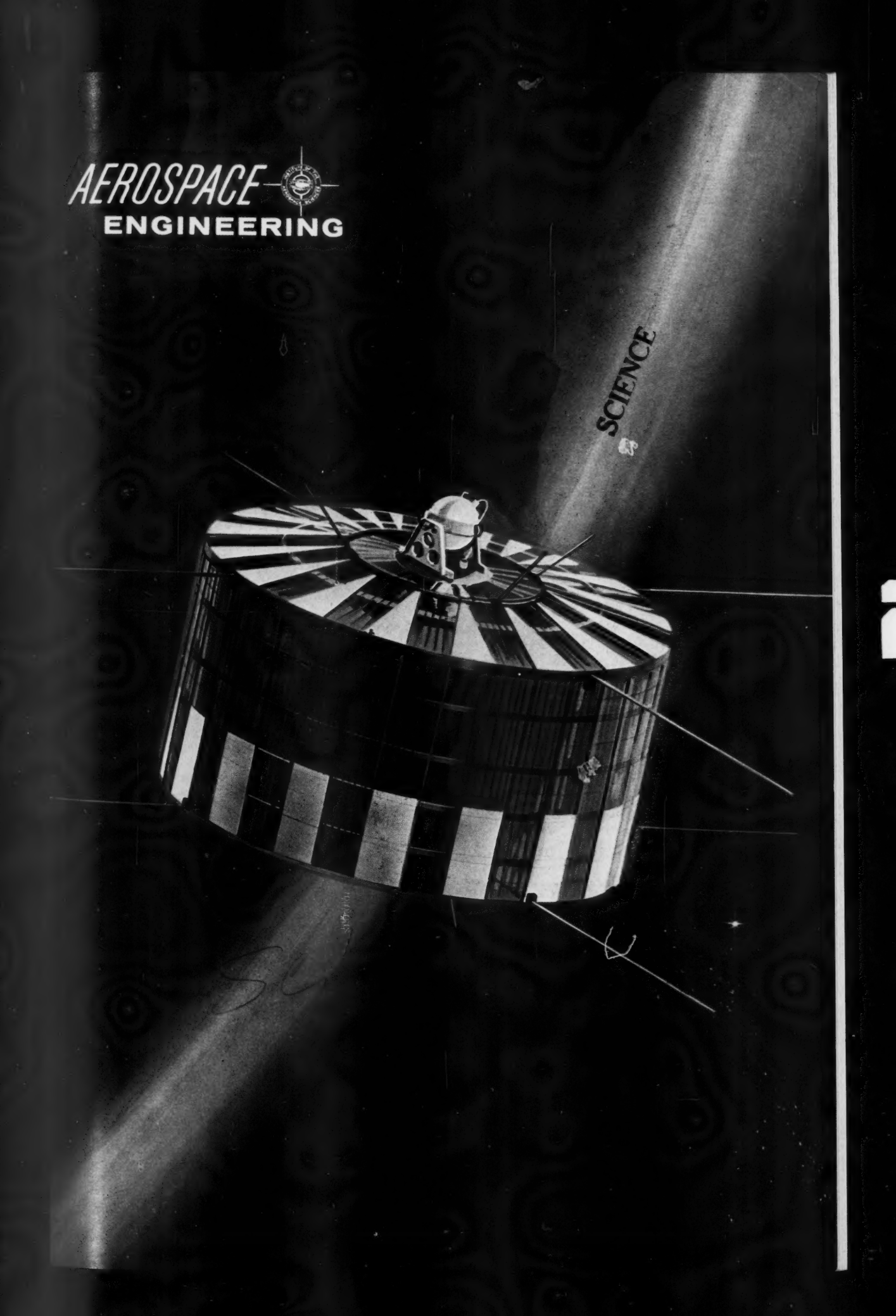
AEROSPACE
ENGINEERING
SCIENCE

Greater Mobility and Reliability for Today's Weapon Systems

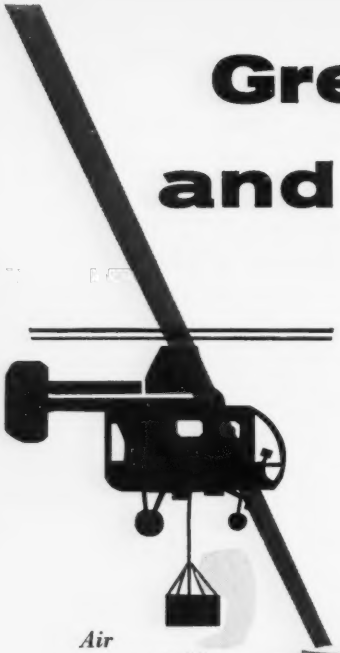

Air transportable

Missile support

Typical AiResearch gas turbine generator set

Ground radar

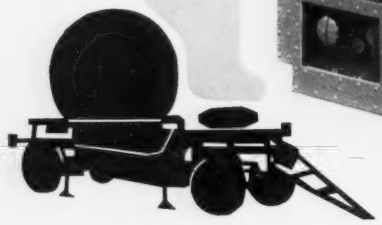

Ground checkout

AiResearch gas turbine generator sets are now providing precise electrical power for mobile weapon systems in compact packages less than half the size and weight of previous systems.

These simplified power packages have fewer parts and provide dependable, quick starting and continuous trouble-free operation in any weather extreme.

Starting, loading and shutdown are completely automatic, push-button operations. And each package has scientifically-designed sound attenuation to minimize noise.

AiResearch is a leader in the design and production of small gas turbine engines and power conversion equipment. Please direct your inquiries to the AiResearch Phoenix Division.

GARRETT **AIRESEARCH MANUFACTURING DIVISIONS** • *Los Angeles 45, California • Phoenix, Ari*

Systems and Components for:
Aircraft, Missile, Spacecraft, Electronic, Nuclear and Industrial Applications

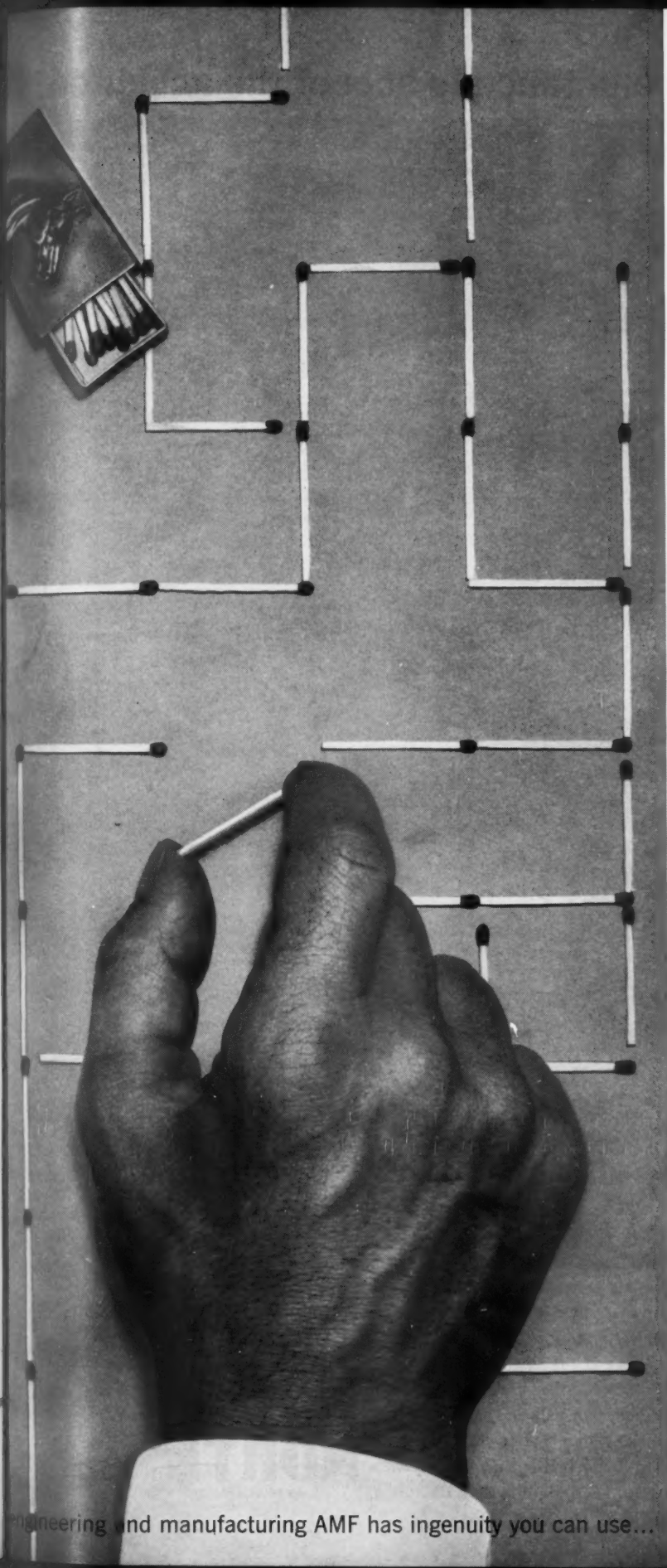

He designed a new interchange for radio traffic

This AMF engineer, part of an AMF-U.S. Army team, solved the problem of traffic delays and personal danger in manual re-connection of jumpers when interchanging R.F. transmitters and antennas.

His solution is a push-button-operated, coaxial crossbar switching system, using vacuum switches for circuit selection. A typical system consists of 4 transmitter inputs, 7 antenna outputs plus a dummy load, in a 4 x 8 matrix that can be mounted in a 19" rack. It can be controlled locally or remotely over any type of communication network having a bandwidth of at least 200 cycles.

AMF's coaxial crossbar switching system provides 100% flexibility in circuit path selection and accommodates power levels as high as 500,000 watts and frequencies up to 30 megacycles. It allows 100% utilization of all transmitting equipment. Stubs are automatically eliminated.

To insure fail-safe operation, power is required for the vacuum switches *only* during change of condition. Selection rate: 1 per second. Operating transmitters are safety-interlocked to insure a load. There are no hazards from open wires or inadvertent application of power to dead-lined antennas.

Single Command Concept

AMF's imagination and skills are organized in a *single operational unit* offering a wide range of engineering and production capabilities. Its purpose: to accept assignments at any stage from concept through development, production, and service training...and to complete them faster...in

- *Ground Support Equipment*
- *Weapon Systems*
- *Undersea Warfare*
- *Radar*
- *Automatic Handling & Processing*
- *Range Instrumentation*
- *Space Environment Equipment*
- *Nuclear Research & Development*

GOVERNMENT PRODUCTS GROUP,
AMF Building, 261 Madison Avenue,
New York 16, N. Y.

AMF

AMERICAN MACHINE & FOUNDRY COMPANY

...gineering and manufacturing AMF has ingenuity you can use...

Do you share his reluctance to accept the accepted?

Doubt is his dogma. He questions everything, takes nothing for granted — not even his own answers.

Do you share his stubborn skepticism? Then come to Northrop, where the breadth and variety of projects give ample scope to the most determined questioner. Northrop's divisional organization makes it possible to support a broad range of programs from countermeasures systems and airborne computer design to techniques for aero-space deceleration and re-entry, and the maintenance of a total human environment in space.

Top priority, just now, goes to senior aerodynamicists and computer circuit designers. But whatever your specialization, if you're the kind of man Northrop needs, there'll always be an opening for you. Why not get in touch with us today and find out more? Just write to Northrop Corporation, Post Office Box No. 1525, Beverly Hills, California.

NORTHROP

AN EQUAL OPPORTUNITY EMPLOYER

"Written Exclusively
By Engineers—For Engineers"

AEROSPACE ENGINEERING

– Established 1934 –

VOLUME 20 / NUMBER 11

NOVEMBER 1961

Featured in this Issue

6 Aerospace Technology as Seen by the Panels
Support—Problems in Concurrent Development and Production. . .William R. Owens
Vehicle Design—Problems Surveyed. . .C. E. Pappas

Jerome G. Morse and Douglas G. Harvey — 8 Nuclear Energy in Space—Radioisotope Auxiliary Power Systems

Lee A. Ohlinger — 10 For the Air Force—A New Scientific Management Technique

Leonard J. Gordon — 12 Trade-Off Between Propellant Specific Impulse and Density

Mortimer J. Lowy and Robert I. Jaffee — 14 On the Development of Low-Cost, Formable, All-Metal Sandwich Panels With Corrugated Cores

Norman R. Cooper — 16 X-15 Flight Simulation Program

Richard Grau and Bruce A. Chubb — 18 The Magnetic Particle Clutch—A Versatile Control Element for Rocket Systems

Frank M. Anthony and Andrew L. Mistretta — 20 Leading-Edge Design With Brittle Materials

W. E. Cox and W. W. Harter — 22 One-Shot Mission Success at Minimum Cost

Shigenori Ando and Jun-ichi Miyashita — 24 Comments on Aerodynamic Drag of Ground Effect Machines

Departments

26 Adventures in Engineering—
Finding Rare Documents. . .Pearl I. Young

30 Sherman M. Fairchild Publication Fund Papers

62 IAS Papers

80 IAS Special Publications and Papers

84 Honors and Awards

85 Personnel Opportunities

86 Index to Advertisers

On our cover

Transit IV-A, carrying nuclear energy into space, is shown in orbit. The white sphere atop the drum-shaped satellite is a radioisotope-fueled SNAP generator, built by The Martin Company's Nuclear Division under contract with the U.S. Atomic Energy Commission. SNAP (Systems for Nuclear Auxiliary Power) drives two transmitters aboard the Navy's navigation satellite. It is discussed in this issue by two Martin Co. authors, J. G. Morse and D. C. Harvey, writing on "Nuclear Energy in Space—Radioisotope Auxiliary Power Systems." The artwork is by Humbert Olivari, Martin illustrator.

AEROSPACE
ENGINEERING
ESTABLISHED 1934

EDITORIAL STAFF

Publisher: Welman A. Shrader, AIAS

Editor: Allan Bernhardt, AIAS

Editorial Production Manager: Vehig S. Tavitian

Editorial Assistant: Helen S. Goldman

Associate Editor: Paul J. Burr, AFIAS

Technical Consultants: R. L. Bisplinghoff, FIAS
Abraham Hyatt, FIAS

AEROSPACE TECHNOLOGY PANELS

* Indicates Chairman

Paul J. Burr, IAS Technical Services Director, Coordinator

Aerodynamics and Fluid Mechanics

Lester Lees*
Seymour M. Bogdonoff
Dean R. Chapman
Antonio Ferri
Paul Germain
Wayland C. Griffith
Hans W. Liepmann
C. C. Lin
Henry T. Nagamatsu
W. R. Sears
John R. Sellars
R. T. Whitcomb
Hideo Yoshihara

Aeroelasticity

R. L. Bisplinghoff*
Y. C. Fung
I. E. Garrick
Martin Goland
Kurt H. Hohenemser
J. C. Houbolt
W. P. Jones
W. J. Mykytow
Robert F. Speaker

Biomedical Sciences

Don Flickinger*
W. Ross Adey
Capt. William Augerson, USA
Stuart Bondurant
A. Scott Crossfield
Cdr. J. H. Ebersole, USN
W. R. Lovelace, II
Capt. Bruce Pinc, USAF
Stanley N. Roscoe
Foreign Correspondent, Hilding Bjurstedt

Communication

P. C. Sandretto*
K. C. Black
James M. Bridges
Harvard L. Hull
Leonard Jaffe
David S. Little
Lt. Cdr. M. M. Macomber
Paul Rosenberg
William J. Sen
Arnold Shostack
Teck A. Wilson

Control and Guidance

Robert N. Brown*
B. Paul Blasingame
S. F. Eyestone
C. E. Gallagher
Percy Halpert
B. J. O'Connor
Robert L. Roderick
S. F. Schmidt
O. Hugo Schuck
H. Philip Whitaker

Energy Conversion

David Altman*
Robert Bromberg
M. U. Clauser
J. Preston Layton
Frank Marble
G. H. Markstein
A. M. Rothrock
Milton M. Slawsky
Martin Summerfield
T. Y. Toong

Flight Mechanics

H. J. Kelley*
Malcolm J. Abzug
H. Julian Allen
A. E. Bryson, Jr.
T. N. Edelbaum
William C. House
George Leitmann
Bernard Maggin
Angelo Miele
John D. Nicolaides
Charles B. Westbrook

Instrumentation

Paul F. Bechberger*
J. M. Hungerford
Max A. Lowy
Walter McKay
M. David Prince
Charles P. Sonett
George I. Toumanoff
Ralph H. Tripp
William A. Wildhack

Management

Edward A. Ledeen*
Garrett C. Covington, Jr.
Maj. Gen. Marvin C. Demler, USAF
Richard G. Folsom
Joel M. Jacobson
Boyd C. Myers
Sidney M. Robbins
Lewis A. Rodert
John H. Sidebottom
R. C. Siebold
T. Paul Torda

Meteorology

Thomas F. Malone*
Robert D. Fletcher
Henry T. Harrison
Joseph Kaplan
Donald T. Perkins
Herbert Riehl
Morris Tepper
Clayton Van Thullenar
Harry Wexler

Nuclear Applications

J. Donald Rauth*
Jack L. Armstrong
Robert W. Bussard
H. M. Dieckamp
R. L. Duncan
Harold B. Finger
Donald J. Keirn
Frank E. Rom
Raymer E. Schreiber
D. Roy Shoults
T. B. Taylor

Operations

Richard V. Rhode*
Maj. Gen. Otis Benson, USAF (MC)
Ernest A. Cutrell
R. Adm. E. E. Fawkes, USN
Melvin N. Gough
Benjamin S. Kelsey
Franklin W. Kolk
Col. J. L. Marinelli, USA
W. E. Rhodes
M. B. Spaulding, Jr.
D. N. Yates

Propulsion Systems

Bruce T. Lundin*
Robert H. Boden
George W. Brady
David Cochran
Elliot Mitchell
Perry W. Pratt
C. C. Ross
John G. Wilder, Jr.
Maurice J. Zucrow

Space Physics

John C. Evvard*
Herbert Friedmann
Leo Goldberg
C. F. Hansen
Arthur Kantrowitz
Bruno Rossi
S. F. Singer
Leo Steg
Fred L. Whipple

Structures and Materials

Nicholas J. Hoff*
Samuel B. Batdorf
Bruno A. Boley
Pol Duwez
R. R. Heldenfels
Samuel Levy
George N. Mangurian
S. S. Manson
Nathan E. Promisel
Ernest E. Sechler

Support

Ernest G. Stout*
Albert D. Brown
Edward I. Brown
Col. Paul T. Cooper, USAF
P. J. Daniel
Paul Hartline
Donald R. Hill
Capt. N. D. Hodson, USN
Lt. Col. George L. Lovett
R. R. Malik
John McKenna
Gilbert Rolan
Richard A. Schmidt
William R. Owens

Vehicle Design

C. E. Pappas*
Adolph Burstein
C. H. Christenson
A. J. Eggers, Jr.
Robert Lichten
E. V. Marshall
Rene H. Miller
John R. Ragazzini
George S. Schairer
George S. Trimble, Jr.

Aerospace Engineering (established 1934) is published monthly by the Institute of the Aerospace Sciences, Inc., at 20th and Northampton Streets, Easton, Pa. Headquarters and Editorial Offices: 2 East 64th Street, New York 21, N.Y. (TEmpleton 8-3800). Western Office: 7660 Beverly Blvd., Los Angeles 36, Calif. Subscription rates: United States and possessions, 1 year, $5.00; single copies, $0.50. Foreign countries including Canada (American currency rates), 1 year, $6.00; single copies, $0.50. Second-class mail privileges authorized at Easton, Pa. This publication is authorized to be mailed at the special rates of postage prescribed by Section 132.122. Notices of change of address should be sent to the Circulation Department, Institute of the Aerospace Sciences, Inc., 2 East 64th Street, New York 21, N.Y., at least 30 days prior to actual change of address.
© Copyright, 1961, by the Institute of the Aerospace Sciences, Inc. Statements and opinions expressed in *Aerospace Engineering* are to be understood as individual expressions and not those of the Institute.

BUSINESS STAFF

Business Manager and Advertising Production

John Phillips

Advertising Director

John R. Cockerell
116 So. Michigan Ave.
Chicago 3, Ill.
ANdover 3-6929

National Advertising Regional Offices

John Cockerell, Inc.
(Headquarters)
116 So. Michigan Ave.
Chicago 3, Ill.
ANdover 3-6929

3757 Wilshire Blvd.
Los Angeles 5, Calif.
DUnkirk 3-1135

380 Lexington Ave.
New York 17, N.Y.
OXford 7-9048

1501 Euclid Ave.
Cleveland 15, Ohio
TOwer 1-8338

915 Olive Street
St. Louis 1, Mo.
GArfield 1-0907

141 N.E. Third
Miami 32, Fla.
FRanklin 1-9941

Contributors Please Note

AEROSPACE ENGINEERING welcomes contributions of full-length technical articles, including manuscripts classified as technical notes, pertaining to all fields of interest in the Aerospace Sciences. (See headings of IAS Aerospace Technology Panels on opposite page.) Manuscripts in either category, which should be addressed to The Editor, *Aerospace Engineering*, 2 East 64th Street, New York 21, N.Y., are acknowledged on receipt. Editorial review—requiring from two to six weeks—is initiated with a promptness dependent upon conformance to standards discussed below. Authors are notified as soon as possible as to acceptance or rejection. To avoid delays and minimize correspondence, contributors are urged to supply the Editor with the original manuscript plus one or two legible (carbon or process) copies complete with clear copies of illustrations. Manuscripts should not exceed 17–20 pages (maximum of 5,000 words). Each should be typed (double-spaced) and every page must be typed with two-inch margins. For each illustration, deduct 350 words; for any tabular matter, deduct an equivalent number of words from text. Detailed instructions for preparation of manuscripts are published monthly on the inside back cover of the *Journal of the Aerospace Sciences*. *Aerospace Engineering* does not pay for contributions.

a new design concept...

HDR SERIES High precision radial ball bearings with maximum ball complements in deep groove races uninterrupted by filling slots or counterbore — extra high capacity — made in four metric series, in ABEC 3 and ABEC 5 precision grades.

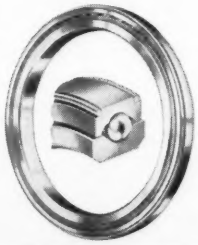

T SERIES Thin-section, high precision radial ball bearings. Type TCR with maximum ball complement and retainer — Type TCF with full race ball complement — Type TWF with unique integral shield.

MIDGET T's Small, thin-section radial ball bearings with maximum ball complements and one-piece retainers — high concentration of load capacity in minimal space results in tremendous space savings.

FUNCTIONAL ADVANTAGES EXCLUSIVE WITH PATENTED SBB BALL BEARING CONSTRUCTION

Split Ballbearings have many advantages over conventional ballbearings because of our exclusive and patented method of construction. The result is a new kind of precision ballbearing with the following superior performance abilities:

MORE LOAD CAPACITY — up to 56% more radial capacity than conventional Conrad-type bearings while maintaining full thrust capacity in either direction. **LONGER SERVICE LIFE** — up to 280% more life than conventional Conrad-type bearings, without sacrificing load capacity. **ONE-PIECE RETAINER** — strong, light, precision made. **SPACE SAVING** — more capacity in a given bearing envelope means smaller bearings may be used. **LOW TORQUE** — maximum ball complements and precision one-piece retainers provide better load distribution within the bearing, effectively reduce starting torque, and minimize running torque. **GREATER RIGIDITY, LESS DEFLECTION, INCREASED RESISTANCE TO SHOCK LOADS** — all these advantages derive from using maximum ball complements in deep groove bearings without filling notches or counterbored rings . . . possible only with Split's patented construction method. **INTEGRAL SHIELDS** — truly integral shields in thin-section bearings . . . no ring distortion. **SPECIAL DESIGNS** — Split Ballbearing's method of construction brings new solutions to difficult bearing problems. As a result, many of these incorporate special bearing designs. You are invited to consult with our Special Bearing Engineering Group for new approaches to your particularly difficult bearing problems.

split ballbearing

SBB DIVISION OF MPB INCORPORATED
LEBANON, NEW HAMPSHIRE

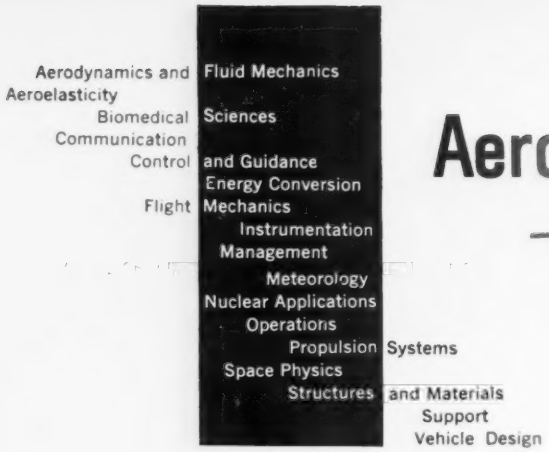

Aerospace Technology

—as seen by the panels

Support

Problems in Concurrent Development and Production

William R. Owens

Mr. Owens is a member of the IAS Aerospace Technology Panel on Support, and a member of the Boeing Company Aerospace Division where he has held project and staff technical assignments on the Bomarc and Minuteman programs.

ONE OF THE MAJOR difficulties the Department of Defense faces today is the problem of hardware deliveries on schedule in a new weapon system involving concurrency between the development program and the production program.

A clear definition of the weapon system requirements, in terms of equipment, facilities, people and data, is the first step in accomplishing a concurrent program on time. Specification MIL-D-9412C establishes the requirement for the conduct of a weapon system functional analysis—viz., preliminary design—resulting in a determination of the following:

(a) All functions (performed by hardware and people) required in the weapon system.
(b) Technical requirements for each item of hardware and facility.
(c) Recommended solutions for (a) above.
(d) Sources of hardware (Contractor-furnished or Government-furnished).
(e) Maintenance requirements.
(f) Spares provisioning consistent with (a) above.
(g) Basis of issue for end item hardware.
(h) Personnel skills and training requirements.
(i) Technical data requirements.

Of the four areas of requirements, perhaps the most difficult to determine is that of equipment, or end items of hardware. The functional analysis attempts to determine the several procurement packages which constitute the end items to be furnished under the production program. (NOTE: In this determination, does an end item for cabling comprise an individual cable or a set of cables for intrasite connections? When a "test set" is comprised of several unconnected units, is each unit an end item, or is the "test set" an end item?) Without much doubt, the biggest detriment to the on-schedule delivery of operational systems has been *late definition* of the elements identified above. A very concerted effort must be put forth sufficiently early in the development program to establish the required elements of the weapon system to know what must be developed and what must go into production. Budget estimates and timing tend to be grossly inaccurate until these elements are known.

Following the completion of the functional analysis and approval of the data by the procuring agency, specifications need to be written. Specification MIL-S-6644A currently requires considerable detailed interpretation to yield satisfactory documents. Definition of a subsystem would logically be assumed to apply to the first subdivision below weapon system, such as missile subsystem, launch control subsystem, etc.; however, this is not generally applied. Why the terms "personnel subsystem" and "launch control system" when these elements have equal importance in the weapon system? Why should it not be clearly stated that an equipment specification must unequivocally define what test results the contractor must obtain to permit acceptance of the equipment. Our communications are hampered by different names for the same thing—"model specification," "detail design specification," "equipment specification." To what level of drawing detail does the contracting agency control and approve configuration changes? Revision of MIL-S-6644A with improved interpretations would help considerably to avoid delays in specification preparation and

approval particularly when production must start within a few months after the first R&D firing.

Concurrency further aggravates the production program because of the volume of changes being fed in by the development program, such as changes in tooling, revision of schedules and price, need for sole sources best capable of performing to program demands, configuration control of hardware by detailed part numbers, changes in long lead operational facilities, and budget limitations preventing enough flexibility to invoke work-arounds to meet program demands.

In summary, the military establishment and industry must place more emphasis on an adequate and early resolution of weapon system elements if we expect to meet the demanding schedules on high-priority complex military weapon systems. *This early weapon system analysis must be conducted to provide a basis for sound program direction.* Having accomplished this objective, the detailed requirement can be developed to add the necessary precision in requirements for equipment, facilities, personnel training, spares, and technical data.

✦ ✦ ✦

Vehicle Design

Problems Surveyed

C. E. Pappas

Mr. Pappas is Chairman of the IAS Aerospace Technology Panel on Vehicle Design, and Assistant to the Vice President—Research and Development, Republic Aviation Corp.

VEHICLE DESIGN encompasses a broad category of flight systems operating in various degrees of the atmosphere, to no atmosphere at all in space. The spectrum extends from conventional aircraft, to missiles, to geocentric satellites and finally deep space spacecraft. Each category requires a special realm of knowledge and engineering design skill. Members of the Vehicle Design Panel will continue to discuss in these columns during the months ahead various problems in these three broad categories to indicate the state of the art and where it is likely to proceed. Perhaps one of the most satisfying results that may ensue from technical data to appear here is that AEROSPACE ENGINEERING readers may determine whether adjustments in individual scientific capabilities and education requirements are necessary to meet challenges ahead.

In extending our design requirements to that of space, we find that in addition to the three basic disciplines of physics, chemistry and mathematics we must now add two more fields—psychology and biology, the latter including botany.

In the past, the aircraft engineer has paid little attention to the psychological factors affecting pilot and crew in the design of aircraft. Today, however, it is essential that he consider the pilot and crew because the success of our manned space efforts will depend considerably upon psychological well-being.

The vehicle designer must synthesize all of these doctrines into one successful operating system. When one accounts for the new concepts being introduced in each one of these fields, the designer really has a formidable task before him.

The designer must have a basic training and understanding of several fields of science. Coupled with this he must have extensive engineering ability and experience. In this regard, vehicle design stands supreme with respect to all other fields; it is no wonder that the designer must proceed with his feet solidly on the ground and must exercise caution as well as sound judgment. Reliability and maintenance considerations will dictate how many new concepts and doctrines he should introduce into a new design in order to attain a certain degree of success.

It is noteworthy that as an engineer's abilities are called upon to design for space conditions, he learns immediately that design depends very heavily upon consideration of weight, systems integration and optimization, weapons system effectiveness, and the new environmental conditions introduced.

As we all know, if we are to achieve proper low structural weight, it is mandatory that we find substantial advances in the state of the art in Structures, Materials, Propulsion, and Electronics; and, in the case of man, closed ecological systems.

It is evident that in order to keep structural weight to a minimum, vehicle shapes of the future must perform several functions. For example, a fuselage may be required to house not only electronics, crew, fuel, etc., but must at the same time be a lifting surface, an air inlet, a combustor, and an exit to be used in conjunction with a propulsion system.

A WORD OF CAUTION: There is a tendency to push forward so fast that the designer finds it very difficult to make the transition between his prior experience with that required in a given new design. On this basis, the overall project contemplated becomes too expensive or too risky. Somehow, we must pause to look around to see what is available to us before plunging too deeply into the unknown. In this case, haste can very well make waste. Common sense and logic must be called upon to resist what certainly is a widespread temptation to plow into darkness without illuminating it first.

We must readjust our ways of research, in industry and Government, if we are to obtain necessary data to design vehicles of the future. We must concentrate more on problems which appear to be more conventional and get factual statistics before tactically useful vehicles capable of sustained flight can be produced. Strict adherence to this concept will assist greatly in obtaining data so necessary for future design.

Nuclear Energy in Space—
Radioisotope Auxiliary Power Systems

Jerome G. Morse • Douglas G. Harvey

The Martin Company

THE SUCCESSFUL launching and operation of a Transit satellite in June 1961 heralded the first application of nuclear power in America's space program. After more than 5 years of development by Martin Company engineers under AEC auspices, a SNAP (Systems for Nuclear Auxiliary Power) generator was put to work driving two transmitters aboard the Navy's Transit IV-A navigation satellite.

The grapefruit-sized device is representative of a family of radioisotope-fueled electrical generators which convert heat to electricity without moving parts—and hence are ideally suited to space missions. They can be used most effectively for low-powered, long-lived earth orbit missions, obviating the need for battery charging. They can function effectively on the dark face of the moon, in the dense atmosphere of Venus, and in any missions away from the sun.

In radioisotopic generators, heat is generated when the particulate and electromagnetic radiations emitted by a sealed quantity of radioisotopic material are absorbed by the source and its surrounding containment material. This heat is then partially converted into electricity by a suitable direct-energy conversion device—thermoelectricity in the case of the Transit IV-A generator—and the remaining heat is dissipated to the external environment.

Two major types of radioactive materials are used: (1) waste materials from the controlled fission of uranium, and (2) alpha-emitting isotopes produced by irradiation of suitable target materials in

Dr. Morse is Director, Auxiliary Power Systems Dept., Martin Nuclear Division. He completed undergraduate studies at City College of New York in 1942, received his M.S. degree from the University of Pennsylvania in 1947, and his Ph.D. in physical chemistry from the Illinois Institute of Technology in 1951. In World War II he was, consecutively, an infantry officer with the U.S. Army and an officer in the Army Air Force. After a year as research chemist with the General Electric Co. in Schenectady, Dr. Morse joined the University of Miami faculty in 1952. He taught chemistry and was Director of the Radioisotopes Laboratory until 1955, when he accepted a post with Martin's Nuclear Division. He is a consultant to the Oak Ridge Institute of Nuclear Studies, and a member of an AEC Industry Advisory Committee on Utilization of Radioisotopes.

Mr. Harvey is Project Engineer in charge of the Space Systems Project of the Auxiliary Power Systems Department in Martin's Nuclear Division. He was graduated from Trinity College (Hartford, Conn.) with a Bachelor's degree in chemistry in 1952, and the following year received his Master's degree in nuclear chemistry from the Massachusetts Institute of Technology. From 1953 to 1956, he served as officer in charge of Radiation Effects Studies at the Wright Air Development Center (Dayton, Ohio), joining Martin in August 1956. In January 1959, after serving in several positions, he was appointed Sales Manager of the Isotopic Power Department, and shortly thereafter became Project Engineer for the SNAP 1A program. His post since has been expanded to include supervision of other Martin-Nuclear Division space power systems as well.

. . . in which, the authors report, this new, rugged, compact and reliable device (converting heat to electricity without moving parts) operates independently of solar transients and is adaptable to power needs in space.

nuclear reactors. Each type of source material has distinct advantages for specific missions; but for space probes into the new environments where one of the properties to be investigated is the ambient electromagnetic radiation, a distinct advantage is found in the use of alpha-emitters as sources of energy. After extensive examination of the alpha-emitters available, it appeared that four isotopes had merit as heat sources—curium-242, polonium-210, curium-244, and plutonium-238. Potential availability and cost, plus the lack of hard gamma radiation, were the deciding factors in the selection of these four isotopes (Table 1).

Two of these four isotopes, curium-242 and polonium-210, are in the short-life, high-power category. Plutonium-238, with its half life of almost 90 years, answers the need for long-lived heat sources. Curium-244 (17.9-year half life) will serve as a source of power for an intermediate-length mission.

Energy Conversion Systems

The heat obtained from radioactive decay may be converted into electricity by means of rotating machinery, thermoelectric devices, or thermionic devices. With efficiency and reliability as guidelines, only the latter two schemes need be considered at power levels of a few hundred watts. Early missions will use thermoelectric converters, but the potential of thermionic systems, offering such significant advantages as high heat-rejection temperatures, lower weight, and higher efficiencies, well justifies extensive (*Continued on page 58*)

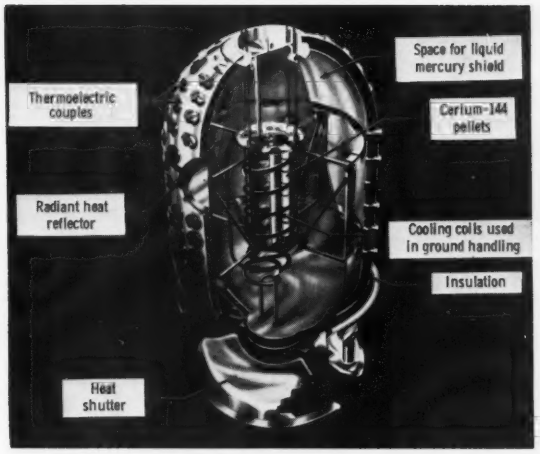

Fig. 1. SNAP 1A thermoelectric generator.

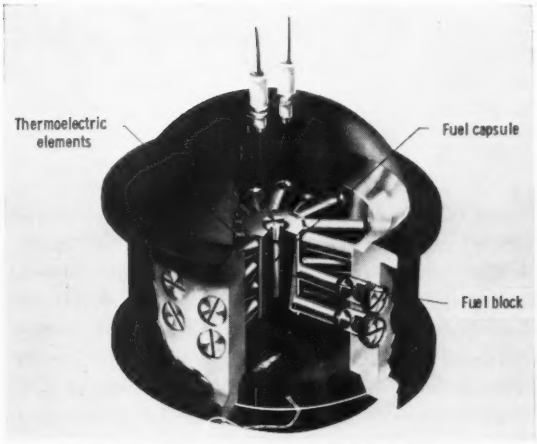

Fig. 2. SNAP 3 thermoelectric generator.

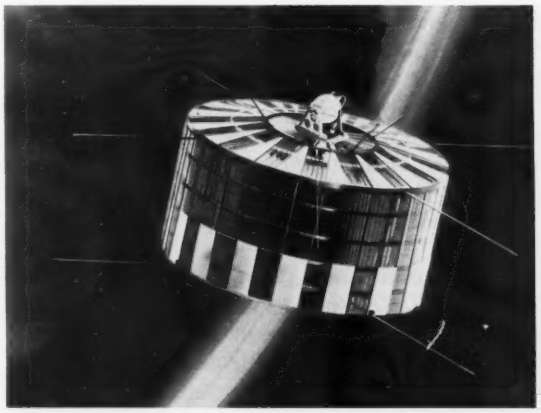

Fig. 3. The first nuclear-powered satellite in orbit (artist's drawing). White sphere atop the drum-shaped Transit satellite is a radioisotope-fueled SNAP generator. Heat produced by the spontaneous decay of plutonium-238 in the core of the generator is converted directly into electric energy by a thermoelectric system.

For the Air Force

A New Scientific Management Technique

Lee A. Ohlinger, *Northrop Corporation*

The author, Director of Northrop's Norair Division Computing and Data Processing Center, is a pioneer and leader in the atomic energy and computing-data processing fields. His 34 years of technical and management experience includes 12 years in his present post, three years as Northrop's Design Specialist and Project Engineer of Nuclear Energy Projects, four years as Assistant Division Director, University of Chicago Metallurgical Laboratory (Manhattan Project) where he made the basic engineering designs for the first nuclear reactors at Hanford, 12 years as Specialty Design Engineer for Standard Oil, and seven years as a consulting structural engineer. He holds over 40 patents in his principal fields.

MOST PEOPLE probably think of the U.S. Air Force (USAF) in terms of "the customer" and not many consider them from "the management" aspect. Nevertheless, what used to be the Air Material Command (AMC) and is now the Air Force Logistics Command (AFLC) has under its jurisdiction or "management" a complex of over 100 weapon systems programs for which it is responsible from a cost and performance standpoint. Classical management theory defines the five principal management functions as planning, control, organizing, staffing, and directing. The Air Force not only exercises all of these within its own structure but also exercises the first two and strongest of these management functions over the program complex continuously, and this certainly classes them as "management."

Unfortunately, the USAF has been faced with the same problem that has harassed industry—the need to recognize management's true place in the total scheme of things and the need for converting the "art" of management to the "science" of management.

In a democratic nation devoted to the concept of free enterprise, it was inevitable that competition would drive industry toward better products at lower cost but too many people believe that the better products and lower costs are simply the result of improved technology and manufacturing skills. Very few seem to realize the importance of management's part in achieving these goals or recognize that a bad management system can ruin the effects of the best skilled engineering and production workers. Industry provides research in science and technology and research in manufacturing techniques but rarely if ever stresses research in management techniques and the development of scientific methods of improving management's functions of decision-making and control.

However, the day of intuitive management by "seat-of-the-pants" techniques is passing, and the new tools of scientific management which we call Operations Research, aided and abetted by the newer mathematical tools and high-speed computing and data-processing equipment, are providing the opportunity for intelligent and realistic decision-making based upon scientific principles.

If scientific management can be applied to in-

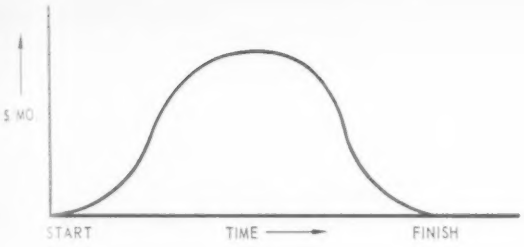

Fig. 1. Expenditure rate curve.

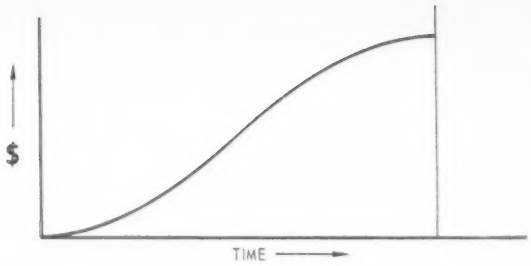

Fig. 2. Expenditure growth (or cumulative expenditure) curve.

. . . the need to recognize management's true place in the total scheme of things. . . . the need for converting the art of management to the science of management. The application of scientific techniques in a joint USAF-Industry effort to remedy a long-neglected management area is reported along with significant results for long-range programing and reprograming.

dustry, it should be equally capable of being applied to the military in their capacity as managers of what amounts to "big business"—this complex of over 100 weapon systems programs. The following is a report of a joint effort of industry and the Air Force to provide the latter with a significant example of the new scientific techniques of management in an area that has sorely needed this aid for many years. The successful demonstration of the principles involved can only lead inevitably to the application of similar scientific techniques to other phases of management in the Air Force and other military agencies but the program described herein can well serve as the pioneering effort to demonstrate the new concepts of management.

The program complex of AFLC is a dynamic one, subject to change at any time brought about by a number of different disturbing factors. For example, Hq USAF may, at any time, perform a simulation or gaming exercise on the program complex based upon economic, military, or even political reasons. The result of the gaming is to raise a number of "What if . . . ?" questions for which Hq USAF, as top management, must have answers in order to evaluate the results of various program shifts and arrive at decisions for immediate or future action. This may range from a quantity, schedule, or product change in a single program to a major change in the force structure, but good decisions are impossible without answers to the "What if . . . ?" questions.

In the past, the request for such answers came through AMC to the affected contractors, very often on a Friday, with a Monday deadline. The result of such queries, even though they might avowedly be only a hypothetical investigation, was the creation of a panic and a drop in morale that reduced production and required some time before things were again on an even keel at the contractor's site.

In addition to the external influences that required the ability to predict the effects of reprograming, there existed within the program complex itself additional reasons for reprograming all or part of the complex. For example, the development of an over-run or over-schedule condition in one or more programs might result in the rupture of the budget ceiling for AMC and necessitate immediate and fast reprograming to cover the exigency. Another example of the cause for reprograming is the inevitable "program growth" that historically always occurred but which no one wanted to recognize until the usual specter of ruptured budget ceilings necessitated reprograming.

For many years, Hq USAF, Air Research and Development Command (ARDC), and AMC were quite concerned with the magnitude of this programing and reprograming problem but they faced the difficulty of finding time in the busy schedules of the top military decision makers and the means within their own organization and industry to do something constructive about it.

The pressure that finally sparked the study described in this paper was (*Continued on page 63*)

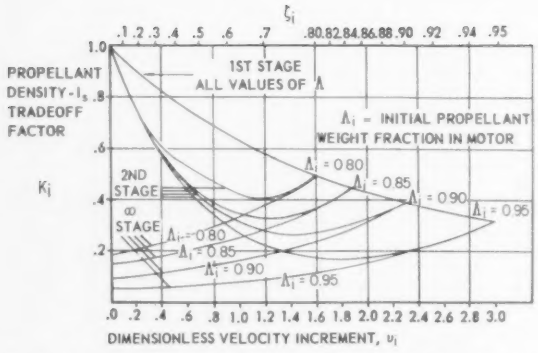
ζ_i
.1 .2 .3 .4 .5 .6 .7 .80 .82 .84 .86 .88 .90 .92 .94 .95
1.0
.8
.6
.4
.2
PROPELLANT DENSITY-I_s TRADEOFF FACTOR
K_i
1ST STAGE ALL VALUES OF Λ
Λ_i = INITIAL PROPELLANT WEIGHT FRACTION IN MOTOR
2ND STAGE
∞ STAGE
Λ_i = 0.80
Λ_i = 0.85
Λ_i = 0.90
Λ_i = 0.95
0 .2 .4 .6 .8 1.0 1.2 1.4 1.6 1.8 2.0 2.2 2.4 2.6 2.8 3.0
DIMENSIONLESS VELOCITY INCREMENT, v_i

Fig. 1. Propellant density-I_s trade-off factor for ideally staged rocket with fixed propellant volume and inert weight in each stage.

Trade-Off Between

Leonard J. Gordon

Aerojet-General Corporation

Mr. Gordon is head of the solid propellant thermodynamics section at Aerojet's Solid Rocket Plant in Sacramento, Calif. He graduated in chemical engineering from the University of Illinois in 1949. After associations with Burgess Battery Co. and the U.S. Naval Ordnance Test Station (Pasadena, Calif.) and graduate study in physical chemistry at UCLA, he joined Aerojet in 1951. Since then he has worked on various aspects of obtaining power from chemicals—primary electric batteries, fuel cell batteries, monopropellants, liquid fuels, and solid propellants.

WHEN SELECTING propellants for rocket applications, one must always consider the trade-off between propellant density and specific impulse values. A relatively simple and straightforward method of determining this trade-off and some typical trade-off values are given here. The method is general with respect to vehicle performance or design criteria, but will be illustrated for only one case—that where a multistage vehicle's inert parts weights and propellant volumes are fixed and a given vehicle burnout velocity is to be maintained.

Geckler[1] has shown that, for multistage rockets, the differential of the ideal vehicle burnout velocity may be written in a form such that the effects of changes in inert parts, propellant, and payload weights of each of the stages are separable. His fundamental equation is

$$dv_b = \sum_{i=1}^{N} \left[v_i dc_i + p_i \frac{dM_p^{(i)}}{M_p^{(i)}} - e_i \frac{dM_e^{(i)}}{M_e^{(i)}} - L_N \frac{dM_L}{M_L} \right] \quad (1)$$

where p_i and e_i are complicated functions which reflect the changes in ith stage weights on the mass ratios of the first to the ith stages. For the special case considered here

$$dM_p^{(i)}/M_p^{(i)} = d\rho_i/\rho_i \qquad \text{(fixed volume)} \quad (2)$$

$$dM_e^{(i)}/M_e^{(i)} =$$

$$dM_L/M_L = 0 \qquad \text{(fixed inert weight)} \quad (3)$$

Using Eqs. (2) and (3) and the fundamental relationship

$$dc_i/c_i = dI_s^{(i)}/I_s^{(i)} \quad (4)$$

Eq. (1) is reduced to

$$dv_b = \sum_{i=1}^{N} \left[c_i v_i \frac{dI_s^{(i)}}{I_s^{(i)}} + p_i \frac{d\rho_i}{\rho_i} \right] \quad (5)$$

If a given vehicle burnout velocity is to be maintained as changes are made in propellant I_s or ρ values,

$$dv_b = 0 \quad (6)$$

For the case where changes are considered only in the ith stage

Propellant Specific Impulse and Density

A general method of determining this trade-off is presented, with one illustration—"that where a multistage vehicle's inert parts weights and propellant volumes are fixed and a given vehicle burnout velocity is to be maintained."

Symbols

- c = effective exhaust velocity
- e = coefficient for inert parts
- I_s = propellant specific impulse
- K = propellant density-I_s trade-off exponent
- L_N = coefficient for payload
- M_e = empty mass rocket motor
- M_L = mass of payload
- M_p = mass of propellant
- M_0 = initial mass of vehicle stage
- N = number of stages in multistage rocket
- p = coefficient for propellant
- v_b = burnout velocity
- v = dimensionless velocity increment
- α_i = stage ratio
- ζ_i = stage propellant fraction
- Λ_i = motor propellant fraction
- Ω = parameter as defined by Eq. (11)
- ρ = propellant density

$$dI_s^{(j)}/I_s^{(j)} = d\rho_{(j)}/\rho_{(j)} = 0 \qquad (\text{all } j \neq i) \quad (7)$$

and Eq. (6) reduces to

$$c_i v_i \frac{dI_s^{(i)}}{I_s^{(i)}} + p_i \frac{d\rho_i}{\rho_i} = 0 \quad (8)$$

Within the range of changes in $I_s^{(i)}$ and $\rho_{(i)}$, for which the assumption of fixed inert parts weights remains valid, Eq. (8) may be integrated to yield

$$\left[I_s^{(i)} \rho_i^{K_i}\right]_1 = \left[I_s^{(i)} \rho_i^{K_i}\right]_2 \quad (9)$$

where

$$K_i = p_i/c_i v_i \quad (10)$$

Equations for computing the coefficients p_i are given by Geckler.[1]

The form of Eq. (9) is well known, having been stated empirically—for example, in Leonard.[2] Often one is interested in substituting one propellant for another of known density and I_s. Inasmuch as I_s appears explicitly in the burnout velocity expressions and ρ does not, it is convenient to cast Eq. (9) into the form

$$\Omega = I_s(\rho/\rho_0)^K \quad (11)$$

where ρ_0 is density of a reference propellant, and Ω is "effective specific impulse."

Figs. 1 and 2 show how K varies from stage to stage of an ideally staged vehicle as a function of the motor propellant fraction Λ_i (*Continued on page 27*)

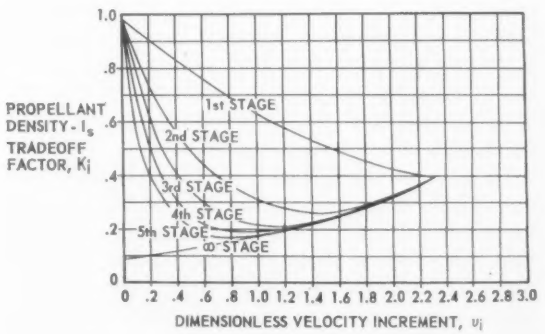

Fig. 2. Propellant density-I_s trade-off factor for ideally staged rocket with fixed propellant volume in each stage. (Initial propellant weight fraction in motor, $\Lambda_i = 0.90$.)

On the Development of Low-Cost, Formable, All-Metal Sandwich Panels With Corrugated Cores

Mortimer J. Lowy, AFIAS, *Douglas Aircraft Company*

Robert I. Jaffee, *Battelle Memorial Institute*

A METHOD OF fabricating all-metal sandwiches by pressure welding the components in a hot-rolling operation was conceived by Dr. Robert I. Jaffee. This sandwich system was developed at Battelle, under the sponsorship of Douglas Aircraft Company, and is referred to as a roll-welded sandwich. Development work on forming the panels and processing after rolling is being conducted at Douglas.

A 3-ft by 6-ft panel (Fig. 1) has been successfully rolled of A-55 titanium by use of conventional rolling equipment. Smaller panels have been made of other titanium alloys, 15-7 Mo stainless steel, and aluminum. Battelle has conducted feasibility studies of application of the technique to René 41, beryllium, molybdenum, and other metals. Work is continuing on these systems. Theoretically, there is no limit to the number of alloy systems that can be fabricated in sandwiches by this process.

The sandwich system of construction for light-gage metal structures has long been viewed by structural designers as a very efficient means of obtaining high strength with minimum weight for structures subjected to compression or bending loads. In general, a lightweight core is used to hold relatively thin sheets ("faces") at an appreciable distance from each other in a panel, thereby affording the panel a degree of stiffness several times greater than it would have if the face material were concentrated in a single homogeneous sheet. Also, the core material supports the face sheets either continuously or intermittently at a pitch distance calculated to afford stabilization of the individual sheet when the sheet is loaded by a compression force lying within its plane. Of course, there must be an attachment between face and core so that the face is restrained from buckling away from the core just as the core itself offers the restraint against buckling into the volume occupied by the core.

During the past 20 years structural designers in the aircraft and, more recently, the missile industries have worked to incorporate sandwich construction in their designs. Many types of core configurations

Mr. Lowy is Technical Assistant to the Chief of Stress, Space Systems Engineering, and has been associated with Douglas since 1948. His responsibilities have included those associated with structural, heat-transfer and material problems encountered in the design of supersonic aircraft, hypersonic glide re-entry, hypersonic testing, solid propellant motor cases, cryogenic tankage, and space cabins. Mr. Lowy received his B.S.M.E. at Illinois Institute of Technology in 1944. In addition to his IAS Associate Fellowship, he is a member of the ARS.

Dr. Jaffee, Technical Manager of the Department of Metallurgy, guides Battelle activities in process, mechanical, physical, fabrication, and chemical metallurgy and metallurgical engineering. His research interests are reflected in the more than 100 reports bearing his name, and the almost three dozen patents based on his contributions. Active in technical and professional circles, he is Chairman of the Alloy Selection Group of the Titanium Alloy Sheet Rolling Panel, and of the Molybdenum Applications Group, Refractory Metals Panel, Materials Advisory Board, National Academy of Sciences.

"The pressure welding accomplished by the hot-rolling process produces joints in which the diffusion across the interface is complete. . . In general, proper control of the combination of surface preparation, rolling temperature, and amount of reduction results in welds in which the joints cannot be distinguished from the parent structures."

have been made, ranging from soda straws glued side-by-side, blocks of balsa wood, and foamed plastics to hexagonal columns arranged in array with axes perpendicular to the faces ("honeycomb core"). Cores in the honeycomb configuration have been made of paper, fiberglass-reinforced plastic, and various metals. Actually, the honeycomb core configuration has given birth to a number of small industrial firms and, of the various core configurations, has received the most attention. In applications where it is not necessary to provide isotropic load-carrying capability, a corrugated core can be used and is often more efficient than the isotropic or nearly isotropic forms. This is especially true when the component of compressive loading in one direction is high and the corrugations are made to run in this direction. In such a case, the corrugated core can serve the dual function of carrying direct load as well as stabilizing face sheets.

Despite the obvious advantages in structural efficiency, wide-scale application of sandwich construction has been slow in coming. Some of the problems which have stood in the way have been:

(1) Joining of sandwiches to each other and to other structures.

(2) Introduction of concentrated loads into the sandwich structure.

(3) Fabrication of contoured surfaces.

(4) Cost.

(5) Nondestructive inspection techniques and quality control.

With the development of hyperperformance aircraft and missile and space systems, attention has again been focused on the sandwich structure because of the exceptionally large exchange ratios, or "payoffs," which attend structural weight-savings on these systems. Ironically, (*Continued on page 28*)

Fig. 1. Finished panel (A-55 titanium; copper cover sheets not stripped).

X-15 Flight Simulation Program

Norman R. Cooper, AIAS

North American Aviation, Inc.

THE IMPORTANCE OF flight simulation in the development and testing of the X-15 research vehicle cannot be overestimated. Flight simulation has been used in all design and testing phases—first to support the configuration and subsystem design; next to test and evaluate subsystems, displays, and control hardware, both in prototype and in final production form; and finally to provide flight-test support and pilot training. This paper will review briefly the overall simulation program conducted during the 5-year development of the X-15 and will describe in detail the unrestricted six-degree-of-freedom mechanization which has been utilized during the past 3 years of the program. It will describe the most important of the many applications in which the simulator has been, and in fact is still being, utilized in the design, development, and flight testing of the X-15. Finally, it will compare the simulation requirements of the X-15 with those of more advanced space vehicles and attempt to interpret problems or deficiencies encountered in the X-15 simulation as they may affect more advanced space mission simulation.

It may be said that many of the X-15 simulation requirements literally "grew" with the program. However, the major simulation objectives were evident at an early date. These included hypersonic stability and control evaluation; control requirements and techniques during the exit, re-entry, and ballistic phase of the mission; stability augmentation requirements and control system design; and hardware testing of the flight control system and related subsystems. As described later, other equally important objectives were accomplished as the program progressed. In all applications, however, it was apparent that the pilot, or operator, was required as an integral part of the control loop, and as a consequence the final flight control simulator as it exists today was included in the initial X-15 simulation plans.

A review of the X-15 vehicle and its intended mission gives an insight into the simulation requirements associated with the program. Fig. 1 shows the X-15 vehicle and the control system configuration. The X-15 has an upper and lower movable

Mr. Cooper received his Bachelor of Science degree (1952) and his Master of Science degree (1953) in aeronautical engineering from the University of Texas. He joined North American Aviation in 1953 as an aeronautical engineer responsible for flight control analysis and simulation, starting with the F-100 series airplane. Mr. Cooper was associated with the flight control system development in the X-15 since its inception and was responsible for the development and direction of the flight simulation program in support of the X-15. (*Aerospace Engineering* regrets to note Mr. Cooper's death in a highway accident last July 4 and wishes to acknowledge his associates' assistance in posthumous publication of his work on these pages.)

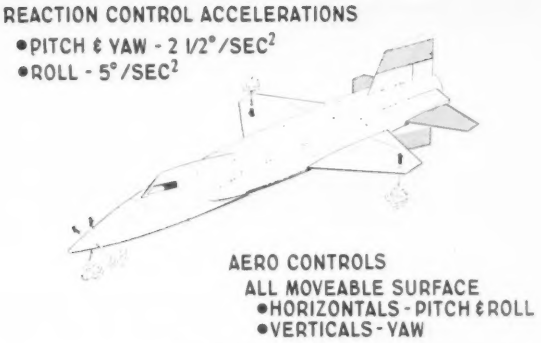

Fig. 1. Flight controls.

"It is believed that the X-15 simulation program pushed analog techniques to their limits . . . Based on these results, it is apparent that digital techniques must be resorted to in future simulations."

Symbols

b = wingspan, ft
$\bar{C}$ = mean aerodynamic chord, ft
C_c = chord force (nondimensional coefficient)
C_l = rolling moment (nondimensional coefficient)
C_m = pitching moment (nondimensional coefficient)
C_n = normal force (nondimensional coefficient)
C_y = side force (nondimensional coefficient)
G = acceleration of gravity, ft/sec²
h = altitude, ft
I_{xx} = moment of inertia about X-body axis, slug-ft²
I_{yy} = moment of inertia about Y-body axis, slug-ft²
I_{zz} = moment of inertia about Z-body axis, slug-ft²
l_T = tail length, ft
m = mass, slugs
M = Mach number
p = roll rate
q = pitch rate
q_c = dynamic pressure, lb/ft²
r = yaw rate
S = wing area
V_o = velocity of center of gravity, ft/sec
V_x = velocity component along X-body axis, ft/sec
V_y = velocity component along Y-body axis, ft/sec
V_z = velocity component along Z-body axis, ft/sec
α = angle of attack
β = angle of sideslip
δ' = differential horizontal stabilizer deflection, roll control
δ_H = horizontal stabilizer deflection, pitch control
δ_V = vertical stabilizer deflection, yaw control
Φ = Euler angle of axial rotation, roll
Θ = Euler angle of elevation, pitch
ψ = Euler angle of azimuth, yaw

vertical stabilizer for yaw control, and differentially operated horizontal surfaces for pitch and roll control while in the atmosphere. The reaction system for attitude control outside the atmosphere consists of small hydrogen peroxide rocket motors in the nose and wing tips. Electronic stability augmentation in the X-15 consists of rate damping about all three axes.

Fig. 2 reviews the design mission and performance capability of the X-15. It is capable of attaining speeds in excess of 6,000 fps, or Mach 6.0, and altitudes to 500,000 ft. The (*Continued on page 71*)

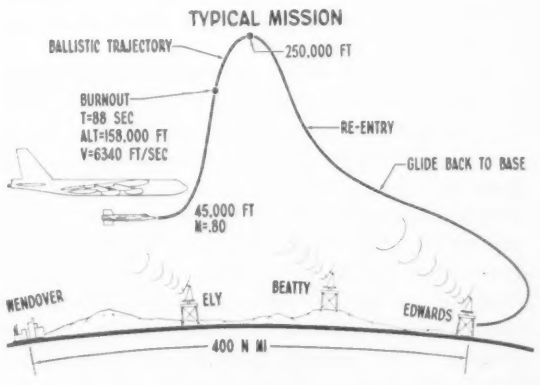

Fig. 2. X-15 research system.

The Magnetic Particle Clutch

A Versatile Control Element for Rocket Systems

Richard Grau • Bruce A. Chubb

Lear, Incorporated

PRIOR TO the development of the clutch servo concept, the engineer had a choice of two conventional types of prime mover—(1) an electric servomotor, or (2) a hydraulic or pneumatic system. The servomotor presented a barrier to high response with its low torque to inertia ratio and inherent damping. The electric motor also had a decided disadvantage in missile applications in that it was a low gain device and therefore required a large power output amplifier. For missile applications, the hydraulic system posed a problem to the engineer regarding shelf life, periodic overhaul, reliability at temperature extremes, periodic leakage checks, sedimentation, and complexity of installation. The simplicity of assembly of the actuator to the vehicle just prior to blast-off was of utmost importance in obtaining high weapon mobility. Fig. 1 shows a hydraulic system as first used to control the four air vanes on a missile, in comparison with four completely separate electric clutch actuators, which replaced all the hydraulics.

The magnetic particle clutch was developed nearly 15 years ago to fill the need for an electric servo that had proportional control characteristics and response suitable for high-performance jet aircraft. Since that time, the magnetic particle clutch has built a proved service record of life, performance, and reliability in almost every field of automatic control. Applications in the rocket field vary from tiny instrument mechanism systems, which have power outputs of only a few watts, to 3-hp missile guidance systems. The magnetic particle clutch servo has broken the barriers of short shelf life, low response, and low power gain associated with electric actuators of the past, and has provided a breakthrough in missile readiness and reliability.

Mr. Grau is a member of the Electro-Mechanical Division. He majored in mechanical engineering at Michigan State University and began his career in 1951 as design engineer for Werner Machinery Co., where he was engaged in food-processing plant layout, machine design, process control, cost estimating, and production engineering. He joined Lear, Incorporated, in 1956 and has devoted his time since to the design of hydraulic actuators, servovalve development, magnetic particle clutch design and development, systems design and engineering, and components and systems analysis.

Mr. Chubb is a member of the Instrument Products Division. He received his B.S. in mechanical engineering from Michigan State University, and followed this with graduate work in electrical engineering at Rutgers University and Michigan State. During his 2-year tour of duty in the U.S. Signal Corps (1957–1959) he performed research and development in the field of electromechanical servomechanisms including supervision in areas of control systems for automatic tracking applications and a precision tape drive incorporated into the Vanguard satellite. He joined Lear in 1959 and has been engaged in the analytical design of servomechanisms including hydraulic servos for flight controls, hydraulic valve analysis, digital accelerometer analysis, gear stiffness and backlash effect study, magnetic particle clutch servoanalysis, and navigation servo studies.

Magnetic particle clutch servos use a continuously rotating prime mover that may be driven by any convenient power source. For example, in rocket system applications, the power source may be a stored propellant, hot gas, or an electric motor

Theory of operation and design of the magnetic particle clutch into numerous missile control packages are described in detail. As case histories, illustrating the versatility of the magnetic particle clutch in solving rocket control problems, three typical servosystems are discussed: (1) a bistable actuator, useful in both aerodynamic control and highly sensitive engine gimbaling; (2) a muscle-type actuator for large rocket vane control; and (3) an instrument-type servo designed for a high response satellite mechanism. This example describes clutch applications in a typical system by the actual design of a servo capable of response up to 250 cps. Results of reliability and service readiness surveys regarding typical clutch actuators are also briefly treated.

(Fig. 2). The prime mover is geared to two counter-rotating clutches. The clutch output members are geared to the common output. By energizing the proper clutch, the output may be made to go in either a clockwise or a counterclockwise direction.

Clutch Characteristics

Fig. 3 illustrates the cross section of a typical magnetic particle clutch. The clutch consists of an electrical coil, a magnetic core structure, and a low inertia drive disc located in the annular air gap. The annular gap is filled with a finely divided magnetic powder. The mechanics involved in coupling the torque of the prime mover to the drive disc have been defined by Bepristis,[1] and may be listed as follows:

(a) When the current is passed through the winding, a flux is built up in the ferromagnetic clutch housing.

(b) In order that the flux complete its path, it must traverse the gap.

(c) In passing through the gap, the flux causes radial alignment of the iron particles.

(d) Since each particle is in a state of magnetization, it is attracted to, and also attracts, neighboring particles thereby forming chains across the gap.

(e) Each particle bears down upon adjacent particles creating a normal force.

(f) The normal force produces a corresponding shear force under conditions of slip or pending motion.

(g) The summation of individual shear forces is equivalent to a resultant shear force which acts in the same direction as the clutch housing.

(h) Increasing or decreasing the total flux in the powder gap accordingly increases or decreases the normal force created by the particles and, therefore, controls the magnitude of the shear force.

(i) The torque of the (*Continued on page 31*)

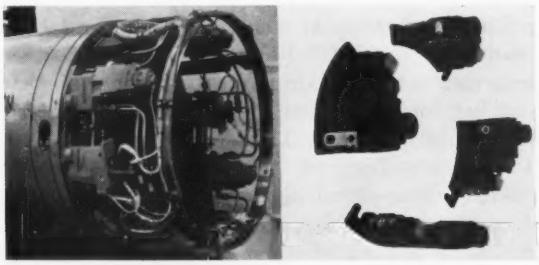

Fig. 1. Comparison of hydraulic system and electrical clutch system for rocket air vane control.

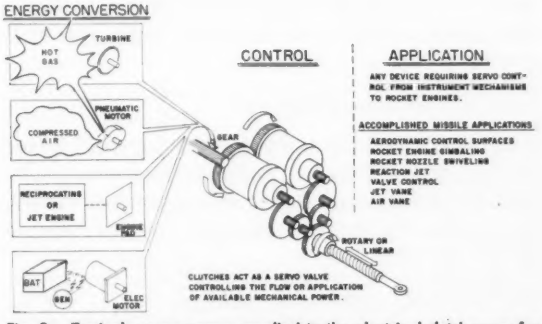

Fig. 2. Typical power sources applied to the electrical clutch servo for rocket applications.

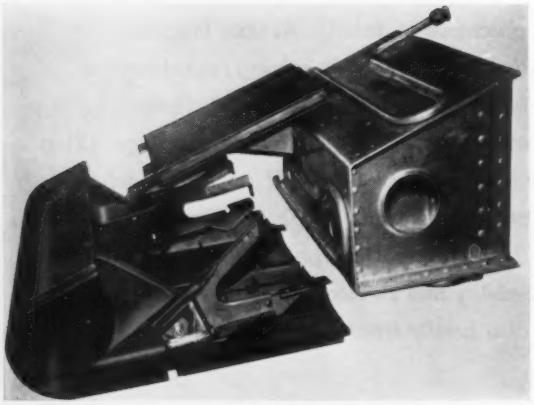

Fig. 1. Graphite leading-edge assembly.

Leading-Edge Design

Frank M. Anthony, AIAS • Andrew L. Mistretta

Bell Aerosystems Company

THE LEADING EDGE of a hypersonic glider is subjected to extreme operating environments. Design of such a structural component requires the consideration of many variables of flight performance requirements, vehicle geometry, material characteristics, and component geometry. The major design problem is to provide a leading edge which will resist the thermal and aerodynamic loadings imposed and will not oxidize despite high operating temperatures.

The many aspects of leading-edge design have been under study at Bell Aerosystems Company for a number of years. Most recently much of this effort has been supported by Materials Central and the Flight Dynamics Laboratory of Wright Air Development Division. It is not possible here to discuss leading-edge design in even a general manner. Approximately 2,000 pages are devoted to the subject in the final report of the Air Force contract.

This paper will discuss the graphite leading edge (Fig. 1) as a structural component designed for a specific application, and the philosophy and methods of analysis used to ensure structural usefulness despite the brittleness of the construction material. The approach should be useful for other materials and other design problems.

Statement of Design Problem

The graphite leading edge was designed for a hypothetical glider of global range flying from east to west at the equator. At the end of the 5-min boost phase the maximum component temperature is about 2,000°F. This increases slowly to 3,000°F after 70 min, then decreases gradually to about ambient at landing after a total elapsed time of about 2 hours.

During the flight, the aerodynamic heating intensity varies considerably, by a factor of 25, from the stagnation point to the upper rear corner. Large chordwise temperature gradients and high thermal stresses result.

External airloadings are very low during the high-temperature portion of flight, but, just before landing, maneuvers are required. Maximum external loadings on the graphite component designed for this program resulted from a pull-up at subsonic speed where temperatures are low.

Basically these brief statements define the structural design conditions. Since we are concerned with structural design, it is the low-temperature, high-load condition which we shall discuss.

Description of the Graphite Leading Edge

After extensive studies of the many variables involved, the graphite leading edge (Fig. 1) was produced. Fig. 2 shows the component prior to coating. The diameter of 5.0 in. was determined by vehicle performance requirements and the maximum allowable temperature of 3,000°F. Lower surface length, 6.50 in., was established so that the support structure would not exceed 2,000°F, thereby permitting the use of conventional superalloys. Length of the upper chord, 4.10 in., was established on the basis of thermal stress minimization. Wall thickness of 3/8 in. was dictated by fabrication considerations. Based upon resistance to airload stresses on the shell, a segment length of 16 in. was established. In Fig. 2, note the relatively large size

This work was supported by the USAF under Contract No. AF33(616)-6034, monitored by Materials Central and the Flight Dynamics Lab., WADD, Wright-Patterson AFB, Ohio. This sponsorship is gratefully acknowledged.

With Brittle Materials

A rational design philosophy and analysis procedure were established to produce the leading edge of a hypersonic glider from graphite • The philosophy and methods can also form the basis for designing other types of ceramic components.

of the attachments dictated by the design philosophy and analysis methods to be discussed. The design approach applies to the leading-edge shell and the attachments. However, attachment design involves more of a structural problem and the following is restricted to this aspect.

Design Philosophy

The most important ingredient of a design philosophy for brittle materials is believed to be the recognition of the absence of yielding. When the stress at any point in a brittle component, no matter how localized, reaches the limit of material capability, fracture will result. In recognition of this fact, the design philosophy formulated at Bell consists of the following five concepts (Fig. 3):

(1) Nonredundant attachments permit the determination of loads at these points, whether the loads are due to externally applied pressures or relative deformations between the leading edge and the wing. If *all* loads are known, the part can be designed with confidence.

(2) Brittle structures cannot be pulled into position during assembly. Any misfit which introduces high local stress could cause failure. Hence, this situation must be avoided.

(3) Proper account must be taken of all stress risers due to section changes, discontinuities, locally applied loadings, etc. Normal analysis of ductile structures under static loadings neglects stress concentration effects because they are reduced to insignificance by microscopic plastic flow. For brittle materials this relief is essentially absent. Stresses are *not* relieved by localized straining.

(4) At some point the refractory nonmetallic component must be joined to a metallic structure. Since the nonmetal part is used to withstand extreme temperatures, the joint would be made at a more reasonable temperature, say 2,000°F, where superalloys could be used. Thermal expansion differences could be quite large. If, however, the projections of all mating metallic and nonmetallic surfaces intersect at a single point, there will be no changes in the fit of the two parts resulting from differential thermal expansion. This design rule is based on the fact that, (*Continued on page 44*)

Mr. Anthony received a B.S. in aeronautical engineering from M.I.T. in 1949, and has attended graduate courses in heat transfer at the University of Buffalo. His 12 years of experience are divided between helicopters and hypersonic vehicles. While with the Bell Helicopter Division, he served as Group Leader, Analytical and Blade Design Group. His work on hypersonic vehicles has emphasized insulated and cooled structures and leading-edge systems, both heat resistant and cooled. Mr. Anthony has contributed to the structural aspect of various weapon system studies including Dyna-Soar. For $2^1/_2$ years he was Project Engineer on Contract AF33(616)-6034, the study outlined here. As Chief, Airframe Development, Vehicle Structures, Aerospace Engineering Dept., he is responsible for development of leading edges, nose caps, structural cooling systems, and thermal protection systems.

Mr. Mistretta received a B.S. in mechanical engineering from the University of Buffalo in 1951 and has also attended graduate courses there. He has 10 years' experience in structural design, analysis, and testing. For the last 4 years, his experience has been in the field of elevated temperature structures using refractory metals and nonmetals. He contributed to the development of a molybdenum leading edge and a graphite leading edge with temperature capabilities to 3,000°F. This work was performed on Contract AF33(616)-6034, a study of the utilization of available refractory metals and nonmetals for hypersonic glider leading edges. At present, he is Structures Engineer, Airframe Development, Vehicle Structures, in the Aerospace Engineering Dept.

One-Shot Mission Success at Minimum Cost

W. E. Cox, AFIAS • W. W. Harter

Northrop Corporation, Norair Division

DEFINING A ONE-SHOT MISSION as a mission for which one successful shot is all that is desired, and letting P be the acceptable probability of obtaining this one successful shot, we may regard the cost of the mission project as the sum of three principal costs: (1) project basic development cost, (2) cost of any reliability improvement program undertaken, and (3) cost of fabricating and launching a sufficient number of vehicles to result in the probability P that at least one shot will be successful.

Determination of a minimum total cost requires a capability of estimating each of these three cost contributions. Since the number of vehicles required is dependent upon the vehicle reliability resulting from the reliability improvement program, it is necessary, in particular, to be able to estimate the cost of the vehicle reliability improvement program required to obtain a given vehicle reliability.

A survey of flight-test development histories of some half-dozen missiles has shown that, when reduced to a common standard of complexity, environment, and duration of flight, the reliability growths of the missiles against calendar time have been approximately the same. Since these missiles were developed under similar philosophies, it appears that this similarity of growth with calendar time confirms that the growth has been, and is, dependent on the accumulated reliability improvement effort.

Although the costs of these improvement efforts have not been determined for all of the missiles surveyed, the reliability improvement costs for one of the more complex missiles are known. Presuming that the improvement effort costs per unit complexity for this missile are representative of those of other missiles, a curve (Fig. 1) may be constructed showing "standard" reliability $\bar{p}$, obtained as a function of improvement dollars spent $\bar{c}$, per unit com-

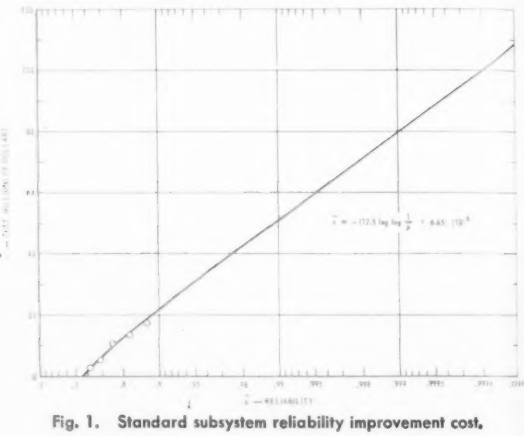

Fig. 1. Standard subsystem reliability improvement cost.

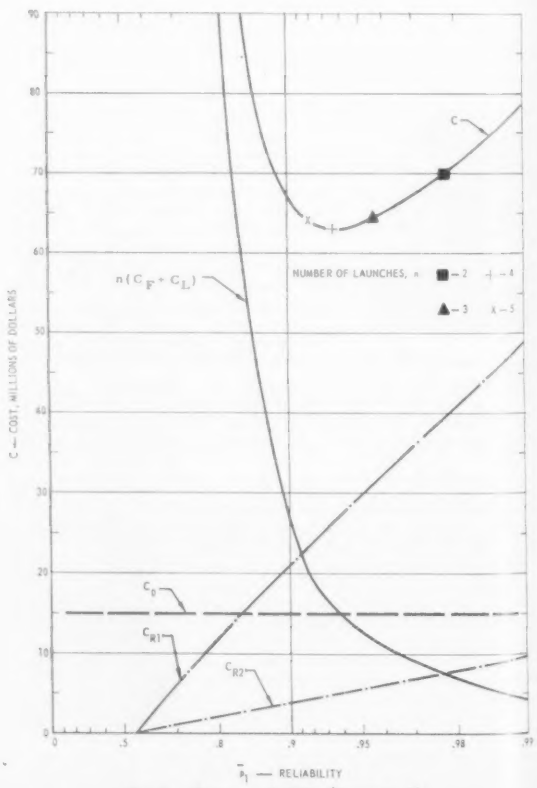

Fig. 2. Cost vs. reliability (Example 1).

"It is possible to define the scope of the reliability improvement program and the on-board redundancy criteria that will result in obtaining a specified probability for success of at least one shot at minimum cost. This paper develops mathematical models for the solution of this optimization problem and presents examples illustrating the application of this model to planning for a one-shot mission success."

plexity. More explicitly, $\bar{p}$ is defined as the probability of successful operation of a subsystem of standard complexity for 10 hours in a standard environment, and $\bar{c}$ is the cost in dollars of the effort resulting in this reliability. Standard complexity has been chosen as the complexity of a subsystem equivalent to 10,000 film resistors in series; standard environment has been chosen as average postboost phase environment. Fig. 1 provides a plot of the "best fit" analytical expression for $\bar{c}$ vs. $\bar{p}$, the data points upon which it is based, and an extrapolation of the curve to higher values of $\bar{c}$ and $\bar{p}$. The complexity of any designed subsystem may be obtained from a parts count of the subsystem and tables of relative complexity of parts, which are fairly well standardized throughout the industry; the complexities of a subsystem not yet designed can be estimated by relative comparisons with complexities of existing subsystems of the same type.

It should be noted that the curve of Fig. 1 is applicable only to subsystems of relatively high complexity. Reliability improvement effort has consisted mostly of the search for possible modes of failure and controls to limit their chance of occurrence; the experienced improvement vs. cost curve of Fig. 1 is, therefore, applicable only when the subsystem is sufficiently complex to contain a number of failure modes sufficiently large to make the law of averages applicable.

With this curve available, it is possible to define the scope of the reliability improvement program and the on-board redundancy criteria that will result in obtaining a specified probability for success of at least one shot at minimum cost. This paper develops mathematical models for the solution of this optimization problem, and presents examples illustrating the application of this model to planning for a one-shot mission success.

Mathematical Model

If an experiment requires P probability for success of at least one shot, the total cost C of the experiment may be expressed

$$C = C_E + C_R \qquad (1)$$

where $C_E \equiv$ cost of fabricating, launching, and supporting the flight of the number of vehicles required to provide probability P for success of at least one shot, and $C_R \equiv$ cost of the reliability improvement program undertaken. (*Continued on page 53*)

Dr. Cox received his B.S. and M.S. degrees from Tulane University and his Ph.D. (1940) in mathematics from Ohio State University. He was Assistant Professor of mathematics at Mississippi State University, and during World War II was in the Army Air Force assigned to the Dynamics Branch, Aircraft Lab., Wright Field. Since 1946 he has been with Northrop (Norair Division), and was Supervisor of the Dynamics Branch until 1956. At present, he is Chief of the Reliability Group which he has headed since its organization in 1956. He is a past member of the NACA Subcommittee on Vibration and Flutter and an IAS Associate Fellow.

Mr. Harter is Supervisor of the Systems Reliability Branch, Norair Division. He received his B.S. degree (1942) and M.S. degree (1947), both in aeronautical engineering, from the California Institute of Technology. With Northrop since 1942 for all but two years, his experience has been in the fields of structural analysis, aerothermodynamics, dynamic loads and vibration analysis, reliability analysis, and reliability program planning for aerospace systems. Mr. Harter joined the Norair Reliability Group in 1956, and has headed the Systems Reliability Branch since its formation in 1957.

Comments on

Aerodynamic Drag of Ground Effect Machines

Shigenori Ando • Jun-ichi Miyashita

Kawasaki Aircraft Co., Ltd.

MANY PAPERS have recently been published concerning possibility of various types of ground effect machines as transport vehicles. Although air curtain (peripheral jet) type has been studied more thoroughly than other types of GEM, nature of the drag still seems to be questionable. For examples, the authors can cite two data concerning drag breakdown of air curtain GEM, presented by Kuhn and Carter[1] and Nixon and Sweeney.[2] These data show that the parasite drag becomes seemingly negative, at least at a lower speed range. H. R. Chaplin[3, 4] made considerable contributions to the field of GEM. However, he paid no attention to the significant character of parasite drag in his theoretical studies of GEM performance.[3, 4] The authors designate reduction of parasite drag "interference thrust," and propose that it must be taken into account on estimating GEM performance because of its large amount. Investigation of mechanism of the interference thrust may be useful to improve GEM performance or to find superior types of GEM.

Mr. Ando was graduated from Kyoto University in 1952. He served in the Kubota Iron Works Co., Ltd., on the cast iron pipe research staff from 1952 to 1956, until he joined Kawasaki Aircraft Co. (Gifu) where, since 1957, he has been on the aerodynamics research staff. At present, his main interest lies in the fields of magneto-aerodynamics and ground effect machines.

Mr. Miyashita, a graduate of Tokyo University, has been an aeronautical engineer at Kawasaki Aircraft Co. (Gifu) since 1959. His special field of interest covers ground effect machines and jet flaps.

(1) Concept of Rotation Loss

It is well known that, sufficiently rearward of any body, flow pattern contains the two kinds of flow—simply retarded (or advanced) flow, and rotational flows whose axes are parallel to the free-stream direction.

Rotational flow causes "rotation loss," and one can consider the following examples:

(1) Trailing vortex induced by a finite span wing.

(2) Separation vortex at leading edge of a delta wing.

(3) Rotational flow in a propeller slipstream.

(4) Trailing vortex induced by the flow ejected from a GEM or ram wing.

The last example (4) is a key point in the present paper. The above examples suggest that once any part of a fluid curls up, all the rotational energy dissipates to heat energy and does not contribute to the propulsive force.

The concept of rotation loss is convenient, particularly in the case where one cannot know what mechanism causes the trailing vortices.

(2) Similarity Between Ram Wing, Plenum Chamber GEM, and Peripheral Jet GEM

First, let us consider a flow pattern around a ram wing (Fig. 1). The "internal" flow is ejected from the both sides and the trailing edge. Wind-tunnel testing showed that one trailing vortex starts at each

A qualitative theory is presented on the aerodynamic drag of GEM's. Several possible methods, effective for canceling a major part of the momentum drag, are suggested on the basis of the flow pattern model around a vehicle.

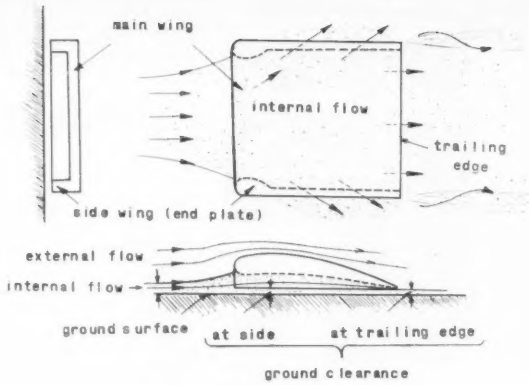

Fig. 1. Airflow around a ram wing.

Symbols

D = total drag of GEM with internal flow
D_{mom} = momentum drag
D_p = drag of GEM without internal flow
D_p' = fictitious parasite drag of GEM without internal flow
$D_{p,p}$ = parasite drag of GEM with internal flow
m = mass flow rate of internal flow
$P_{t\infty}$ = total pressure of free stream (gage)
P_{tj} = total pressure of jet (gage)
S_b = area of base surface of GEM
T_{int} = interference thrust
T_j = jet thrust at nozzle exit
T_j' = fictitious jet thrust
T_s = propulsive thrust produced by separate engine
V_∞ = velocity of free stream
V_c = characteristic velocity
V_j = jet velocity at nozzle exit
V_j' = fictitious velocity reached by ejected air, $\sqrt{2P_{tj}/\rho}$
W = total weight of vehicle
α = longitudinal attitude angle (radian) of GEM, positive when front part of GEM is up

wing tip. When the flight altitude is very large relative to the wing span, then the drag due to the trailing vortices is reasonably termed "induced drag"—the drag can be interpreted "aft-tilt of lift vector" due to downwash. However, when the clearance between the lower extremity of side wings and ground surface is very small, the authors may hesitate to term the vortex drag "induced drag" for the following reasons:

(1) The vortex-generating mechanism is very similar to the one in a plenum chamber GEM.

(2) Curling up of the flow discharged under the side wings may be caused partly by the negative pressure over the upper wing surface like a conventional wing, but caused partly through flow separation from the outer surface of the side wings.

(3) Trailing vortices are more strongly localized at the wing tips than for a conventional wing—the situation is rather similar to tip clearance loss of ducted propeller.

(4) Downwash due to finite span is much less in the ram wing than in the conventional wing, because of proximity to the ground surface.

It may be difficult and improper to calculate the vortex drag by integrating pressure change induced by the vortex over the surface. Instead, the vortex drag should rather be estimated by calculating directly the rotational energy of the fluid, in the whole space, added by the vortex per unit flight distance. The latter method, of course, would be carried out semiempirically.

Second, let us consider a plenum chamber GEM. Of particular interest and importance is the fact that the air ejected from the periphery (excluding some part of the front) may behave in a similar manner as in a ram wing. In fact, a plenum chamber GEM traveling at speed $V_\infty = \sqrt{2(W/\rho S_b)} = \sqrt{2}V_c$ can be regarded as a "modified" ram wing, because the power required for lift becomes very small owing to a ram effect. In the case of plenum chamber GEM, one also could observe a trailing vortex starting at each side which causes rotation loss and thus internal drag. According to today's custom, drag resulting from internal flow is termed "momentum drag" for a plenum chamber GEM and "induced drag" for a ram wing.* It is noteworthy, however, that drag generating mechanism is very similar for the both cases. (*Continued on page 79*)

* Recently Chaplin treated the internal drag of a ram wing as a momentum drag.[8]

Adventures in Engineering

Finding Rare Documents

Pearl I. Young, MIAS

Miss Young has been associated with aeronautics since graduating from the University of North Dakota in physics and reporting for duty at the NACA laboratory at Langley Field in 1922. She divides her time between technical writing and editing, and teaching physics to college engineering and physics students. Having just completed a definitive biography of Octave Chanute (for whom the IAS awards are named), Miss Young is teaching physics at Fresno State College this academic year, thus permitting a professor to have a year's leave.

WHEN AN ENGINEER overhears people talking of a "rare" document, he sidles away pretty fast because he is sure they are wasting work time discussing their latest find in some musty old bookstore. He should snuggle up a little closer and find out where to locate rare new documents in engineering—pamphlets, periodicals, or books.

For many rare items are not chronologically old. But the engineer has never seen them and suddenly up they pop in ever so many footnotes and references. They may be rare because they were published in a source or by a publisher never tapped by *Engineering Index* or *Science Abstracts*.

The best thing he can do, rather than spend fruitless hours in an aimless way, is to appeal to the better nature of a library hound; one with an intuitive feeling for sources and the memory of an elephant. It may be necessary to bet the hound a dollar he cannot locate the item, and a second buck that he can't buy a copy.

The writer's biggest adventure in locating rare documents came in 1958 when departing for Europe on a private research hunt for material ending at 1910. A distraught librarian deposited two slips of paper in my hand with the request that a few minutes be spent in New York and London to locate the items and to determine how to buy them for aeronautical engineers hastily being retreaded into space scientists.

En route to New York, I looked at the two slips. The requests seemed very simple. One called for a group of articles on celestial navigation in *Navigation;* the other, for a book on "The Upper Atmosphere." Both were recent. Grand Central Station is so close to the New York Public Library that walking is convenient. Experience prompted an immediate visit to Science and Technology. The librarian never hesitated. She just reached behind her on the shelf, handed over a few copies of *Navigation* and suggested the writer work on that item while she looked up the book.

It seemed that one didn't subscribe to *Navigation* but joined a society and this periodical came along. I wrote it all down on a slip of paper and put it in an envelope and left it open for the book information. This, however, was another story. "The Upper Atmosphere" was written by a professor in Calcutta and, although they could supply the publisher's name, they doubted if the book could be found nearer than London.

The letter mailed, back with the passport went the augmented book slip. Locating a rare engineering item is easy in London only if you know Frank Smith—librarian at the Royal Aeronautical Society and author of "On the Shelf" in the weekly, *Engineering*. So the book slip eventually got dumped on top of the clutter on Frank's desk. Such telephoning, such waiting for calls, such digging through source books, such delaying of luncheon, cannot be detailed. But, finally, two new slips of paper were in my possession, each with a bookshop proprietor's name and address—both back of the British Museum, both importers of Asian books. So hopping on the bus with a map, I dismounted where the conductor said was the proper stop, and walked to store No. 1. There was a lock on the door, and a note suggesting "Come get me at other store," which was No. 2. But No. 1 was correct, according to the proprietor, as we walked back. He had sold out his few copies of "Upper Atmosphere" very rapidly, but did have an invoice for the reorders. "They are likely in the Suez Canal," he said, and it struck me they were coming by boat. All that was needed was to pay the whopping price for the book and leave an American name and address and the second commission was completed.

Any adventure with a successful outcome is surely a worthwhile adventure.

Propellant Specific Impulse & Density

(Continued from page 13)

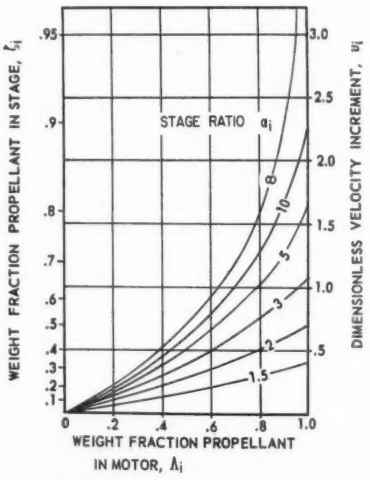
WEIGHT FRACTION PROPELLANT IN STAGE, ζ_i
DIMENSIONLESS VELOCITY INCREMENT, v_i
STAGE RATIO α_i
WEIGHT FRACTION PROPELLANT IN MOTOR, Λ_i

Fig. 3. Relationships among rocket design parameters.

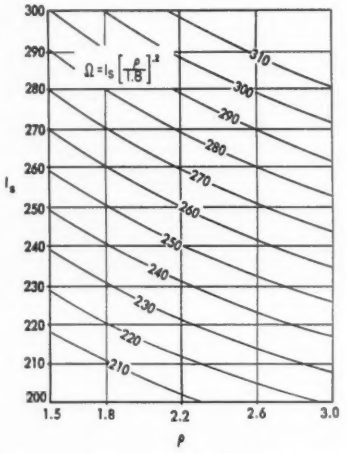

Fig. 4. Effective specific impulse as function of I_s and ρ ($K_i = 0.2$).

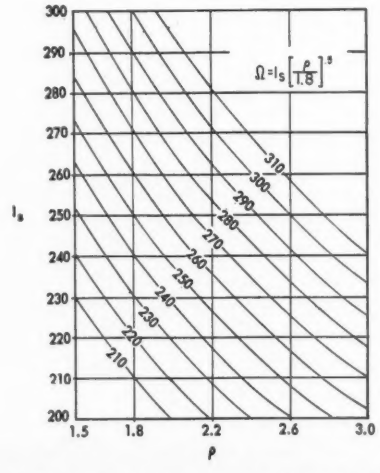

Fig. 5. Effective specific impulse as function of I_s and ρ ($K_i = 0.5$).

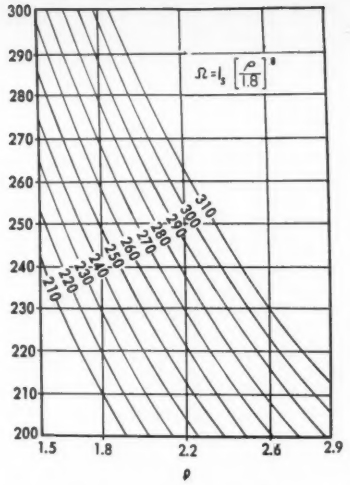

Fig. 6. Effective specific impulse as function of I_s and ρ ($K_i = 0.8$).

and the velocity increment v_i. Note that, because of the effect of propellant weight changes on the mass ratios of all previous stages, K_{i+1} is always less than K_i, but the K_i always converge to a finite value for K_∞. The values of K_∞ and the rate of convergence are functions primarily of the motor propellant fraction Λ_i and the stage ratio α_i. The summary at the end of this paper gives the relationships among Λ_i, α_i, ρ_i, and v_i, and Fig. 3 is helpful in visualizing these relationships.

Noting that for most real vehicles K_i takes values from about 0.2 to 0.8, Figs. 4, 5, and 6 present values of Ω as a function of I_s and ρ based on an arbitrary value of $\rho_0 = 1.8\ \mathrm{g} \times \mathrm{cm}^{-3}$.

Summary of Basic Relationships for Multistage Vehicle Performance

$$\Lambda_i = M_p^{(i)}/[M_p^{(i)} + M_e^{(i)}]$$

$$\zeta_i = \frac{M_p^{(i)}}{M_p^{(i)} + M_e^{(i)} + M_0^{(i+1)}} = \Lambda_i \frac{\alpha_i - 1}{\alpha_i}$$

$$\alpha_i = M_0^{(i)}/M_0^{(i+1)}$$

$$v_i = (V_b + gt)/c = \ln 1/(1 - \zeta_i)$$

References

[1] Geckler, R. D., *Ideal Performance of Multistage Rockets*, J. ARS, pp. 531–536, June 1960.

[2] Leonard, A. S., *Some Possibilities for Rocket Propellants, Part III*, Jet Propulsion, No. 72, p. 13, June 1947.

Notice

Readers desiring information on English language translations of Soviet technical literature published in the U.S.—in addition to data published in AEROSPACE ENGINEERING, Vol. 20, No. 7, p. 42—may request it from the National Science Foundation or U.S. Department of Commerce, Office of Technical Services.

Corrugated Core Sandwich Panels

(Continued from page 15)

although completely satisfactory solutions had not been found for the less rigorous applications, these later problems added the environmental rigors of elevated temperatures. The all-metal sandwich has been investigated for possible applications using many of the metals that have favorable properties at elevated temperatures. Titanium alloys, steels, refractory metals, and the so-called "super" alloys have been of interest. Methods of fastening faces to cores by means of brazing, resistance welding, and high-temperature adhesives have been investigated, to mention a few. Most of these methods have required the use of specially developed tooling, and none of them allowed for forming without development of costly tooling. Also, the service temperatures are limited in the case of brazed and adhesive bonded systems to temperatures well below those permitted for the higher temperature alloys.

The principal advantages of the roll-welded sandwich described here are lowest cost of any known all-metal sandwich, service temperature limited only by properties of parent metal (no adhesive or brazing alloy), producibility on existing rolling mill equipment with size limited only by width of mill, formability on existing equipment (e.g., Hydropress, power roll, etc.), and ease of providing edge members and inserts for concentrated loads.

Panels are made by first laying up the faces and core in a "picture frame" yoke with "matrix" bars shaped to fit the core corrugations laid in place. Solid inserts and shaped edge members can be inserted at this time. Cover sheets are placed over the entire assembly which is then sealed for protection at the elevated rolling temperature. Figs. 2 and 3 show, respectively, a schematic representation of the lay-up and the actual operation of laying up a pack. The entire pack is then heated and rolled parallel to the corrugations to a predetermined reduction of thickness. This hot-rolling process produces

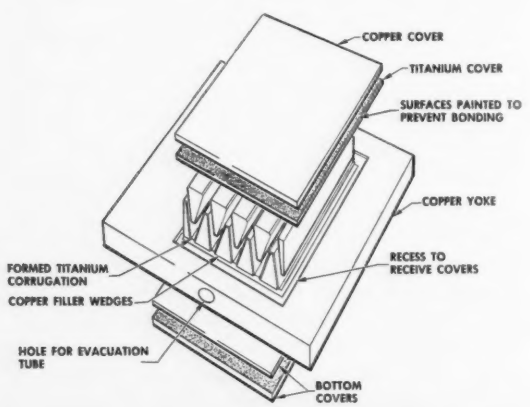

Fig. 2. Elements of the sandwich pack.

a pressure-welded assembly in which the very thin faces and core of the sandwich are joined together while the matrix material supports the thin gages to prevent buckling and wrinkling. Some of the processing parameters which must be predetermined in order to achieve successful welds include selection of suitable matrix material which can be removed by preferential leaching or other means and which has rolling characteristics and physical properties compatible with the material chosen for the sandwich; choice of rolling temperature, amount of reduction, and number of passes to accomplish the reduction; and preprocessing surface treatment for contact surfaces. Another factor which influences the choice of matrix material is the effect on workability and formability of the panel after welding.

The pressure welding accomplished by the hot-

Fig. 3. Assembling elements of core.

rolling process produces joints in which the diffusion across the interface is complete. Photomicrographs (Fig. 4) indicate that the diffusion across the joint is so complete that it is difficult to locate the interface after welding except for the alclad 2014 aluminum alloy, in which the welding takes place in the alclad layers. In general, proper control of the combination of surface preparation, rolling temperature, and amount of reduction results in welds in which the joints cannot be distinguished from the parent structures. Reductions of 60 to 80 percent have been used for the panels fabricated to date.

After rolling, the panels are formed to desired shape. Pilot studies have produced single and double contoured parts (Fig. 5).

Upon completion of all forming operations, the matrix material is removed. Up to the present, this has been accomplished merely by soaking the part in a tank of nitric acid solution until the matrix material is dissolved.

Development work is continuing at both Battelle and Douglas. Studies are under way to extend the

system to other metals and combinations of metals, and surface treatments and the interplay of amounts of reduction and rolling temperatures with weld quality are being investigated. Also, studies of more readily removable matrix systems are in progress. One which holds considerable promise involves the use of a matrix bar that has a hole running its entire length. This hole is filled with a low-melting-point metal. The ends of the matrix bar are sealed so that the low-melting-temperature material will not run out during the panel rolling operation. After the panel has been rolled, the ends of the matrix bars will be opened and the low-temperature material melted out. Then the leaching solution will be able to attack large areas of matrix material simultaneously, thereby greatly reducing the time for the leaching operation. Interestingly enough, it has already been determined in forming studies that much sharper radii can be formed if holes are drilled along the axes of the matrix bars prior to forming. Thus it appears that there might be a double payoff in the use of a hollow matrix bar. Current development work is concerned mainly with forming techniques and methods for reclaiming leaching reagents and dissolved matrix material (mostly copper in the work to date).

Despite the continuing development effort, it is felt that the process is ready for "hardware" application. The reason for this attitude lies in the fact that fabrication and forming of a large, "usable" size panel has already been demonstrated—development work will merely extend the range of application of the system and allow for further cost-savings.

Cost analysis of a sample 3-ft by 6-ft cylinder made

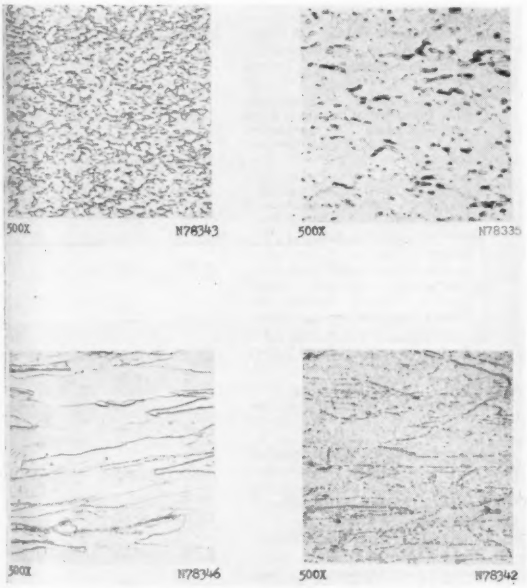

Fig. 4. Photomicrographs of bonds of two-layer sandwiches of various materials. (*Top left:* Ti-6Al-4V alloy rolled at 1,550°F; *top right:* A-110AT titanium rolled at 1,550°F. *Bottom left:* Unalloyed molybdenum rolled at 1,800°F; *bottom right:* René 41 rolled at 1,800°F.)

SENIOR RESEARCH STAFF POSITIONS for expanding DEPARTMENT OF MECHANICAL SCIENCES

A long range program of expansion and growth has opened up challenging and rewarding research positions in these areas:

DYNAMICS

for work in the field of dynamics and stability and control, ranging from hydrofoil boats to large rocket booster systems.

FLUID DYNAMICS and HEAT TRANSFER

for theoretical and experimental studies in hydrodynamics for application in astronautics and naval engineering, and in new problem areas in heat transfer.

Ph.D. applicants preferred; however, careful consideration will be given if you have a B.S. or M.S. plus experience. Salaries for these positions will be top bracket for those outstanding engineers and scientists who meet our requirements.

Picturesque San Antonio enjoys a year round healthful climate. You will like the casual outdoor living of the Alamo City. Southwest Research Institute is an independent research and development organization located on a 1500-acre campus eight miles west of downtown. Our well equipped laboratories provide the scientific climate conducive to creativity and individual accomplishment.

Please send resume and salary requirements to:

R. C. Mays, Director of Personnel

SOUTHWEST RESEARCH INSTITUTE

8500 Culebra Road
San Antonio 6, Texas

All qualified applicants will receive consideration for employment without regard to race, creed, color or national origin.

Fig. 5. Eight-in.-radius partial dome formed from 15-in. sq. pilot panel of A-55 titanium (copper matrix removed).

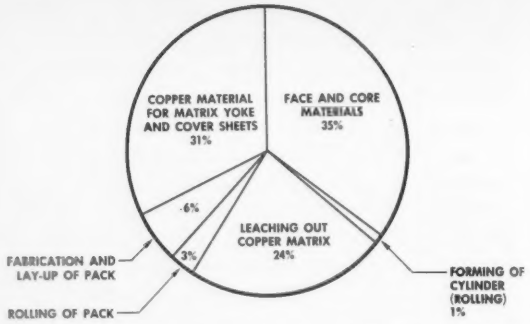
COPPER MATERIAL FOR MATRIX YOKE AND COVER SHEETS 31%
FACE AND CORE MATERIALS 35%
6%
LEACHING OUT COPPER MATRIX 24%
3%
FABRICATION AND LAY-UP OF PACK
ROLLING OF PACK
FORMING OF CYLINDER (ROLLING) 1%

Fig. 6. Cost breakdown for roll-welded sandwich cylinder (6Al-4V titanium sandwich cylinder, 3 ft diameter by 6 ft length).

of all-titanium, corrugated-core sandwich shows that the system yields parts at less than half the cost of the nearest known competitive process. This cost advantage results even when the crude, albeit successful, matrix removal methods reported here are applied and all reagent and dissolved matrix material are assumed to be discarded. The pie chart (Fig. 6) shows the relative size of the cost components in a cylinder to be made of 6A1-4V titanium alloy. As demonstrated in this chart, 55 percent of the cylinder cost goes for the matrix material and the leaching operation. Thus, it is seen that any success in improving the matrix removal process or reclaiming either matrix material or leaching chemicals would have an excellent chance of being reflected in additional cost advantage for this system. No mention is made at this time of further implied capitalization cost advantages which follow from the utilization of existing equipment for rolling and forming the panels.

✦ ✦ ✦

SHERMAN M. FAIRCHILD PUBLICATION FUND PAPERS

No.		Member	Nonmem.
FF-29	Design Principles for a General Control Computer—R. Alonso and J. H. Laning, Jr.	$3.00	$6.00
FF-28	Elementary Mechanics of Turbulent Fluid Motion—Max M. Munk	2.00	4.00
FF-27	A Magnetic Support for Floated Inertial Instruments—P. J. Gilinson, Jr., W. G. Denhard, and R. H. Frazier	2.00	4.00
FF-26	2nd Supersonic Transport Proceedings—L. J. Line, D. J. Maglieri, H. H. Hubbard, J. B. Pearson, Jr., R. J. Pfeiffer, B. C. Monesmith, R. A. Bailey, and R. H. Miller.	1.50	3.00
FF-23	A Matrix Approach to Flutter Analysis—William P. Rodden.	0.75	1.50
FF-22	Methods of Boundary-Layer Control for Postponing and Alleviating Buffeting and Other Effects of Shock-Induced Separation—H. H. Pearcey and C. M. Stuart.	1.50	3.00
FF-18	On the Main Spray Generated by Planing Surfaces—Daniel Savitsky and John P. Breslin.	0.75	1.25
FF-17	Atomic Reactors (a Symposium).	1.25	1.75
FF-14	Engineering Management Philosophies (a Symposium).	0.50	1.00
FF-12	Transonic Testing Techniques (a Symposium).	1.85	2.50
FF-10	Improved Solutions of the Faulkner and Skan Boundary-Layer Equation—A. M. O. Smith.	0.75	1.25
FF-7	Natural Flight and Related Aeronautics—James L. G. Fitz Patrick.	2.65	3.50

No.		Member	Nonmem.
FF-4	Finite Deflections of Curved Sandwich Plates and Sandwich Cylinders—F. K. Teichmann and Chi-Teh Wang.	$0.50	$0.85
FF-3	The Penetration of a Fluid Surface by a Wedge—Experimental Towing Tank, Stevens Inst. of Tech.	1.20	1.60
286	Linearized Treatment of Supersonic Flow Through Axi-Symmetric Ducts with Prescribed Wall Contours—Charles E. Mack, Jr., and Ignace I. Kolodner.	0.75	1.25
229	Wave Profile of a Vee-Planing Surface, Including Test Data on a 30° Dead-Rise Surface—Experimental Towing Tank, Stevens Inst. of Tech.	1.20	1.60
170	Wave Contours in the Wake of a 10° Deadrise Planing Surface—Exp. Towing Tank, Stevens Inst. of Tech.	1.20	1.60
168	Wave Contours in the Wake of a 20° Deadrise Planing Surface—Exp. Towing Tank, Stevens Inst. Tech.	1.20	1.60
167	On the Pressure Distribution for a Wedge Penetrating a Fluid Surface—Experimental Towing Tank, Stevens Inst. of Tech.	0.75	1.00
106	Measurement of Ambient Air Temperature in Flight—W. Lavern Howland.	0.35	0.50
104	Tensor Analysis of Aircraft Structural Vibration—Charles E. Mack, Jr.	1.85	2.50
102	Electrical Resistance Strain Gages Applied to Wind-Tunnel Balances—Elmer C. Lundquist.	0.60	0.80
101	Introduction to Shock Wave Theory—J. G. Coffin.	2.65	3.50
100	Blade Pitching Moments of a Two-Bladed Rotor—R. W. Allen.	0.75	1.00

Order by number from: Special Publications Dept., IAS, 2 E. 64th St., New York 21, N.Y.

Magnetic Particle Clutch

(Continued from page 19)

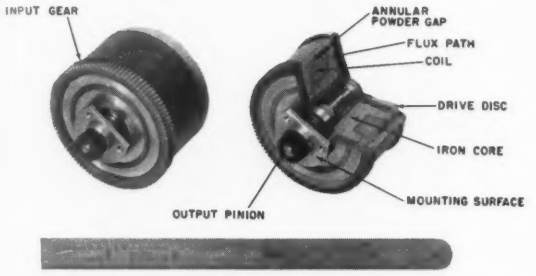

Fig. 3. Drive-disc type of magnetic particle clutch, rotating coil.

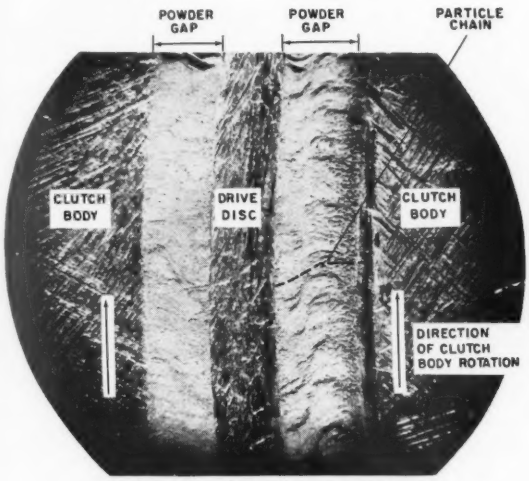

Fig. 4. Action of particles in magnetic gap.

clutch is the product of the shear force and the drive disc radius.

The characteristics of the shear surfaces occurring between particle layers are similar to the action of a fluid between two moving cylinders—that is, there appears to be no relative motion between the particles and the surfaces at the drive disc and clutch housing boundaries. Shearing action takes place between adjacent particle layers, and thereby gives the magnetic particle clutch the properties of a friction clutch, while overcoming any limitations due to wear on the fixed surfaces. Fig. 4 is a photograph showing the action of the magnetic particles in the powder gap. The powder is a dry medium, and therefore the coefficient of kinetic friction is essentially independent of the shearing velocity, resulting in the clutch torque being independent of slip speed.

High torque-to-inertia ratios are achieved since the large inertia members (prime mover and clutch core structures) are continuously rotating and only the low inertia clutch drive disc must be accelerated to achieve output motion. Power gains of 3,000:1 are attainable since only a few milliamps of control current are required for full torque output.

The equation that mathematically defines the torque transmitted by the clutch is

$$T = 5.59 \times 10^{+8}[fK_qR/A]\phi^2 \qquad (1)$$

where

T = torque transmitted by clutch, in-lb
f = coefficient of kinetic friction between the powder particles (nominal value = 0.26)
A = cross-sectional area of powder gap normal to flux, sq in.
K_q = ratio of actual area occupied by particles to available area normal to flux path (nominal value = 0.80). (K_q approaches unity for a finely divided powder of sufficient quantity to fill effectively working portion of gap.)
ϕ = total flux through powder gap, webers
R = radius to clutch shear surface, in.

The total flux ϕ developed around the flux path, as a result of the signal current I, is given by

$$\phi = NI/(R_g + \Sigma R_i) \qquad \text{(webers)} \qquad (2)$$

where

N = number of turns
I = current, amp
R_g = effective reluctance of gap and powder combination, 1/henries
ΣR_i = summation of reluctance values around iron path exclusive of gap, 1/henries

Since the permeability of the iron is much greater than that of the gap,

$$R_g \gg \Sigma R_i \qquad (3)$$

and for a gap with parallel surfaces,

$$R_g = 39.37\ (L_g/\mu_g\ A) \qquad \text{(1/henries)} \qquad (4)$$

where L_g = length of gap, in., and μ_g = permeability of powder gap, henries/meter.

Therefore, the flux ϕ may be determined as

$$\phi \cong \mu_g\ NIA/39.37\ L_g \qquad \text{(webers)} \qquad (5)$$

From Eqs. (1) and (5) it is seen that, if the permeability of the magnetic particle gap were constant

AERO/THERMODYNAMICIST

Ph.D.

Immediate research position available for senior aerodynamicist with specific experience and interest in the following areas: Hypersonic Boundary Layer Theory, Separated Flows, Chemical Kinetics, Non-Equilibrium Hypersonic Flows.

This position offers exceptional opportunity for personal and professional advancement.

Please address inquiries to

Mr. D. L. Smelser

ELECTRO-OPTICAL SYSTEMS, INC.
125 North Vinedo Avenue, Pasadena, California

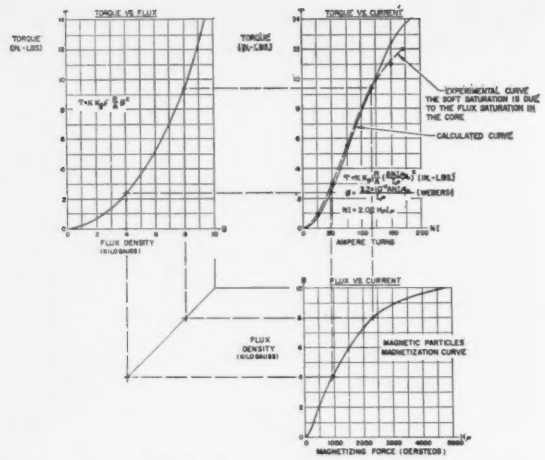

Fig. 5. Calculated and experimental torque vs. current curve.

over the range of excitation, the torque of the clutch would be proportional to the current squared. An experimental curve and a calculated curve are shown in Fig. 5. The linearizing effect of the powder is clearly evident. There remain two regions of nonlinearity, one near null and the other as the clutch becomes magnetically saturated.

Use of a pair of biased contrarotating clutches directly removes the nonlinearity about null, thereby resulting in zero dead space and linear operation through the null region. The amount of quiescent current required is determined by the intersection of the extended linear portion of the torque current curve and the current abscissa. The bias currents also preload each gear of the parallel gear train in the same direction as its power transmission, and thereby effectively eliminate the backlash under all conditions of powder transmission and null. If the torque saturation is objectionable, a derated clutch must be used to guarantee linear operation.

The torque output of the magnetic particle clutch is proportional only to the input control current and is independent of the slip speed (Fig. 6). The "zero damping" characteristic makes the clutch an ideal component for either the Type II proportional or the on-off type of control in missile systems where rapid response is desired. The clutch (Fig. 6) can operate continuously at any point under the 5-watt maximum rating shown. Because of the manner in which the torque is conveyed by the particle mechanism and because of the processing techniques used in particle manufacturing, exceptionally long life and service without adjustments are given by the magnetic particle clutch. The ability of a clutch to yield a constant torque for a given current after many hours of use is called "torque stability." A typical torque stability curve is shown in Fig. 7.

The clutch dynamic transfer function can become quite complex for certain design types; the most complex is required for the large nonlaminated versions. The complexity is a result of the hysteresis and eddy current losses and the dynamic lag between the magnetic flux and torque. The transfer function that describes the current to flux characteristics of the larger nonlaminated versions was developed by Blackburn[2] and is given by

$$\frac{\phi(s)}{I(s)} = \left[\frac{\dfrac{C}{R_c + R_o}}{1 - \dfrac{\Delta R(s)}{R_c + R_o}}\right]\left[\frac{\phi(0)}{u(0)}\right]\left[\frac{\tanh\sqrt{L^2\, s/k}}{\sqrt{L^2\, s/k}}\right] \tag{6}$$

where

$\phi(s)$ = total flux
$I(s)$ = signal current
C = a constant of proportionality
R_c = core reluctance
R_o = air gap reluctance
ΔR = frequency-sensitive component of reluctance
s = Laplace variable
$\frac{\phi(0)}{u(0)}$ = static gain of total flux vs. flux density at boundary
k = ratio of resistivity to permeability
L = plate thickness

Because of the clutch inductance, there is also a lag between the voltage applied and the current.

$$\frac{I(s)}{E(s)} = \frac{\dfrac{1}{R_s + R_e}}{(\tau_e\, s + 1)} \tag{7}$$

where

$I(s)$ = signal current, amp
$E(s)$ = source output voltage (unloaded), volt
R_e = clutch coil resistance, ohm
R_s = source resistance, ohm
τ_e = clutch electrical time constant
$\tau_e = L_c/(R_e + R_s)$, sec
L_c = clutch inductance, henries

In the general case, the magnetic particle clutch may be defined from torque output to voltage input by the product of the transfer functions given in Eqs. (6) and (7) and using Eq. (1) to determine the

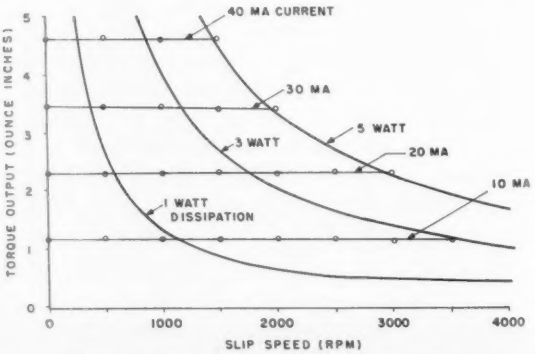

Fig. 6. Torque speed and power dissipation curves.

AIRCRAFT ENGINEERS

THIS is an Invitation

. . . to join us here where there is a future for you second to none. Here our projects include Giant C-141 jet transports . . . Intercontinental C-130 turbo-prop transports . . . JetStar passenger craft . . . "Hummingbird" type VTOL aircraft . . . Missiles . . . Rockets . . . Nuclear Products . . . Nuclear Research . . . Avionics Research . . . Operations Research . . . Cryogenics Research . . . and scores more interesting long-range projects.

Openings in the fields of: Aircraft Design Engineering • Engineering Drawings Checking • Aircraft Structures • Basic Loads • Flutter and Vibration • Sound and Vibration • Aircraft Specifications Engineering • Reliability Engineering • Operations Research • Aircraft Research Engineering.

Write to: Hugh L. Gordon, Professional Employment Manager, Lockheed-Georgia Co., 834 W. Peachtree St., Atlanta 8, Georgia. Dept. DD-77.

All qualified applicants will receive consideration for employment without regard to race, creed, color or national origin.

THE ENGINEERING CENTER
LOCKHEED-GEORGIA COMPANY
A DIVISION OF LOCKHEED AIRCRAFT CORPORATION

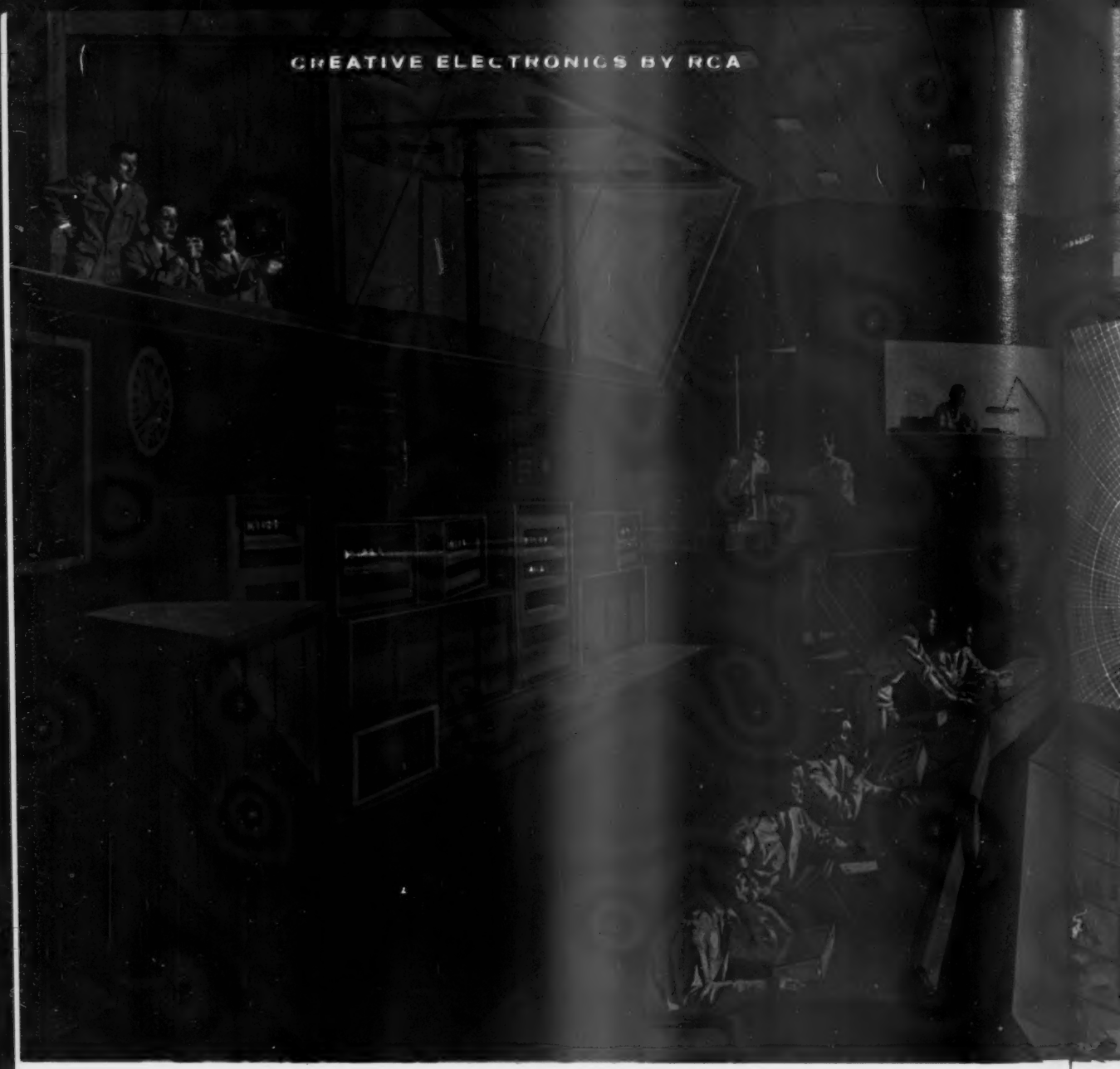

NORAD ON THE ALERT

Inputs from BMEWS Provide Instantaneous Missile Data Direct to NORAD Headquarter

From our vast outer defense perimeter, over thousands of miles, to the nerve center of the North American Air Defense Command at Colorado Springs, the most advanced concept of data handling and checkout is being utilized in the BMEWS system. The stakes are high, for the purpose is defense of the North American Continent.

At BMEWS installations operated by USAF Air Defense Command, computers read out missile tracking data from giant radars. This information is simultaneously relayed to NORAD's Combat Operations Center.

The Radio Corporation of America is prime systems contractor for BMEWS. At the COC, RCA's Display Informatio Processor computing equipment automatically evaluates missi sightings, launch sites and target areas. By means of data pro essing and projection equipment installed by RCA and a team other electronics manufacturers, the findings are displayed huge, two-story high map-screens in coded color symbols, pr viding the NORAD battle staff with an electronic panora of the North American and Eurasian land masses.

The handling of BMEWS inputs at NORAD is an example how RCA data processing capabilities are assuring the high d gree of reliability so vital to continental defense.

NORAD Headquarters, RCA computing equipment, the Display Information Processor (control console shown here) receives sightings data from BMEWS and processes it for automatic readout.

RCA is prime system contractor for the sprawling BMEWS three-site radar network whose probing electronic fingers reach deep into space to provide early warning of missile attacks.

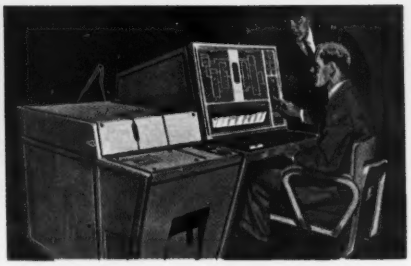

RCA's Automatic Checkout & Monitoring equipment continuously tests and checks performance of portions of the system and alerts an operator when a monitored signal exceeds certain limits.

...t of the defense needs of today a new generation of RCA electronic data ...cessing equipments has been born. For tomorrow's needs RCA offers one of ...e nation's foremost capabilities in research, design, development and produc... ...on of data processing equipment for space and missile projects. For information ...n these and other new RCA scientific developments, write Dept. 434, **Defense ...ectronic Products,** Radio Corporation of America, Camden, N. J.

RCA®

The Most **Trusted** Name in Electronics

RADIO CORPORATION OF AMERICA

ENGINEERS:

THE NEXT 2.15 MINUTES COULD CHANGE YOUR ENTIRE

FUTURE!

If you are an experienced engineer with the desire to participate in challenging research assignments and programs of New Product Development, the 2.15 minutes it takes you to read this could mean a lifetime of professional advancement and satisfaction for you. If you are "lost in the crowd" in your present position and have very little opportunity to freely express your ideas and theories, you'll like the way we work at Boeing/Wichita. • At present our engineers are advancing the state of the art in Variable Sweep Wing technology, conducting studies and tests in the operation of high-performance aircraft at low level, design of land- and carrier-based V/STOL vehicles, and are conducting studies in the areas of Fire Control, Bombing, Navigation, Guidance and Reconnaissance and Surveillance systems. If you feel your background and experience qualify you to make a contribution in any of the following areas, we want to talk with you.

ELECTRICAL-ELECTRONIC-PHYSICS-MATH

1. Equipment Design
2. Fire Control Systems
3. Servo-Mechanisms
4. Computer Technology
5. Systems Analysis
6. Applied Physics
7. Reliability
8. Instrumentation Design

AERONAUTICAL-MECHANICAL-CIVIL

1. Propulsion Systems
2. Stress Analysis
3. Flight Controls
4. Structural Dynamics
5. Mechanical Controls
6. Stability & Control Analysis
7. Weight Control
8. Reliability

To save time send us a complete resume today. You'll get an immediate reply. Or fill in the coupon below and we will send you an application. Send your resume or coupon to Mr. Melvin Vobach, The Boeing Company, Wichita Division, Wichita 1, Kansas.

BOEING WICHITA

An Equal Opportunity Employer

Please send information about Boeing/Wichita and your "Opportunities Brochure OAN."

Name_____

Address_____

City_____ **State**_____

Degree(s)_____ **Years Experience**_____ **Areas of Interest**_____

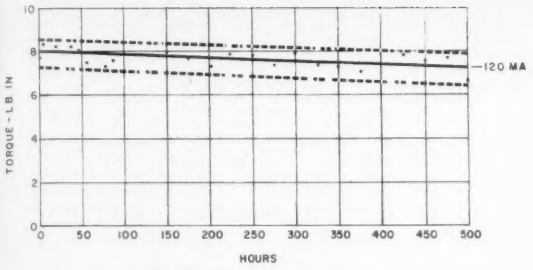

Fig. 7. Torque stability curve.

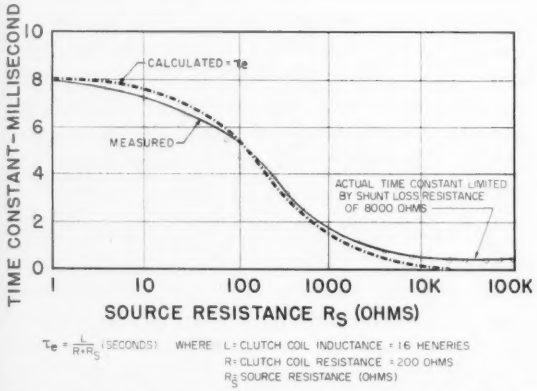
TIME CONSTANT - MILLISECOND
CALCULATED = Te
MEASURED
ACTUAL TIME CONSTANT LIMITED BY SHUNT LOSS RESISTANCE OF 8000 OHMS
SOURCE RESISTANCE Rs (OHMS)
Te = L/(R+Rs) (SECONDS) WHERE L = CLUTCH COIL INDUCTANCE = 16 HENERIES
R = CLUTCH COIL RESISTANCE = 200 OHMS
Rs = SOURCE RESISTANCE (OHMS)

Fig. 8. Effect of source resistance on clutch electrical time constant.

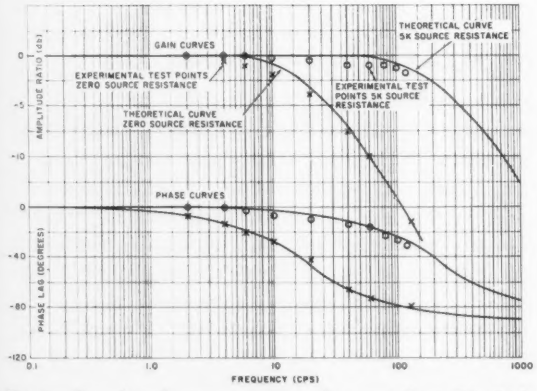

Fig. 9. Open-loop frequency response of a magnetic particle clutch.

constant relating flux to torque. Fig. 8 shows the electrical time constant τ_e as a function of the source resistance. The voltage to current relationship is seen to be quite linear, and the time constant can be made about as small as desired by using a high source resistance.

The closed-loop stability of a system containing the current to flux relationship, Eq. (6), can be determined from a Bode plot, and the closed-loop frequency response may be obtained through the use of a Nichols diagram. Methods are also available for using root locus representation.

The current to flux relationship, Eq. (6), essentially approaches a constant term for laminated core construction and/or small clutch configurations. For a laminated core, the resistivity becomes much greater than the permeability, resulting in large values of the ratio k in Eq. (6), and the eddy current function approaches unity. In addition, the core reluctance R_c becomes large compared to both R_o and $\Delta R(s)$; therefore, the flux becomes related to the current by essentially a constant. Fig. 9 illustrates the frequency response and linearity attainable with the laminated and/or small magnetic particle clutch. The only lag is essentially that associated with the electrical time constant τ_e.

A somewhat less accurate but more useful form of the transfer function of Eq. (6) can be obtained. The first term in brackets can be adequately defined by a simple lag-lead transfer function. Blackburn has shown that the meromorphic function can be approximated by choosing a sufficient number of pole-zero pairs (series expansion of the third term in brackets). The transfer function to use in preliminary design employing the larger nonlaminated type would then have the form

$$\frac{T(s)}{I(s)} = K_c \left[\frac{Z_o s + 1}{P_o s + 1}\right]\left[\frac{(Z_1 s + 1)(Z_2 s + 1)}{(P_1 s + 1)(P_2 s + 1)}\right] \quad (8)$$

where K_c = clutch torque gain, in-lb/amp.

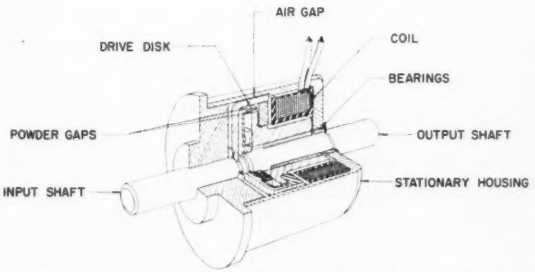

Fig. 10. Drive-disc type of magnetic particle clutch, stationary coil.

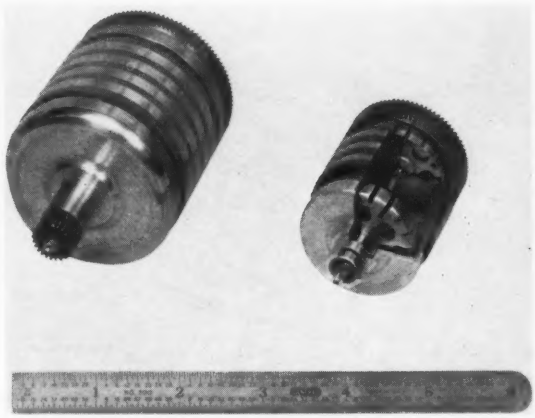

Fig. 11. Coaxial type of magnetic particle clutch.

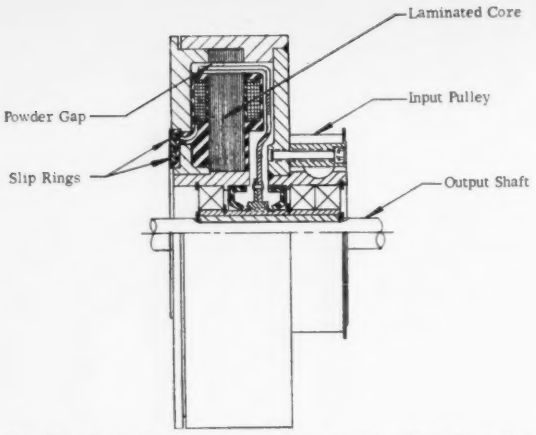

Fig. 12. Drive-disc type of magnetic particle clutch, laminated.

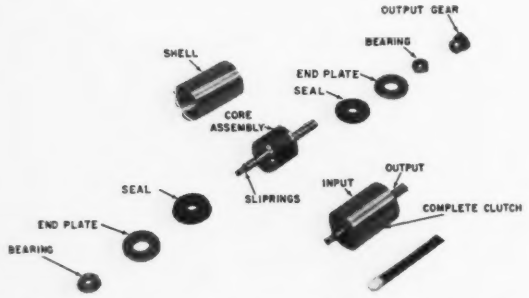

Fig. 13. Barrel-type magnetic particle clutch, rotating coil.

Clutch Configurations

The introduction of clutches into various sizes and shapes of mechanical actuators has yielded a diversified line of clutch types and configurations:

(A) Drive-disc type (low inertia output)
  (1) Rotating coil
  (2) Stationary coil
  (3) Coaxial clutches
  (4) Laminated iron core

(B) Barrel type
  (1) Rotating coil
  (2) Stationary coil
  (3) Laminated iron core

The most popular type has proved to be the rotating-coil drive-disc clutch (Fig. 3). Extreme smoothness and high power gains are typical characteristics. The stationary-coil type (Fig. 10) is easier to install, but requires higher excitation power because of the reluctance of an additional air gap. Hysteresis reduction due to the extra air gap is an advantage. Coaxial (two-in-one) clutches (Fig. 11) are solutions to difficult packaging problems. A common iron path allows a weight-saving over the use of two single clutches. Clutches of the laminated drive-disc type (Fig. 12) appear to be the only answer for large high-performance applications where both a small time constant and a high torque-to-inertia ratio are demanded.

The barrel clutch has also had widespread usage. Little attempt is made to provide a low inertia output in the design. In general, the barrel clutch is simpler, having fewer parts than an equivalent drive-disc clutch. A clutch of the rotating-coil barrel type is shown in Fig. 13, the laminated version in Fig. 14, and a stationary-coil barrel clutch in Fig. 15. The same remarks made for the stationary-coil drive-disc clutch are applicable here also.

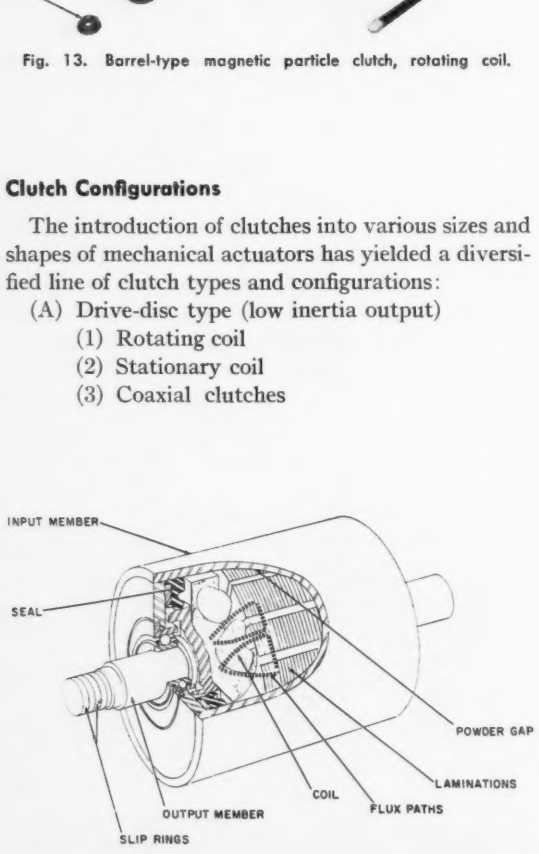

Fig. 14. Barrel-type magnetic particle clutch, laminated.

Typical Rocket System Applications

It is fortunate that the magnetic particle clutch servoactuator concept is equally well adapted to provide rapid response with either proportional or nonproportional control methods. The clutch actuator is desirable in the proportional concept because (1) zero dead space and zero backlash features are obtainable with two clutches operating in push pull, and (2) the torque output is a linear function of current and is completely independent of speed.

The clutch drive is also proving to be increasingly desirable in the more recently developed nonproportional modes of operation (Fig. 16). Nonproportional control usually requires that the actuator output be capable of switching between states. The clutch type of actuator is ideally suited for this operation since the prime mover runs continually in the same direction and only the clutch output switches state. The tristable and quinstable modes are considered to be of major importance because of the reduced power consumption for a given missile flight.

The magnetic powder clutch has a decided advantage over any type of spring or friction clutch in its capability of operating in the quinstable or even higher modes. This feature is possible since the control output level of the actuator is a function of only the input current. The only control requirement is

that different levels of command error switch corresponding levels of current into the clutch.

In comparison to a simple electric drive motor, the clutch type of actuator has two definite advantages:

(1) The clutch control power required is greatly reduced compared with the required motor power.

(2) The clutch actuator response is faster because only the low inertia of the clutch drive disc must be accelerated.

Example of Nonproportional Actuator

Fig. 17 illustrates the first typical missile application to be discussed. The requirement is for four identical interchangeable bistable servoactuators to be fitted around the rocket blast tube in order to control the position of each of the four control surfaces. The actuator housing is the structural member and provides full support for the control surface. Some of the physical characteristics are as follows:

Control power input	20 watts maximum
Weight	9 lbs
Output travel	±90 deg
Efficiency	50% at rated torque
Motor power input	1,440 watts maximum
Mechanical power output	450 watts maximum

The servoactuator consists of, basically, a unidirectional compound-wound d.c. motor driving a pair of contrarotating magnetic particle clutches. The output shafts of the clutches are coupled to the actuator output shaft through three stages of parallel spur gearing.

The actuator is, in itself, open loop and is part of the overall guidance loop that is closed through the missile aerodynamics. The actuator operates continually in a bistable mode, being full-on in either one direction or the other. Using the bistable control mode, the missile is subjected to a constant low-amplitude roll oscillation. This continually stresses the missile structure in roll, thereby providing stiffness in the longitudinal axis. The actuator driving source need not be a proportional amplifier but only an electronic switch. Still another advantage to bistable operation is that nearly full actuator torque is applied at all times and the output shaft is continuously in motion, thereby resulting in greater sensitivity since the friction and stiction characteristics become negligible. In this particular application, worm gearing was not required and, therefore, spur gearing was used for greater efficiency. A worm gear drive provides more complete load isolation, and may be incorporated into the magnetic clutch servoactuator when specifications require.

Lending itself directly to bistable operation, the clutch actuator combines the features of the low inertia output drive with the high inertia prime mover to obtain the fast response required for the modern rocket. On the one hand, the clutches provide a unique, rapid-reversal coupling device between the prime mover and the control surface, enabling the

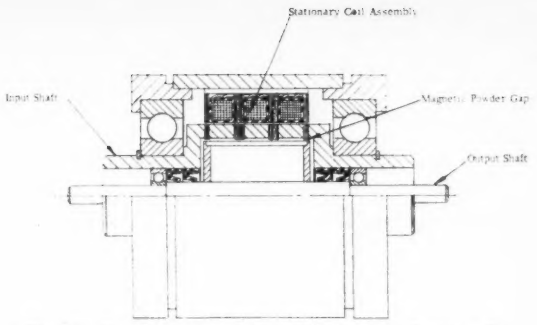

Fig. 15. Barrel-type magnetic particle clutch, stationary coil.

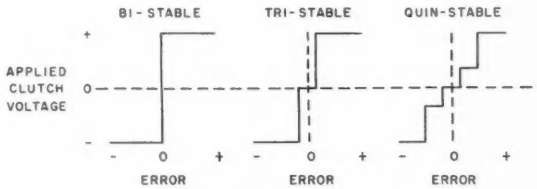

Fig. 16. Nonproportional modes of control.

missile control surface to obtain the desired rate or position in a minimal length of time. On the other hand, the prime mover provides the static torque-speed curve needed to accomplish a required power level with a minimal amount of overdesign. The high inertia of the prime mover and clutch housings provides a flywheel effect enabling the actuator to sustain high peak loads and also contribute to a low drift rate. If properly utilized, the flywheel effect can also reduce the power requirement of the motor and power supply.

Three actuator dynamic requirements typifying the performance specifications associated with bi-

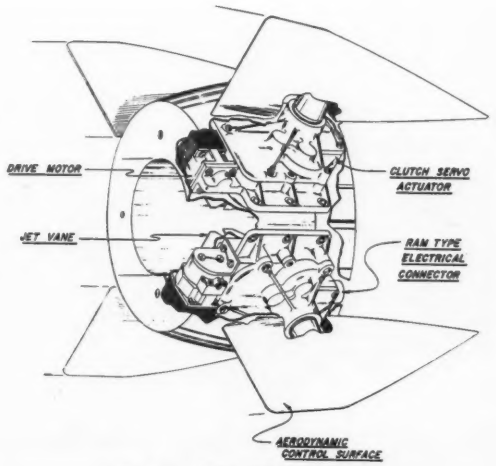

Fig. 17. Missile flight control servo.

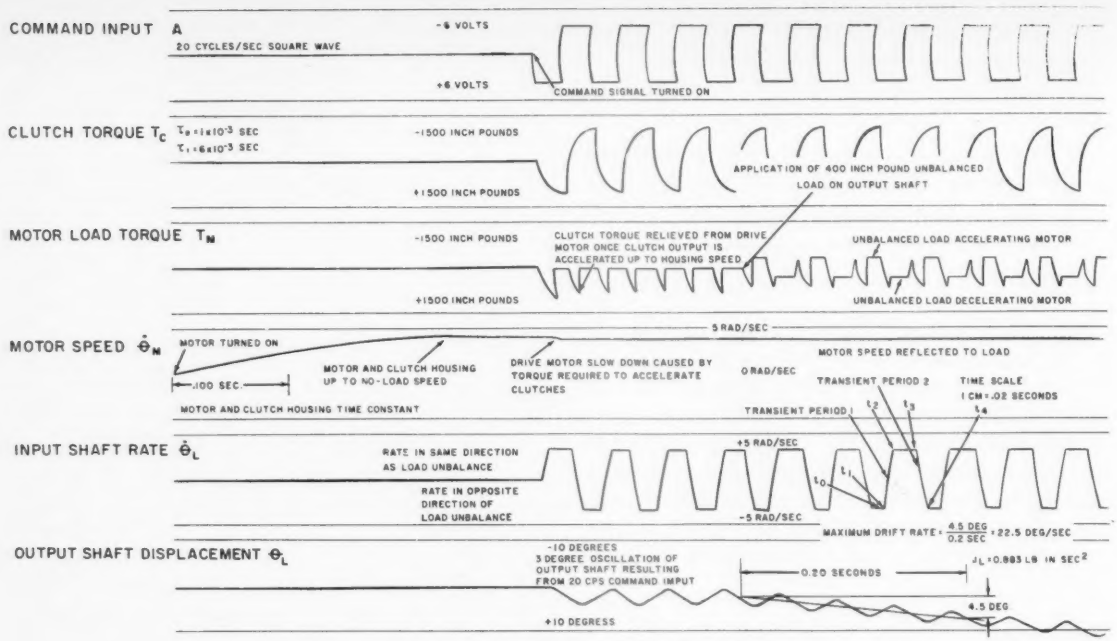
COMMAND INPUT A
20 CYCLES/SEC SQUARE WAVE
-6 VOLTS
+6 VOLTS
COMMAND SIGNAL TURNED ON
CLUTCH TORQUE T_C
τ_e = 1x10⁻³ SEC
τ_i = 6x10⁻³ SEC
-1500 INCH POUNDS
+1500 INCH POUNDS
APPLICATION OF 400 INCH POUND UNBALANCED LOAD ON OUTPUT SHAFT
MOTOR LOAD TORQUE T_M
-1500 INCH POUNDS
+1500 INCH POUNDS
CLUTCH TORQUE RELIEVED FROM DRIVE MOTOR ONCE CLUTCH OUTPUT IS ACCELERATED UP TO HOUSING SPEED
UNBALANCED LOAD ACCELERATING MOTOR
UNBALANCED LOAD DECELERATING MOTOR
MOTOR SPEED $\dot{\theta}_M$
5 RAD/SEC
MOTOR TURNED ON
.100 SEC.
MOTOR AND CLUTCH HOUSING UP TO NO-LOAD SPEED
DRIVE MOTOR SLOW DOWN CAUSED BY TORQUE REQUIRED TO ACCELERATE CLUTCHES
0 RAD/SEC
MOTOR SPEED REFLECTED TO LOAD
TRANSIENT PERIOD 2
TIME SCALE 1 CM = .02 SECONDS
MOTOR AND CLUTCH HOUSING TIME CONSTANT
TRANSIENT PERIOD 1
t_2
t_3
t_4
INPUT SHAFT RATE $\dot{\theta}_L$
RATE IN SAME DIRECTION AS LOAD UNBALANCE
RATE IN OPPOSITE DIRECTION OF LOAD UNBALANCE
+5 RAD/SEC
-5 RAD/SEC
t_0
t_1
MAXIMUM DRIFT RATE = $\frac{4.5 \text{ DEG}}{0.2 \text{ SEC}}$ = 22.5 DEG/SEC
OUTPUT SHAFT DISPLACEMENT θ_L
-10 DEGREES
3 DEGREE OSCILLATION OF OUTPUT SHAFT RESULTING FROM 20 CPS COMMAND IMPUT
0.20 SECONDS
J_L = 0.883 LB IN SEC²
4.5 DEG
+10 DEGRESS

Fig. 18. Bistable actuator drift characteristics.

stable operation are maximum drift rate, dead time to speed, and recovery time. The clutch servo is able to excel in each of the aforementioned figures of merit because of the combination of low inertia output and high inertia input.

Maximum drift rate: The drift rate of a bistable actuator is a measure of the actuator's ability to ignore a load disturbance. The rate is defined by the number of degrees the control surface will drift per second when the input is symmetrically switched while an unbalanced load is applied. The larger the drift rate, the more deviation in attitude the rocket will obtain, when an unbalanced aerodynamic load is applied, before the guidance loop can compensate.

The clutch actuator achieves a low drift rate by rapidly coupling the control surface to a relatively slow response prime mover thus effectively holding back the control surface. The primary consideration in determining drift rate is the fact that, when the control surface is accelerated up to the reflected motor speed, the output shaft can then further increase only if (1) the larger motor and clutch housing inertia is accelerated, or (2) the clutch torque is exceeded by the load so that the clutches are made to slip.

In one specific actuator, the unbalanced aerodynamic load specified is 4 times less than the available clutch torque, and the motor and clutch housing inertia is 40 times greater than the clutch output and load inertia. Therefore, since neither of the previously mentioned conditions can take place, the control surface is "locked" to the motor. To obtain a desired drift rate, the control surface must be made to accelerate rapidly to the reflected motor speed. This is accomplished by properly choosing the clutch time constant τ_e and the output torque-to-inertia ratio.

Fig. 18 shows the actuator response from motor start to insertion of a 20-cps input signal, and then application of a 400-in-lb unbalanced load. It is seen that the resulting drift rate is 22.5 deg/sec. It is also seen that the amount of drift is the same for each cycle. This drift rate can be reduced, if required, by use of a laminated clutch and/or a nonreversible worm and gear segment.

Mathematically, the drift rate may be calculated

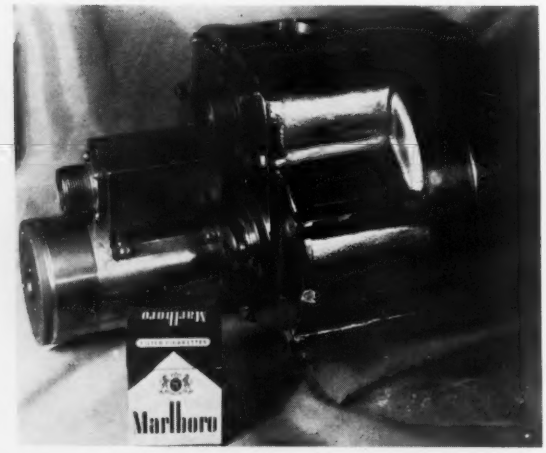

Fig. 19. Muscle-type clutch actuator.

by following closely the actuator's behavior for one complete cycle.

Dead time to speed: Another criterion of bistable actuator performance is the time required to reach a predetermined speed. This is a measure of the actuator's ability to respond rapidly to a command input. It is defined as the time it takes for a bistable actuator to reach 63.2 percent of the control surface rate when the input command is switched to one of the on-states.

Recovery time: A figure of merit with regard to the ability of a bistable drive to recover from a stall condition is its recovery time. With the clutch actuator design concept, the output shaft may be stalled by application of the maximum aerodynamic torque, causing the clutches to slip. The drive motor continues to run at a decreasing rate, depending upon its speed-torque curve. The actuator recovery time, once the stall torque is removed, depends upon clutch response, drive motor response, and length of time stall torque was applied.

Muscle-Type Actuator

A large missile vane control servo is shown in Fig. 19. The rugged construction is required to withstand the blast-off vibration and acceleration. This unit contains two drive-disc type clutches which are rated at 175 in-lbs. The actuator specifications and performance are tabulated here for reference.

Unit Specifications

Unit weight	48.8 lbs
Maximum output speed	17 rpm
Maximum output torque	16,000 in-lbs
Peak output power	1.36 hp
Rated load	1,400 in-lbs
Total travel	±27 deg
Duty cycle	5 min on, 25 min off, without cooling

Unit includes position feedback transducer, velocity transducer, and RIV filter.

Dynamic Performance

Bandwidth (with inertia load)	2.5 cps
Accuracy	0.04%
Stiffness under load torque	7,000 in-lbs/deg

With a larger motor, this unit could easily deliver 3 hp.

Examples of Proportional System With 250-cps Bandwidth

Fig. 20 shows the mechanism involved. The servo is required to position the slide in a satellite mechanism. This is accomplished by using a rack connected to the slide and two pinions connected to the counterrotating clutches, thereby achieving zero backlash. The clutches are driven continuously by the motor. The follow-up consists of a conductive plastic linear potentiometer connected directly to the output. The actuator uses two miniature barrel-type clutches as shown in Fig. 13. Some of the specification requirements are listed in Table 1.

Table 1. Miniature Clutch Servo Requirements

Specification	Requirement	Servo Capability
Maximum slide velocity	25 in./sec	30 in./sec
Maximum slide acceleration	100 in./sec²	1,130 in./sec²
Stroke of slide	±0.5 in.	±0.5 in.
System static positional accuracy (with 0.316-lb friction)	0.005 in.	0.0002 in.
System damping (equivalent to second order)	0.3 to 0.7	0.45 approx.
Servo must follow a ±0.010-in. amplitude input at 5 rad/sec smooth and with a phase lag less than	3 deg	0.6 deg
Bandwidth: Servo must have less than 90-deg phase lag at	80 cps	250 cps

Because the magnetic particle clutch torque output is independent of speed, the clutch is capable of producing a Type II servo. The clutch servo may be reduced, if desired, to a Type I by adding output rate damping. Type II servo theory shows the servo to have zero positional error with both static and constant velocity conditions. A constant positional error exists only during periods of constant acceleration. The Type II system was chosen because better accuracy and faster response are obtainable.

Fig. 21 shows a mathematical block diagram of the system. To obtain a Type II system, it is necessary for the total open-loop transfer function to contain a double-integration term ($1/s^2$). Considering a system with inertia load, clutches, amplifier, and follow-up (the system of Fig. 21 without the compensating block), the open-loop transfer function would be

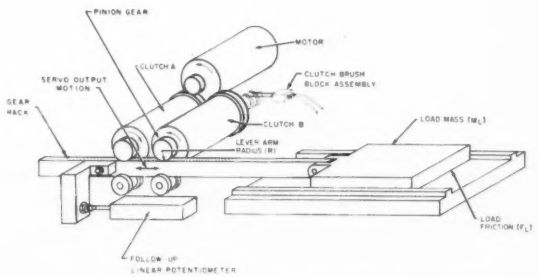

Fig. 20. Diagram of a clutch-type linear servoactuator.

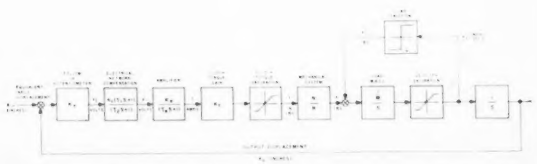

Fig. 21. Mathematical block diagram of a Type II clutch servo.

$$\frac{\text{Output}}{\text{Error}} = \frac{X_o(s)}{E(s)} = \frac{K_f K_a K_c\ [N/R]\ [1/M]}{s^2\ (\tau_e s + 1)} = \frac{K_F/M}{s^2(\tau_e s + 1)} \quad (9)$$

The closed-loop transfer function would then be

$$\frac{\text{Output}}{\text{Input}} = \frac{X_o(s)}{X_{in}(s)} = \frac{1}{[M\tau_e/K_F]\ s^3 + [M/K_F]\ s^2 + 1} \quad (10)$$

This indicates an absolutely unstable system (the coefficient of the s^{+1} term is zero) with zero damping. Damping may be introduced into the system in the form of either output or error rate. If output rate is used (such as velocity generator feedback), the open-loop transfer function has the form

$$\frac{X_o(s)}{E(s)} = \frac{K_V}{s(\tau_e \tau_g s^2 + \tau_g s + 1)} \quad (11)$$

The use of a velocity generator will stabilize a clutch system, but it is noted that the resultant system is Type I. The Type II capabilities may be maintained by using error rate rather than output rate damping. This may be accomplished by using a passive electronic lead network. The voltage output to voltage input transfer function for the network is

$$\frac{V_{out}(s)}{V_{in}(s)} = \frac{K_1(\tau_1 s + 1)}{(\tau_2 s + 1)} \quad (12)$$

where $\tau_2 < \tau_1$ and $K_1 = \tau_2/\tau_1$.

The open-loop transfer function of the complete servo then becomes

$$\frac{X_o(s)}{E(s)} = \frac{K_A(\tau_1 s + 1)}{s^2(\tau_e s + 1)\ (\tau_2 s + 1)} \quad (13)$$

where $K_A = K_F/M$ = servo acceleration constant, and $K_F = K_f K_1 K_a K_c\ [N/R]$ = servo force constant.

The closed-loop transfer function becomes

$$\frac{X_o(s)}{X_{in}(s)} = \frac{\tau_1 s + 1}{\left[\frac{\tau_e \tau_2}{K_A}\right] s^4 + \left[\frac{\tau_e + \tau_2}{K_A}\right] s^3 + \left[\frac{1}{K_A}\right] s^2 + \tau_1 s + 1} \quad (14)$$

Using Routh's test for stability, it is seen that the servo is stable with error rate damping, provided that

$$\tau_1\tau_e + \tau_1\tau_2 - K_A\ \tau_1^2\tau_2 > (\tau_e + \tau_2)^2 \quad (15)$$

The individual component parameter values were determined to satisfy the inequality shown in Eq.

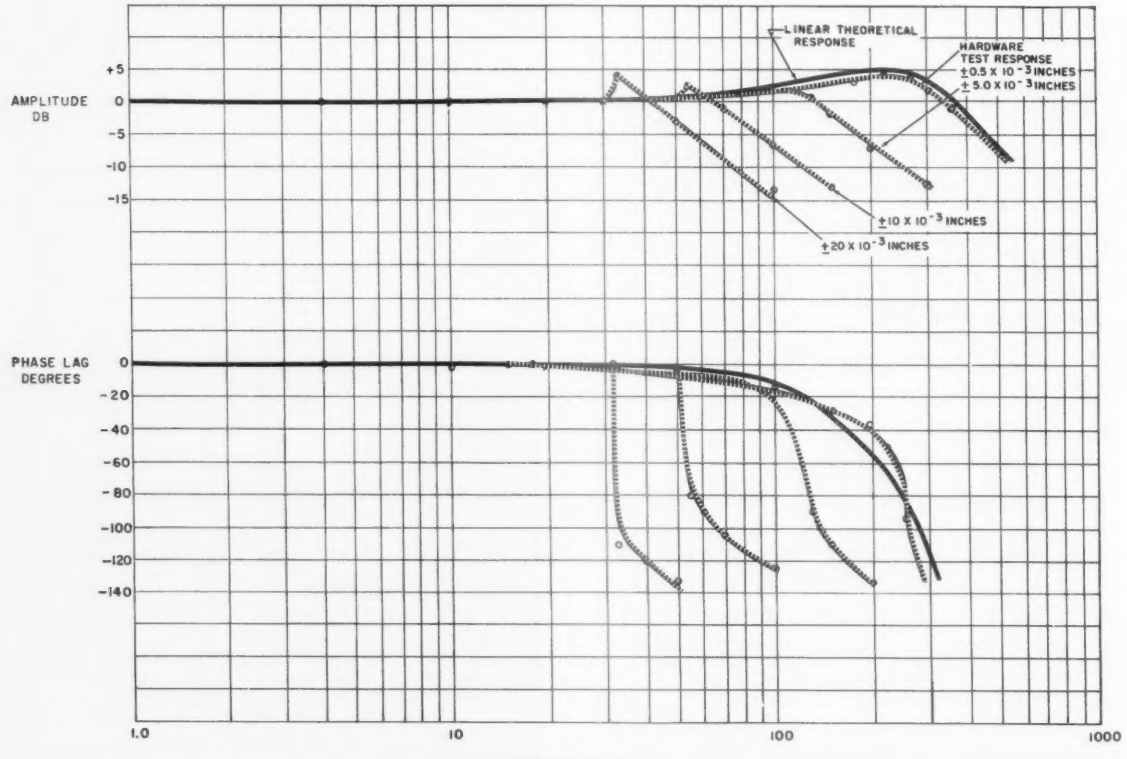

Fig. 22. Closed-loop frequency response of Type II clutch servo.

(15), as well as to provide adequate phase margin and damping.

Fig. 22 illustrates the frequency response obtainable with the clutch Type II actuator. The theoretical linear curve is shown, along with a small signal hardware test curve which closely follows the linear curve because the high force gain makes the friction essentially negligible. For large-amplitude inputs, there are two saturation characteristics that must be considered as shown in Fig. 21—torque saturation caused by magnetic flux saturation of the clutch core, and velocity saturation since the maximum speed of the clutch output is equal to the clutch housing speed.

The effect of torque saturation is seen in Fig. 22 with larger input amplitudes. The curves are typical of Type II systems since the torque saturation effectively lowers the force gain and thereby decreases the bandwidth and phase margin. The decrease in phase margin shows up in the increased resonant peaking and rapid phase fall-off. The response curves follow the linear results until saturation occurs. The effect of velocity saturation is not apparent from the frequency response plot because, for sinusoidal inputs, the acceleration limit is dominant. For step inputs, the velocity limit would yield a greater rise time for larger step amplitudes.

Clutch System Reliability and Shelf Life

Since production first started on the particle clutch type of servo, considerable reliability data have been accumulated. Most of the statistical data available are from the numerous aircraft employing the clutch servo.

An extensive survey of 2,800 autopilots disclosed a total of only 185 failures in approximately 478,000 hours of operation. Since each autopilot has three clutch servos, this gives a mean time to failure for the servos of 7,750 hours. Assuming a 2-hour average mission time, the reliability index is 0.9998. Additionally, a 6-month survey revealed that, of 1,800 servos in operation, only 17 required any servicing.

Another survey of 125 autopilots showed three servos (roll, pitch, and trim) to have an EMTBF of 3,300 hours, resulting in a reliability index of 0.9998. The pitch trim servo displayed an EMTBF of 30,000 hours with a 0.9999+ reliability index.

A third survey of 27 autopilots showed the roll, pitch, and yaw servos to have an EMTBF of 5,143 hours, resulting in a reliability index of 0.9996, while the pitch trim servo yielded an EMTBF of 25,718 hours and a reliability index of 0.9999+.

These three reliability surveys pointed out the high reliability obtainable with the clutch-type servos. Another form of reliability that is of special interest to missile engineers is shelf life. Shelf life of any unit is, of course, a debatable concept and may be measured only through actual field experience.

Various data corroborate the claim to "long shelf life" associated with clutch-type actuators. Tests were conducted on one servo which was stored for 5 years after it had completed 1,000 hours of service in an autopilot system. It was found that the slope (pound-inch/milliamp) of the torque current curve (clutch gain) had changed from 5.8 before use to 5.0 after 1,000 hours' service and was 4.7 after a 5-year storage period. In January 1958, three servos were removed from Government bond and submitted to various tests. These actuators were fabricated in the first half of 1951 and so were at least $6^1/_2$ years old at the time of the test. They were first submitted to production acceptance tests and all were close to the nominal, well within the allowable limits. Following the acceptance tests, all three were submitted to a life test, using the original qualification test cycle. One servo completed 268.75 hours, the second 345.5 hours, and the third 1,634 hours of life. Cause of failure of the first two units was gear failure due to lubricant breakdown, and the third unit was still operating satisfactorily when the test was terminated. From test data, Lear has concluded that the magnetic particle clutch servo can be logically expected to produce desired performance after at least 5 years of storage and to have adequate reserve life to provide typical missile operation reliably.

References

[1] Bepristis, A., *An Analytical Approach to the Design of Dry Powdered Clutches*, Lear, Inc., Engrg. Memo. Report No. 40, March 24, 1958.

[2] Blackburn, E. P., Jr., *A Mathematical Model for a Dry Powdered Magnetic Clutch*, M.S. thesis, Univ. of Calif., June 1960.

AN AUTHORIZED BINDING FOR

Aerospace Engineering

Arrangements have been made by the Institute of the Aerospace Sciences for members and subscribers to have their magazines bound carefully and economically. Simply write for details to:
Publishers' Authorized Bindery Service Ltd., 430 West Erie St., Chicago 10, Ill.

Brittle-Materials Leading-Edge Design

(Continued from page 21)

while the dimensions of a structural element change with temperature, all angles remain constant.

(5) Because of the brittleness of the material and the lack of yielding capability, the stress concentrations produced by material flaws precipitate material failure. (The term *material flaws* refers not to defective materials as such, but rather to those macroscopic or submicroscopic items—such as inclusions, voids, density variations, lattice defects, etc.—which cannot be detected by available inspection techniques and are an inherent characteristic of the particular material as produced by present technology.) Since the flaws are a random occurrence, the design allowable strength must be based upon a desired probability of survival under given loading conditions. The flaw concept appears to be most satisfactory in defining the structural performance of brittle materials—particularly, a Weibull statistical distribution function. The effect of the unknown flaws or stress concentrations within the material may be treated on a statistical basis as an effect on the allowable stress—that is, allowable strength values are chosen to ensure a prescribed probability of survival. This procedure requires that material strength properties be determined statistically by conducting tests of a large number of specimens for each experimental condition. Furthermore, since the presence of other than gross flaws cannot be detected by currently available inspection techniques, it is necessary to relate allowable stresses to a particular process control procedure in order to ensure similarity between the test bar and component material.

Fig. 4 illustrates the fifth concept of the design philosophy. We have a plot which essentially depicts the variability of various refractory nonmetals. The ordinate is a safety factor, the ratio of mean strength to the strength at a prescribed probability of survival. The abscissa is a material constant m, an index of the number of flaws, derived from fitting the Weibull distribution function to the experimentally determined data. Two survival rates are shown along with m values for various materials. Of the materials investigated at Bell, m values ranged from about 1.5 to 15, with the higher values representing the more reproducible materials. Mild steel at room temperature, which was not part of our evaluation, has an m of 58 and requires a safety factor of almost negligible magnitude, 1.1 to 1.2. If we take as examples the most variable and least variable materials investigated, we have

m	99%	99.99%
1.5	19	300
15	1.4	1.9

That is, for a material which has an m of 15, the mean strength must be divided by 1.4 to obtain an allowable strength at which the chance of fracture is only 1 in 100. With graphite, as used for the present leading edge, the m value is about 8, which requires that the mean strength be divided by 1.7 in order to give an allowable stress that will ensure that the chance of fracture is only 1 in 100.

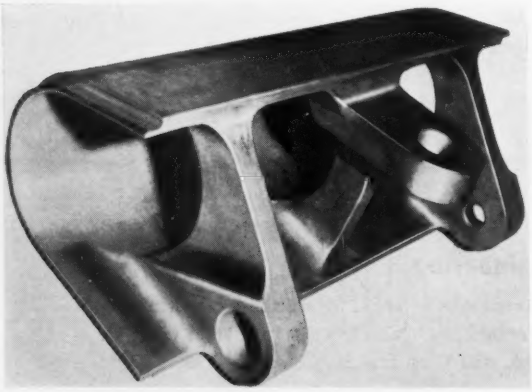

Fig. 2. Graphite leading edge prior to coating.

Method of Analysis

In discussing methods ot analysis for brittle materials, the factors which may influence the strength of such a component, for a material whose processing and inspection is well controlled, include stress state, size, strain rate, temperature, and—for some materials—atmospheric conditions.

If the material performs according to Weibull's statistical function, stress state and size effects may be predicted from analytical relationships. At the present time, however, it is desirable to define experimentally these and the other effects. The analysis of a component, then, requires consideration of these factors in addition to the inclusion of stress concentration effects. For a potentially critical cross section, stresses are found by standard analysis methods and multiplied by the stress concentration in that region. This maximum local stress is then compared with the design allowable strength, the mean strength as corrected for the following:

(1) Desired probability of survival.
(2) Type of stress at the cross section—bending, torsion, tension, compression.
(3) Size of the cross section.
(4) Rate of load application.
(5) Temperature at the cross section.
(6) Atmospheric conditions.

From this it is obvious that the problem in analyzing brittle structures is that of establishing the design allowable strength. Experimental evaluation programs must be designed to yield the required information.

During the extensive evaluation of the mechanical properties of siliconized ATJ graphite, the varia-

PROBLEM	SOLUTION
1. ATTACHMENT LOADS	NON-REDUNDANT ATTACHMENTS
2. TOLERANCES AND FITS	SELF-ALIGNING AND ADJUSTABLE SURFACES
3. STRESS CONCENTRATIONS	REFINED STRESS ANALYSIS
4. THERMAL EXPANSIONS	INTERSECTION OF MATING SURFACES
5. MATERIAL FLAWS	STATISTICALLY DETERMINED STRENGTH

Fig. 3. Design with brittle materials.

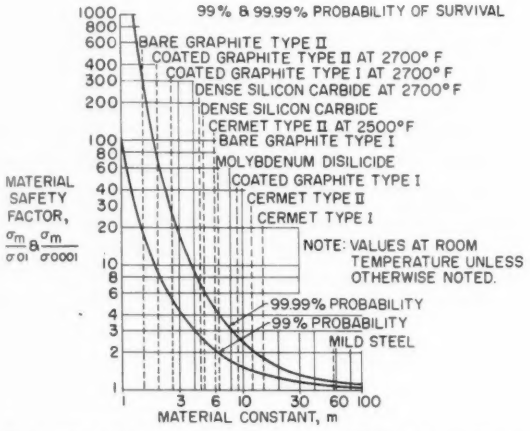

Fig. 4. Variation of material safety factor with material constant *m*.

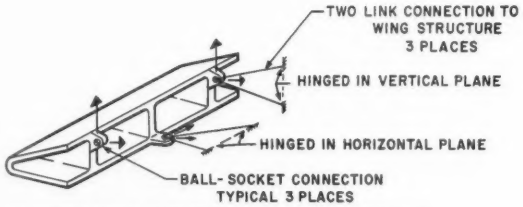
TWO LINK CONNECTION TO WING STRUCTURE 3 PLACES
HINGED IN VERTICAL PLANE
HINGED IN HORIZONTAL PLANE
BALL-SOCKET CONNECTION TYPICAL 3 PLACES

(a) THREE POINT ATTACHMENT FOR LARGE SEGMENTS

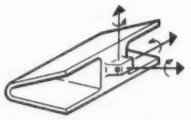

(b) SINGLE POINT ATTACHMENT FOR SMALL SEGMENTS

Fig. 5. Basic attachment schemes for leading-edge segments.

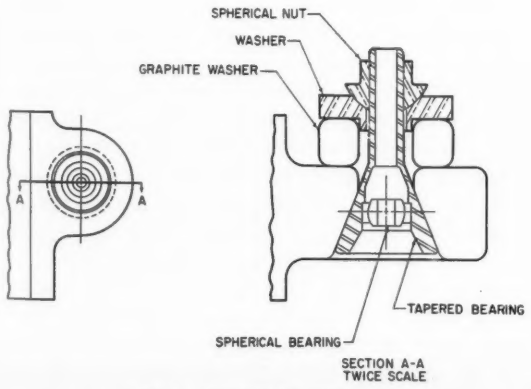

Fig. 6. Standard lug attachment.

bility of coating thickness on a single specimen resulted in the overshadowing of many of these effects. It was necessary, therefore, to use bending strength results as the basis for analysis. Corrections with regard to stress state were made by use of analytically derived relationships. Size effects were not included. The strain rate effect was overshadowed by other variables and had to be neglected. Temperature effects were accounted for by employing strength data obtained at various temperatures. All tests were conducted in air to simulate atmospheric conditions. The method applied to obtain design allowables for the ATJ graphite, as well as the various stress-state interrelationships, are presented in the Appendix.

The evaluations of uncoated ATJ graphite were limited to room temperature bend tests at a slow strain rate. Therefore, the allowables established for the attachments subjected to experimental evaluation, to be discussed later, were corrected only for the desired probability of survival and analytically derived corrections for stress size. Size effects were neglected, but both the bend test material specimens and the typical attachments were evaluated in air at slow strain rates and at room temperature. Corrections for these effects should therefore be negligible. From the bend test bars, the average strength was 3,400 psi which when corrected gave a design allowable of 2,000 psi for a 99 percent survival.

Attachment Designs

Arrangements for attaching the leading edge to the wing are shown in Fig. 5. Both meet the design philosophy previously discussed, plus the additional requirement that restraint of thermal deformations of the leading edge be minimized. This latter requirement minimizes shell thermal stresses. The three-point attachment is well suited for leading edges of large diameter. Each attachment takes loads in only one plane. This is ensured by deflection clips or hinges designed into each support truss. The vertical trusses accommodate axial growth by deflection of these clips. Rotational restraint is eliminated by the use of spherical bearings.

In the single-point attachment, all loads and moments are resisted at one point. Relative deformation problems between the leading edge and the wing do not induce extraneous loads.

Since the graphite leading-edge design had a large diameter, the three-point arrangement was selected, and the most promising attachment was a design referred to as the standard lug (Fig. 6). This design is easy to machine as an integral part of the leading edge, enables incorporation of a spherical bearing, involves relatively simple metal parts, and accommodates differential thermal expansion. However, the concentration factor due to the hole must be considered, and the resulting size is quite large. The spherical bearing is carried in a metal housing which is tapered to fit into a tapered hole in the

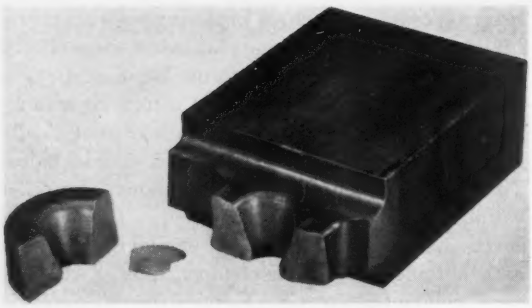

Fig. 7. Standard lug test failure.

graphite lug. The housing is held in place by a washer and nut. A graphite washer is used so that the apex of the tapering cone intersects the plane of the flat metal washer. This ensures that the fit does not change despite temperature changes. In this design a good fit is required at the taper but other tolerances are easily accommodated. The spherical nut is used to avoid problems in perpendicularity between the axis of the hole and the face of the nonmetallic.

Comparison of Predictions and Test Results

For this and other promising attachment designs, typical assemblies were fabricated and tested. Some typical fractures were tensile fracture through the hole in the standard lug (Fig. 7), tensile fracture of a protrusion loaded in shear (Fig. 8), tensile fracture for a single-point attachment loaded in tension (Fig. 9), and complex fracture for a single-point attachment loaded in bending (Fig. 10).

Experimental and analytical results are compared in Table 1, which lists the various designs, along with the types of loading and failure loads which may be compared with predictions based on design allowables for 99 percent survival probability and with predictions based upon mean strength. In no case did failure occur below the design load. In most cases the fracture load was in reasonably good agreement with the failure load predicted on the basis of mean strength, ranging from 0.7 to 1.5 of the mean predicted failure load.

Table 1. Summary of Attachment Tests

Type of Attachment	Type of Loading	Failure Load Lbs	Predicted Failure Load - Lbs	
			One Failure in One Hundred	Mean Strength
Standard Lug Bare ATJ	Tension	1800	800/640[1]	1320/1050[1]
Standard Lug Coated ATJ	Tension	850	700/560[1]	1240/990[1]
External Lug Bare ATJ	Bending load on one leg of "V" groove	1180	480	780
External Lug Bare ATJ	Shear on one strap seat	140	-	-
Redesigned External Lug Bare ATJ	Shear on strap seats	1050	790	1360
Single Point Attachment	Tension	1720, 1640, 2500 1840, 2380	914	1550
Single Point Attachment	Bending	414, 391, 414, 411, 403	341	580

(1) Loads calculated by use of theory of elasticity. The other loads were calculated by use of stress concentration factors.

The promising results obtained from these tests and the potential usefulness of the standard lug type of attachment led to the investigation of various lug geometries (Fig. 11). Lug proportions were varied and a simplified geometry was used rather than the tapered hole. Failure loads were predicted on the basis of tension allowables and bending allowables for survival probabilities of 99 and 50 percent. Comparison of experimental failure loads and predicted values are shown in Table 2, which lists types of specimen, predicted fracture loads based on 99 percent survival and on average strength for both tension and bending stress states, and failure loads. The predicted failure loads were based on two sets of data—first, tests of specimens cut from random graphite blocks, and second, tests of specimens cut from the blocks used to produce final leading-edge shapes. The lug specimens were machined from surplus material from the leading-edge blocks. The tension allowable employed was based on an analytical correction of bend test data. The correction factor was a function of the material constant m. For the random block tests, analysis of the data gave $m = 8$, while for the specimens cut from the leading-edge blocks $m = 18$.

For specimens of Types A, B, and C, there were no failures below the design load which is based on an allowable stress corresponding to a 99 percent survival. The average strength of each of these three designs agrees very well with the failure load predicted on the basis of average bending strength of the leading-edge block material.

The agreement for the Type D specimens is not as good. These specimens were the same as the Type B but twice as wide. A size effect should have been found and it was. Comparing the experimental data for specimens of Types B and D indicates that doubling the thickness increased the strength by an average factor of only 1.4 rather than 2.0. This does not agree very well with the factor of about 1.9 expected from analytical considerations. However, size effect aside, comparison of experimental and analytical results for Type D specimens indicates reasonably good agreement between actual and predicted failure loads.

Aside from further demonstrating the general suitability of the design test methods employed, these results can be used to gain specific information about design procedures. Since the net cross-sectional area for lugs of Types A, B, and C was the same, fracture loads should have been the same if stress concentrations could be neglected. Comparison of predicted and measured fracture loads indicates that concentration factors must be included and that the factors used in the design work are approximately correct. Design allowables based on bend tests should be used when stress gradients exist (Fig. 12). The average strengths measured during the tests have been plotted and compared with bending and tension allowables. The use of tension

allowables is seen to be quite conservative. Better correlation is obtained with bend allowables. The use of $m = 18$ also provides better correlation between experimental and analytical results than $m = 8$. This might be expected since the lug test specimens were cut from leading-edge block material as were the test specimens which gave $m = 18$. The use of the lower m value is conservative.

Testing of Graphite Leading-Edge Assembly

The graphite leading-edge assembly was subjected to three types of test which included (1) static load to failure at room temperature, (2) moderate time-temperature cycling to obtain thermal strain data, and (3) time-temperature cycling to simulate flight conditions.

Results of the static test have not been thoroughly analyzed as yet. The assembly failed at 170 percent of design limit load, with fracture occurring in a metal part. This precipitated fracture of the graphite leading edge at several locations. At several locations the cracks went through strain-gage grids. This should provide an indication of fracture strain.

Thermal strain measurement analysis has not been completed either. Preliminary indications show only fair comparison between measured and calculated strains.

The major testing involved five cycles of simulated flight which attempted to follow the program shown in Fig. 13. Limitations of available quartz lamp radiant heaters prevented the attainment of 3,000°F. A maximum temperature of about 2,300°F was achieved and held constant from one side of the program to the other. The first assembly tested withstood the test conditions, for five cycles. There were no structural failures, although oxidation resistance was not completely adequate (Fig. 14). Some oxidation failures are obvious. These progressed quite gradually. After the first cycle, the specimen appeared to have suffered no damage. Redesign of the edge to minimize oxidation failures in these areas would be a relatively simple matter.

A second graphite leading-edge assembly tested under the simulated flight temperature history failed structurally during the first cycle. The failure was attributed to insufficient clearance between the horizontal truss and the upper cover panels, which introduced loads into the center lug. Post-test examination indicated an available clearance of 0.010 in. at a place where it should have been 0.030 in.

The component test results further illustrate the potential usefulness of brittle materials in structural applications.

Conclusion

All indications point to the fact that brittle materials can be used for reliable structural components, such as leading edges, if proper design philosophies and methods are employed. In the work described, brittleness was recognized. The construction material was characterized as to variability by means of experimental observation and statistical method. Sound design principles were formulated to eliminate indeterminate load distribution and to account for tolerance problems, stress concentrations, differential expansions, and material variability. As a result, comparisons of experimental results with analytical expectations have been very encouraging.

The magic material which the airframe industry wanted yesterday has not been developed even today. Chances are that we shall not have it tomorrow either. However, many interesting nonmetals, having brittle characteristics, are currently available or semiavailable for use in air at temperatures up to 3,000°F. These might be used successfully if enough effort is expended in learning

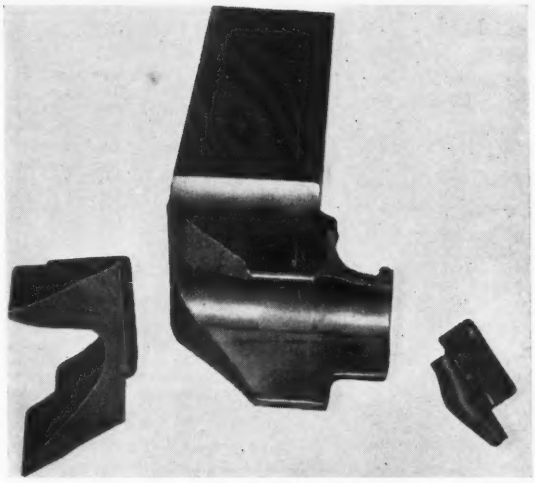

Fig. 8. External lug test failure.

Table 2. Summary of Stress Concentration Specimen Testing

	Predicted Failure Load - Lbs				
	Tension Allowable		Bend Allowable		
Specimen Type	99% Survival	Average Strength	99% Survival	Average Strength	Failure Load-Lbs
A					435
0.250 in. hole					441
1.250 in. lug dia.					480
0.500 in. thick					333
					463
					450
	125 (205)	215 (285)	180 (250)	310 (350)	Av. 434
B					627
0.500 in. hole					580
1.500 in. lug dia.					600
0.500 in. thick					563
					535
	190 (305)	320 (425)	270 (370)	460 (520)	Av. 581
C					757
1.000 in. hole					730
2.000 in. lug dia.					742
0.500 in. thick					627
					803
	260 (425)	445 (595)	375 (520)	640 (730)	Av. 732
D					817
0.500 in. hole					928
1.500 in. lug dia.					705
1.000 in. thick					930
					688
	380 (610)	640 (850)	540 (740)	920 (1040)	Av. 813

Note: Numbers in parentheses are predicted failure loads based on large bending specimens tested after Battelle Memorial Institute had completed the testing program reported in reference 3.

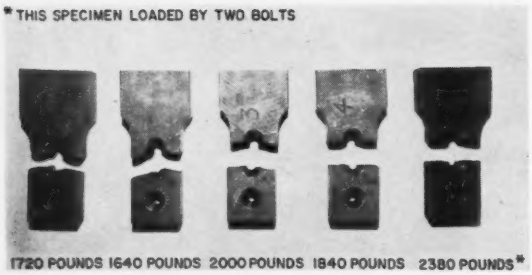

Fig. 9. Test failures of single-point attachment tension specimens.

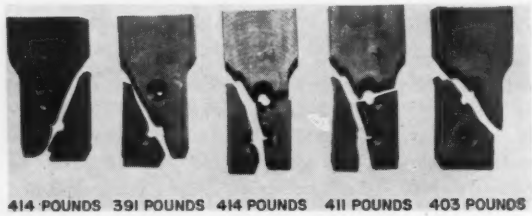

Fig. 10. Test failures of single-point attachment bend specimens.

how to design with them. The primary need is for a better understanding of the strength behavior of nonmetals. Currently available statistical theories are of great help, but they do not account for all observed characteristics. Improved and more comprehensive behavior theories are needed; so are more refined structural analysis methods. Better testing techniques and equipment would permit a more accurate determination of material performance which, in turn, would permit more effective use of the material. Efforts to improve the reproducibility of nonmetals are also desirable. Both processing refinement and inspection technique development should be pursued. These items, and others of a similar nature, represent refinements required to extend and exploit the sound approach presented for the use of brittle materials in reliable structural components, such as leading edges for hypersonic gliders.

Appendix I. Tentative Design Allowables for Siliconized ATJ Graphite

This Appendix discusses the method of establishing design allowable strengths for a brittle material, and presents tentative strength allowables for siliconized ATJ graphite used at Bell for design of the graphite leading-edge component.

Of the statistical theories available, Weibull's theory of strength showed the most immediate promise of predicting certain aspects of brittle material behavior, and this was the theory applied. The relationships formulated for various stress states and size effect from Weibull's theory[1, 2] were considered adequate for the design of components whose function was to demonstrate feasibility.

The following relationships which have been derived from Weibull's theory of strength are:

Stress State

$$\frac{\sigma_b}{\sigma_d} = \left[\frac{2(m+1)V_d}{V_b}\right]^{1/m}$$

$$\frac{\sigma_b}{\sigma_T} = \left[\frac{(2m+1)\ (2m+2)\beta_1' V_T}{2(m+2)V_b}\right]^{1/m}$$

$$\frac{\sigma_b}{\sigma_T} = \left[\frac{(2m+1)\beta_1'\ V_T}{2(m+2)V_d}\right]^{1/m}$$

where

σ_b = average bending or allowable stress
σ_d = average tension or allowable stress
σ_T = average torsion or allowable stress
m = Weibull's material constant
V_b = volume of material in bending
V_d = volume of material in tension
V_T = volume of material in torsion

$$\beta_1' = \frac{\Gamma(m+1)\ \Gamma\left(\frac{m+1}{2}\right)}{\Gamma\left(\frac{2m+1}{2}+1\right)\Gamma\left(\frac{m}{2}+1\right)}$$

Γ = gamma function

Size Effect

$$\sigma_{bS}/\sigma_{bL} = (V_{bL}/V_{bS})^{1/m}$$
$$\sigma_{dS}/\sigma_{dL} = (V_{dL}/V_{dS})^{1/m}$$
$$\sigma_{TS}/\sigma_{TL} = (V_{TL}/V_{TS})^{1/m}$$

where

σ_{bS} = average failure stress or allowable of small bend specimen
σ_{bL} = average failure stress or allowable of large bend specimen
σ_{dS} = average failure stress or allowable of small tension specimen
σ_{dL} = average failure stress or allowable of large tension specimen
σ_{TS} = average failure stress or allowable of small torsion specimen
σ_{TL} = average failure stress or allowable of large torsion specimen
V_{bS} = volume of small bend specimen
V_{bL} = volume of large bend specimen
V_{dS} = volume of small tension specimen
V_{dL} = volume of large tension specimen
V_{TS} = volume of small torsion specimen
V_{TL} = volume of large torsion specimen

or for size effect for any stress state

$$\sigma_S/\sigma_L = (V_L/V_S)^{1/m}$$

where

σ_S = failure stress of small specimen
σ_L = failure stress of large specimen
V_S = volume of small specimen
V_L = volume of large specimen

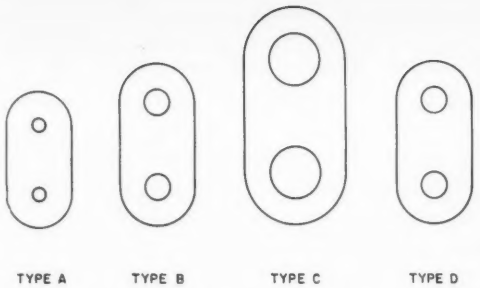

Fig. 11. Stress concentration specimens, graphite.

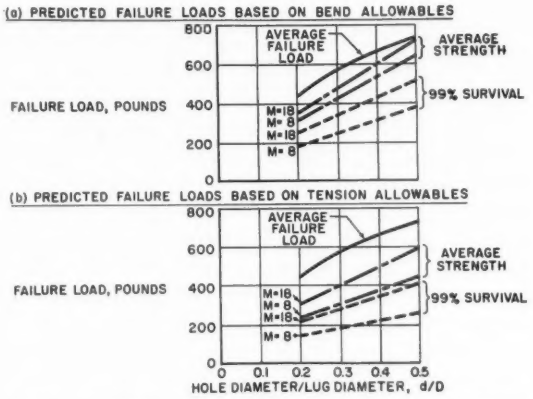

Fig. 12. Predicted failure loads for stress concentration specimens.

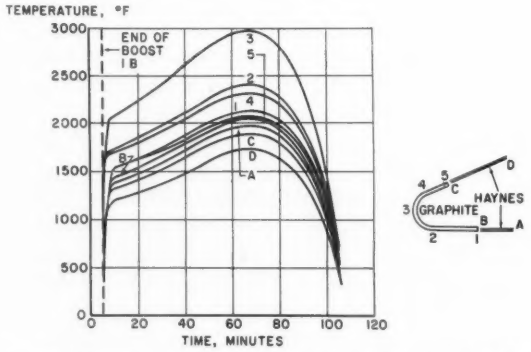

Fig. 13. Temperatures of graphite leading edge during boost and glide (D = 5.0 in., Λ = 60°, W/SC_L = 150 psf, ϵ = 0.55).

From the foregoing relationships, it can be seen that if a material is defined by Weibull's theory, the results of strength tests for one stress state may be used to determine the average failure stresses in the other stress states. The effect due to size may also be determined. Weibull's theory states that the material constant m should not vary with stress state, so that m determined in one stress state may be used in other stress states. Plots of stress ratios vs. m for the various stress states for equal volumes of

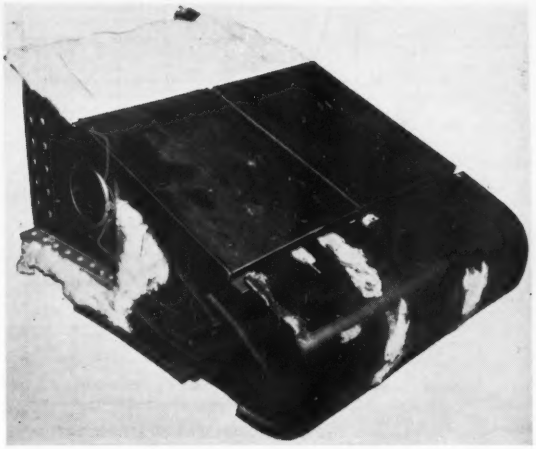

Fig. 14. Graphite leading edge after approximately 10 hours at elevated temperatures.

material are shown in Figs. 15, 16, and 17. Fig. 18 is a carpet plot showing the effect of size for any stress state with parameters of stress ratio, volume ratio, and the material constant m.

The design of the leading-edge component was based on results from bare and coated large bend specimens. The design data presented here must be considered to be tentative since the coating is still in its developmental stage and it was not possible to isolate completely the effects of the coating variation from the material variables under investigation. The effect of coating variations were of the same order of magnitude as some of the effects investigated experimentally, such as strain rate. Despite the limitations, the tentative design allowables established are considered adequate for the design of components whose function is to demonstrate feasibility.

During testing of the large coated bend specimens, it was observed that the coating cracked during the initial stages of loading, leaving the substrate to carry the entire moment until failure. The failure mechanism of the coating was not fully understood at the time so that the failure stresses were calculated by assuming an elastic beam having the cross-sectional dimensions of the substrate only. The coating was considered to be 0.030 in. thick. Later in the program it was found that the coating on the tension surface cracked but the coating on the compression surface retained its load-carrying capacity, making the foregoing analysis of failure stresses somewhat conservative.

The Weibull material constant m was obtained from the following relationship which was derived in reference 3:

$$\frac{a^2}{\bar{\sigma}_f} = \frac{\Gamma[1 + (2/m)]}{\Gamma^2[1 + (1/m)]} - 1$$

where

a = standard deviation

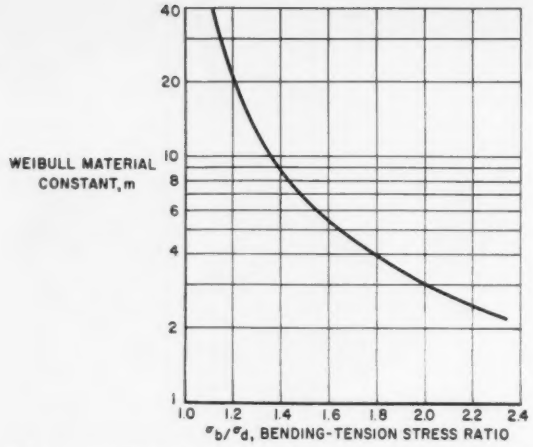

Fig. 15. Variation of bending to tension stress ratio with Weibull material constant *m*.

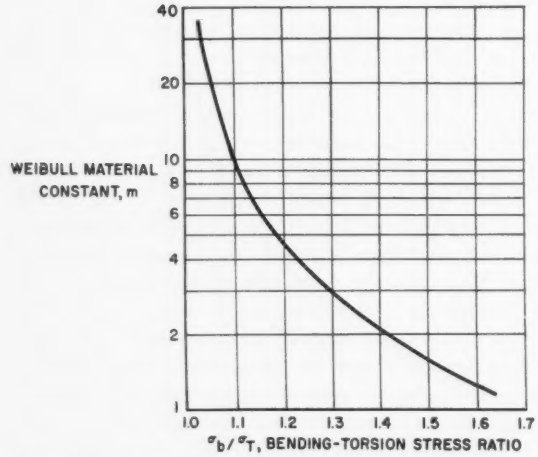

Fig. 16. Variation of bending to torsion stress ratio with Weibull material constant *m*.

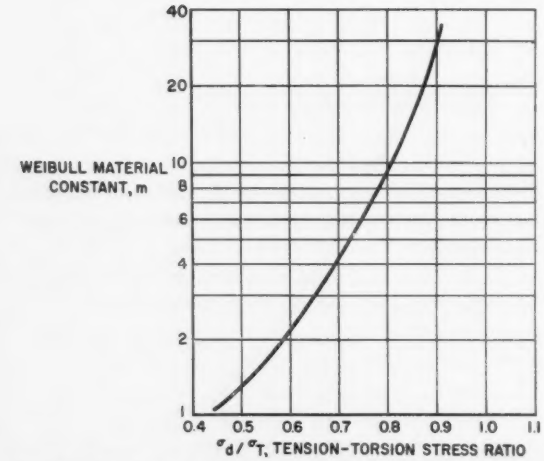

Fig. 17. Variation of tension to torsion stress ratio with Weibull material constant *m*.

$\bar{\sigma}_f$ = average failure stress
Γ = gamma junction
m = Weibull material constant

It should be noted that the material constant m may also be calculated from the stress-state and size-effect relationships, but since the only test data available when the leading-edge component was designed were one stress state and one size, the relationships could not be used to determine m.

The following tabulation shows the average fracture stresses, calculated from the beam flexure equation assuming 0.030 in. of coating thickness and material constant m at the test temperature.

Temperature, °F	Average Fracture Stress, psi	Material Constant m
80	3,080	7.5
2,000	4,160	7.3
2,500	4,050	14.5
2,750	4,360	7.8

For purposes of the leading-edge study, a survival probability of 99 percent at ultimate loads was considered adequate for design. A plot of probability of failure vs. allowable bend stresses (Fig. 19) shows that, at 1 percent probability of failure (99 percent probability of survival), the allowable stress is 1,800 psi. A component stressed to 1,800 psi at ultimate load would be stressed to 1,200 psi at limit load (ultimate load equals 1.5 times limit load). At limit load this would correspond to a probability of failure of 0.06 percent, or 99.94 percent probability of survival. In terms of number of components, 99 percent survival corresponds to 1 failure out of 100 components, and 99.94 percent survival corresponds to 1 failure out of 1,665 components. Thus, at limit load the probability of survival is much higher than at ultimate load. The factor of safety with regard to probability of survival between limit and ultimate condition is approximately 17; with regard to load, it is only 1.5.

Fig. 20 presents the variation of factors of safety vs. the material constant m for various probabilities of survival. The average failure stress in bending vs. temperature, as well as the 99 percent probability of survival stresses, are shown in Fig. 21. At temperatures above 2,000°F, the average strength and the 99 percent probability curve have reverse trends. The average strength curve dips at 2,500°F, whereas the 99 percent probability curve peaks at 2,500°F. The material constant at 2,500°F was approximately twice the value at the other test temperatures, and, with this higher value of the material constant, a lower factor of safety was applied to the average failure stress. To be conservative, since the reason for the increased value of m and the decrease in the average strength at 2,500°F (graphite has the well-known property of increasing in strength with temperature) was unknown, the allowable stress at 2,000°F was used for all temperatures above 2,000°F.

By use of Figs. 15 and 16 the allowable stresses in

the other stress states were obtained as the following stress ratios:

Temperature, °F	Allowable Bend Stress, psi	Ratio — Bending Tension	Ratio — Bending Torsion
80	1,760	1.45	1.130
2,000	2,310	1.45	1.132
3,000	2,310	1.45	1.132

By dividing the allowable stress in bending by the stress ratio, the allowable stress may be found for a volume of material equal to the bend specimen, in tension or torsion. The allowable stress in compression was taken as twice the allowable stress in bending, which is conservative. Effect due to size may be included, with the use of Fig. 18. Size effect was not included in the analysis of the leading-edge component. The allowable stresses as determined from the bend specimens were used.

The design allowables as established in this Appendix were obtained by transforming the coated specimens to bare graphite and then obtaining the properties. It may be reasoned, therefore, that it would be satisfactory to use allowables obtained from bare specimens, but this is not the case. The coating lowers the strength of the graphite substrate. The reduction in the strength of coated specimens is apparent in Fig. 22, which shows—for both coated and uncoated specimens—the variation of bending stiffness and fracture moment with specimen grain direction. The degree of the reduction in strength depends upon specimen orientation, with specimen cut zero-degrees to the grain direction having the largest reduction in strength. The coated specimens showed a mark increase in bending stiffness between the $22^1/_2$ and 45-deg specimens, with the bending stiffness remaining essentially constant beyond that point. A more complete discussion of the effect of the coating on the properties of ATJ graphite is included in reference 3.

Appendix II. Repeated Load Considerations

The question of the effect of repeated loadings on brittle components has been raised. This Appendix presents the limited information available and outlines some aspects of the problem.

Little is known of the effect of repeated loads on the structural integrity of a brittle material structure. Limited test data may shed some light on the question, although they are not considered conclusive. A standard lug made in bare ATJ graphite (identical to the standard lug shown in Fig. 7) was subjected to 300 repeated load cycles which were varied from 0 to 1,200 to 0 lbs without failure. Static load was then applied to failure, which occurred at 1,800 lbs. This failure load was identical to the bare standard lug reported in Table 1. The lug reported in Table 1 was tested first, and the repeated load cycle for the second lug was arbitrarily taken as two thirds of the failure load, or equal to 1,200 lbs. It will be noted that two predicted failure loads are given in

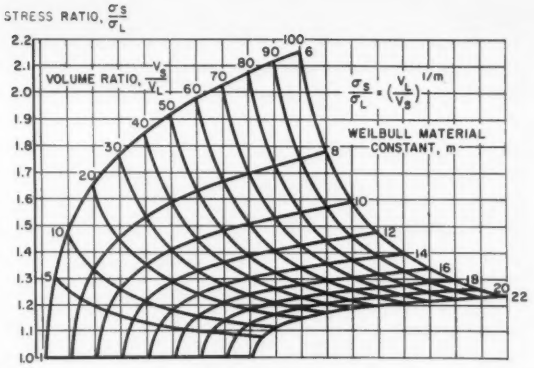

Fig. 18. Variation of small specimen to large specimen stress ratio with volume ratio and Weibull material constant *m*.

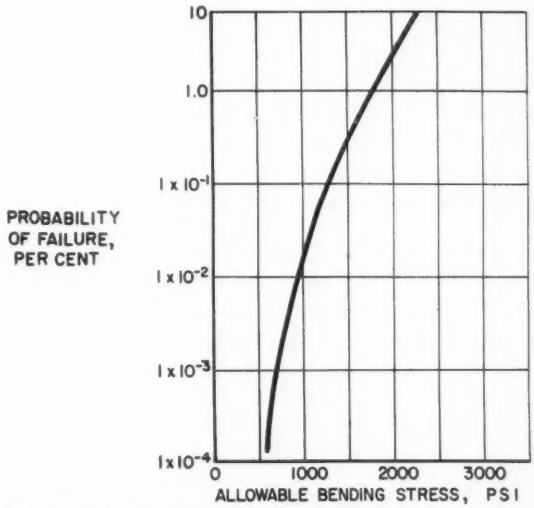

Fig. 19. Variation of probability of failure with allowable bending stress for $m = 7.5$.

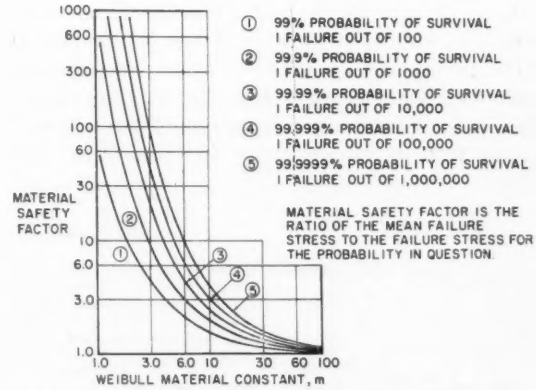
① 99% PROBABILITY OF SURVIVAL 1 FAILURE OUT OF 100
② 99.9% PROBABILITY OF SURVIVAL 1 FAILURE OUT OF 1000
③ 99.99% PROBABILITY OF SURVIVAL 1 FAILURE OUT OF 10,000
④ 99.999% PROBABILITY OF SURVIVAL 1 FAILURE OUT OF 100,000
⑤ 99.9999% PROBABILITY OF SURVIVAL 1 FAILURE OUT OF 1,000,000
MATERIAL SAFETY FACTOR
MATERIAL SAFETY FACTOR IS THE RATIO OF THE MEAN FAILURE STRESS TO THE FAILURE STRESS FOR THE PROBABILITY IN QUESTION
WEIBULL MATERIAL CONSTANT, m

Fig. 20. Variation of material safety factor with Weibull material constant *m* for various probabilities of survival.

Table 1 for the bare standard lug, 800 and 641 lbs. The predicted load of 800 lbs was calculated by means of stress concentration factors and the 641 lbs by use of the theory of elasticity. For this discussion

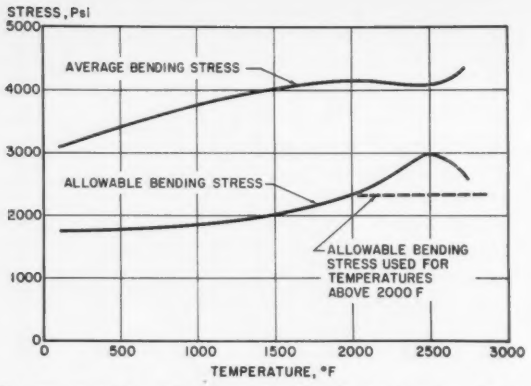

Fig. 21. Variation of average and allowable bending stress for 99 percent probability of survival with temperature.

the 800-lb load will be used, since use of the theory of elasticity leads to a more conservative lug design. The 1 failure out of 100, or the 800-lb load, is considered the ultimate load for the standard lug so that the limit load is 535 lbs. The repeated load which was applied then was 1.5 times ultimate design load which could have caused failure with the application of such a load to a metallic structure, but in the case of most metals the allowable stresses are well defined. The allowable stresses in a brittle material are not well defined, but are based on a given probability of failure, in this case 1 out of 100. Assuming that the material did follow a mathematical law, 1 specimen out of 100 would fail at or below the ultimate design load and the other 99 would fail above the ultimate design load. Both lugs failed at loads 2.5 times the ultimate design load, which is not considered unusual for the limited number of specimens tested.

Repeated load tests were also conducted on a subsequent external lug attachment specimen. A repeated load of 750 lbs was applied to the specimen which was again two thirds of the failure load of 1,050 lbs reported in Table 1. Failure of the specimen occurred after 15 cycles. In this case, the repeated load was only 95 percent of the ultimate design load or approximately 140 percent of limit load.

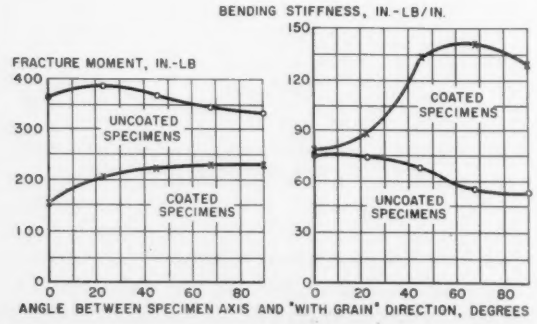

Fig. 22. Anistropy of ATJ graphite as indicated by bend tests.

With only two tests, no conclusions may be drawn as to the effect of repeated loads. It should be pointed out that when metallic structures are designed for static loads, the effects of stress concentrations are not included and problems may arise when fatigue enters the picture. When designing with a brittle material, severe stress concentrations are avoided, if possible, and the effects of stress concentrations are included in the static strength analysis. Hence, one of the basic problems which has plagued metal components—stress concentrations which result in premature failures—is considered in detail for nonmetallic components. Normally, repeated loads are lower than static design loads so that inclusion of stress concentration factors in the static analysis of brittle material parts should tend to reduce potential problems from repeated loads.

Let us extend this point of view, in a speculative manner, to the material behavior. For ductile materials, minute defects such as inclusions, etc., do not affect static strength but do reduce fatigue strength. For brittle materials, such defects do reduce static strength. It might be reasoned, therefore, that the ratio of fatigue strength to static strength should be larger for a brittle material than for a ductile material. Unfortunately, the fatigue strength of brittle materials has not been investigated. However, this line of reasoning would tend to suggest that repeated loadings may not be so detrimental to brittle materials as they are for ductile materials.

To explore the effects of repeated loadings fully, a large number of tests must be performed because of the variability of a brittle material. The primary objective of the program under which this work was performed was to determine the feasibility of designing a structural component which would be useful for five missions, and thus the effects of repeated loadings with the use of stress concentration factors were considered adequately covered. When coating development has progressed further so that oxidation is not the criterion which determines the life of a structural component, then repeated loadings may assume greater importance.

References

[1] Salmassy, O. K., Duckworth, W. H., and Schwope, A. D., *Behavior of Brittle-State Materials*, WADC TR 53-50, Pt. I, June 1955.

[2] Salmassy, O. K., Bodine, E. G., Duckworth, W. H., and Manning, G. K., *Behavior of Brittle-State Materials*, WADC TR 53-50, Pt. II, June 1955.

[3] Rudnick, A., Carlson, R. L., and Manning, G. K., *Investigation of Feasibility of Utilizing Available Heat-Resistant Materials for Hypersonic Leading Edge Applications*, Vol. VI, "Determination and Design Application of Mechanical Properties of Bare and Coated Graphite," WADC TR 59-744, July 1960.

[4] Anthony, F. M., Merrihew, F. A., Mistretta, A. L., and Dukes, W. H., *Investigation of Feasibility of Utilizing Available Heat-Resistant Materials*, Vol. I, "Summary," WADC TR 59-744, Jan. 1961.

One-Shot Mission (Continued from page 23)

The number of vehicles launched, n, is related to the probability of success for any one shot, P_u, by the relation

$$n = [\log (1 - P)]/[\log (1 - P_u)] \qquad (2)$$

The total cost, excluding reliability improvement costs, of launching n vehicles may be expressed

$$C_E = n(C_F + C_L) + C_o \qquad (3)$$

where $C_F \equiv$ cost of fabricating and delivering one vehicle, $C_L \equiv$ cost of launching and supporting the flight of one vehicle, and $C_O \equiv$ nonrecurring costs, including design development, ground support equipment, etc.

Cost C_F may be assumed proportional to the total complexity of the vehicle. Letting K_i be the nonredundant complexity of the ith "in series" vehicle subsystem and m_i the number of each ith subsystem used for "stand-by" redundancy, then the total complexity of equipment associated with the ith function in one vehicle is m_iK_i, and

$$C_F = k_F\left[\sum_{i=1}^{N'} K_i + \sum_{i=(N'+1)}^{N} m_iK_i\right] = k_F\left[\sum_{i=1}^{N} m_iK_i\right], \; m_i = 1 \text{ for } i = 1, \ldots, N' \qquad (4)$$

where k_F is a constant, N is the number of "in series" subsystems in the vehicle, and N' is the number of those subsystems for which no stand-by redundancy is possible.

Similarly, assigning the cost of any booster used in launching (and not developed for the particular project) to the cost of launching, and assuming that the cost of such boosters is a function of the weight (and, therefore, the total complexity) of the vehicle,

$$C_L = f_L\left(\sum_{i=1}^{N} m_iK_i\right) \qquad (5)$$

For the ith vehicle subsystem, the cost of the reliability improvement program may be expressed

$$C_{Ri} = K_i (\bar{c}_i - \bar{c}_{io}) \qquad (6)$$

$$C_R = \sum_{i=1}^{N} C_{Ri} = \sum_{i=1}^{N} K_i (\bar{c}_i - \bar{c}_{io}) \qquad (7)$$

where $(\bar{p}_{io}, \bar{c}_{io})$ is the point on the curve (Fig. 1) at which the ith subsystem may be regarded as located at the beginning of design development of the vehicle, and $(\bar{p}_i, \bar{c}_i)$ the point to which this subsystem progresses as a result of the reliability improvement program.

The reliability of one set of ith subsystem equipment for a mission requiring $10t_i$ hours of operation, in an environment of severity s_i relative to the standard environment, is then given by the expression

$$p_i = \bar{p}_i^{K_is_it}$$

Letting p_i^E be the reliability of the ith function, composed of m_i stand-by redundancies of the subsystem whose reliability is p_i, the reliability of the ith function may be expressed

$$p_i^E = 1 - (1 - \bar{p}_i^{K_is_it_i})^{m_i} \qquad (8)$$

The reliability of one vehicle is then

$$P_u = p_L \prod_i p_i^E = p_L \prod_i [1 - (1 - \bar{p}_i^{K_is_it_i})^{m_i}] \qquad (9)$$

where p_L is the probability of successful booster operation.

Total cost C, Eq. (1), can then be written

$$C = n\left\{k_F \sum_{i=1}^{N} m_iK_i + f_L\left(\sum_{i=1}^{N} m_iK_i\right)\right\} + C_o + \sum_{i=1}^{N} K_i (\bar{c}_i - \bar{c}_{io}), \; m_i = 1 \text{ for } i = 1, \ldots, N' \qquad (10)$$

where

$$n = \frac{\log (1 - P)}{\log\left\{1 - p_L \prod_i [1 - (1 - \bar{p}_i^{K_is_it_i})^{m_i}]\right\}} \qquad (11)$$

$$\bar{c} = f_R (\bar{p}) \qquad \text{(Fig. 1)} \qquad (12)$$

The problem of finding the set of values of $\bar{p}_i$, m_i, and n which minimize C can be reduced to that of finding the set minimizing

$$C' \equiv C - (C_o + \sum_{i=1}^{N} K_i \bar{c}_{io}) = n\left\{k_F \sum_{i=1}^{N} m_iK_i + f_L\left(\sum_{i=1}^{N} m_iK_i\right)\right\} + \sum_{i=1}^{N} K_i f_R (\bar{p}_i) \qquad (13)$$

under the condition

$$n = \frac{\log (1 - P)}{\log\left\{1 - p_L \prod_i [1 - (1 - \bar{p}_i^{K_is_it_i})^{m_i}]\right\}}, \quad m_i = 1 \text{ for } i = 1, \ldots, N' \qquad (14)$$

Procedures for solving this minimization problem are derived and applied to typical examples in the next section—first, for the special case of no on-board subsystem redundancies.

Special Case

Assuming no on-board redundancies, or $m_i = 1$, and letting $K = \sum_i K_i$, Eqs. (13) and (14) for this special case reduce to

$$C' = n\left[Kk_F + f_L (K)\right] + \sum_{i=1}^{N} K_i f_R(\bar{p}_i) \qquad (15)$$

$$n = \frac{\log (1 - P)}{\log [1 - p_L \prod_i \bar{p}_i^{K_is_it_i}]} = \frac{\log (1 - P)}{\log (1 - P_u)} \qquad (16)$$

Finding the values of $\bar{p}_i$ which minimize C' is separated into two steps, the first of which is the establishment for any n, and therefore P_u, of $\bar{p}_2 \ldots$

$\bar{p}_N$ in terms of $\bar{p}_1$ minimizing $\sum_{i=1}^{N} K_i f_R(\bar{p}_i)$. Assume $f_R(\bar{p})$ to be given by the analytical expression of Fig. 1, $\bar{c} = f_R(\bar{p}) = A \log \log 1/\bar{p} + B$. Then the minimization may be accomplished by the method of Lagrangian multipliers, letting

$$F(\bar{p}_i, \lambda) = \sum_{i=1}^{N} K_i (A \log \log 1/\bar{p}_i + B) + \lambda[\prod_i \bar{p}_i^{K_i s_i t_i} - P_u/p_L]$$

and employing the conditions $\partial F/\partial \bar{p}_i = 0$, $\partial F \div \partial \lambda = 0$, or

$$\left.\begin{aligned} \frac{K_i A}{\bar{p}_i \log \bar{p}_i} + \lambda K_i s_i t_i \bar{p}_i^{K_i s_i t_i - 1} \prod_{j \neq i} \bar{p}_j^{K_j s_j t_j} = 0 \\ \prod_j \bar{p}_j^{K_j s_j t_j} - P_u/p_L = 0 \end{aligned}\right\} \quad (17)$$

Substituting from the second equation into the first,

$$A/\log \bar{p}_i = -\lambda s_i t_i P_u/p_L$$

Dividing the first of Eqs. (17) by the ith, the following relationship is obtained:

$$\bar{p}_i = \bar{p}_1^{s_1 t_1 / s_i t_i} \qquad i \neq 1 \quad (18)$$

It follows from Eqs. (17) and (18) that

$$P_u/p_L = \prod_i \bar{p}_i^{K_i s_i t_i}$$

$$= \bar{p}_1^{K_1 s_1 t_1} \prod_{i \neq 1} \bar{p}_1^{(s_1 t_1 / s_i t_i) K_i s_i t_i}$$

$$= \bar{p}_1^{K_s t_s}$$

$$n = \frac{\log (1 - P)}{\log (1 - p_L \bar{p}_1^{K_s t_s})} \quad (19)$$

The minimization of C' may then be accomplished by plotting Eq. (15) against $\bar{p}_1$, using Eqs. (18) and (19), thereby graphically determining the minimum value of C' and the value, $\bar{p}_{1M}$, of $\bar{p}_1$ which provides this minimum. The cost of the effort to be expended then on reliability improvement of the ith subsystem is

$$C_{Ri} = K_i[f_R(\bar{p}_{1M}^{s_1 t_1 / s_i t_i}) - f_R(\bar{p}_{io})] \qquad i \neq 1 \quad (20)$$

The reliability expected to be obtained for each subsystem is

$$p_{iM} = \bar{p}_{iM}^{K_i s_i t_i} \quad (21)$$

and the number of vehicles to be built and launched is

$$n = \frac{\log (1 - P)}{\log (1 - p_L \bar{p}_{1M}^{K_s t_s})} \quad (22)$$

This special case is applied to an experiment for which it is presumed that a 95 percent probability of success of at least one shot is needed for a vehicle made up of a guidance and control subsystem, $i = 1$, a power supply subsystem, $i = 2$, and an instrumentation subsystem, $i = 3$. Cost, mission operation, and subsystem complexity parameters are given by Fig. 1 and Example 1.

Example 1

$s_1 = s_2 = s_3 = 1$
$t_1 = 6, t_2 = 6, t_3 = 0.1$
$K_1 = 1, K_2 = 0.2, K_3 = 0.5$
$\bar{p}_{1o} = \bar{p}_{2o} = \bar{p}_{3o}, p_L \cong 1$
$\bar{c}_{1o} = 0$
$k_F = 0.2(10)^6$ dollars
$f_L(K) = [0.1(10^6) + 2(10)^6 K]$ dollars
$C_o = 15(10)^6$ dollars
$P = 0.95$

Employing the foregoing values, Eqs. (15) and (16) become

$$C' = 3.84(10)^6 n + 1.2 f_R(\bar{p}_1) + 0.5 f_R(\bar{p}_1^{60}) \quad (23)$$

$$n = \frac{\log (0.05)}{\log (1 - \bar{p}_1^{10.2})} \quad (24)$$

A plot of total program cost C vs. $\bar{p}_1$ (Fig. 2) is the same curve that would be obtained by Eq. (23) except that its ordinate is greater by the fixed amount C_o. Values of $\bar{p}_1$ for which n, the number of launches, is an integer are indicated by the markings in the curve representing C. This plot shows that $\bar{p}_{1M} = 0.935$, minimum program cost $C_M = 63(10)^6$ dollars, and n is four. Components of C are also plotted in Fig. 2 to show their relative contribution to the total cost; a tabulation of these is presented in Table 1.

For this particular example it is evident that a significant difference is indicated in reliability improvement expenditures for the three subsystems; note that no funds at all should be spent on reliability improvement of the instrumentation subsystem. This example also indicates that the reliability improvement expenditure required to result in a minimum cost program may exceed by a substantial amount the basic design development cost.

Although the basic design development, fabrication, and launch support cost data employed for this example may appear to be somewhat on the low side for the type of mission chosen, it is apparent from Fig. 2 that the effect of an increase in these costs would be to raise the curve for C_L, thereby moving the minimum cost point to the right and requiring higher reliability improvement expenditures.

Table 1. Cost Components for Minimum Total Cost Program (Example 1)

Item	Cost, Dollars × 10^{-6}
Fixed cost (basic design development)	15
Fabrication and launch costs for four shots	16
Reliability improvement costs:	32
Guidance and control (Subsystem 1)	(27)
Power supply (Subsystem 2)	(5)
Instrumentation (Subsystem 3)	(0)
Total	63

Reliability improvement costs for the optimum program would, therefore, still amount to about 50 percent of the total program cost, even though the basic cost figures were increased.

General Case

The method used in the preceding section to obtain the minimization of Eq. (13) under condition (14) for the special case $m_i = 1$ is applied here to the general case. Let

$$(m_{1k}, m_{2k}, \ldots m_{ik} \ldots m_{Nk}), m_{ik} = 1 \text{ for } i = 1, \ldots, N'$$

be a given set of values of m_i; then for this set of values of m_i and for any n, the relationships between $\bar{p}_i$ minimizing

$$\sum_{i=1}^{N} K_i f_R(\bar{p}_i) = \sum_{i=1}^{N} K_i \left[A \log \log (1/\bar{p}_i) + B\right]$$

and therefore C' of Eq. (13), under the condition (14) are, by the method of Lagrangian multipliers, those values of $\bar{p}_i$, with λ, minimizing

$$F(\bar{p}_i, \lambda) = \sum_i K_i \left[A \log \log (1/\bar{p}_i) + B\right] + \lambda \left\{\prod_i \left[1 - (1 - \bar{p}_i^{K_i s_i d_i})\right]^{m_{ik}} - \frac{P_u}{p_L}\right\} \quad (25)$$

The following minimization expression results:

$$\left.\begin{aligned} &\frac{AK_i}{\bar{p}_i \log \bar{p}_i} + \lambda \left\{K_i s_i d_i m_{ik} \bar{p}_i^{K_i s_i d_i - 1} \times (1 - \bar{p}_i^{K_i s_i d_i})^{m_{ik}-1} \times \prod_{j \neq 1} \left[1 - (1 - \bar{p}_j^{K_j s_j d_j})^{m_{jk}}\right]\right\} = 0 \\ &\prod_i \left[1 - (1 - \bar{p}_i^{K_i s_i d_i})^{m_{ik}}\right] - \frac{P_u}{p_L} = 0 \end{aligned}\right\} \quad (26)$$

Letting

$$q_i \equiv 1 - p_i = 1 - \bar{p}_i^{K_i s_i d_i} \quad (27)$$

Eq. (26) may be written

$$\left.\begin{aligned} &\frac{AK_i}{\log (1 - q_i)} + \lambda m_{ik} (1 - q_i) q_i^{m_{ik}-1} \times \prod_{j \neq 1} (1 - q_j^{m_j}) = 0 \\ &\prod_i (1 - q_i^{m_{ik}}) = \frac{P_u}{p_L} \end{aligned}\right\} \quad (28)$$

Multiplying the first equation by

$$\frac{1 - q_i^{m_{ik}}}{m_{ik} (1 - q_i) q_i^{m_{ik}-1}}$$

and using the second relationship,

$$AK_i X(q_i, m_{ik}) = -\lambda (P_u/p_L) \quad (29)$$

where

$$X(q, m) = \frac{1 - q^m}{m(1 - q) q^{m-1} \log (1 - q)} \quad (30)$$

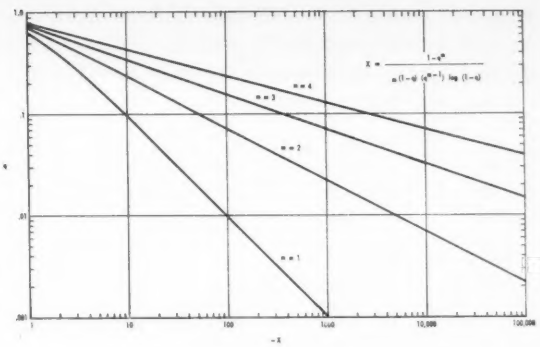

Fig. 3. Plot of q vs. X.

$X(q, m)$ is plotted against q for various values of m (Fig. 3).

Dividing the ith Eq. (29) by the first equation,

$$X(q_i, m_{ik}) = \frac{K_1}{K_i} X(q_1, m_{1k}) \quad (31)$$

Since $\bar{p}_i$ is related to q_i by definition (27), Eq. (31) provides $\bar{p}_i$ in terms of $\bar{p}_1$, minimizing $\sum_i K_i f_R(\bar{p}_i)$ for any value of n—that is, for any value of $\bar{p}_1$, $\bar{p}_i$ can be determined from Eqs. (27) and (31).

As in the preceding section, the set of values $\bar{p}_{iM}$ $(m_{1k}, \ldots, m_{Nk})$ minimizing C' for a given set of values $(m_{1k}, \ldots, m_{Nk})$ can now be found graphically by plotting C' against $\bar{p}_1$. By determining and comparing $\bar{p}_{iM}$ $(m_{1k}, \ldots, m_{Nk})$ over the complete set of integral values of $(m_{1k}, \ldots, m_{Nk})$, the values of m_i and $\bar{p}_i$ minimizing C', and therefore C, are obtained.*

This procedure is next applied to two examples:

(a) Example 2 is similar to Example 1 of the preceding section except that it is presumed that part of the guidance and control subsystem, the power supply subsystem, and the instrumentation subsystem may be made redundant.

(b) Example 3 is a much longer mission but requires guidance and controls and power supply subsystems of relatively low complexity.

Example 2

Letting that portion of the guidance and control

* A simple analytical solution exists[1] for the case $n = 1$, $\bar{p}_i$, and therefore q_i fixed and known, and $q_i << 1$. In this case, the problem reduces to minimizing

$$C'' = k_F \sum_i m_i k_i + f_L \left(\sum_i m_i k_i\right)$$

under the constraint

$$P/p_L = \prod_i (1 - q_i^{m_i}) \cong 1 - \sum_i q_i^{m_i}$$

and by the method of Lagrangian multipliers used in the foregoing, it can be shown that m_i values are given by

$$q_i^{m_i} = (1 - P/P_L) \frac{K_i/\log q_i}{\sum_j K_j/\log q_j}$$

subsystem which is not capable of redundancy be denoted by the subscript 1, and the remainder by the subscript 4, we then give the basic data for this example as follows:

$s_1 = s_2 = s_3 = s_4 = 1$
$t_1 = 6, t_2 = 6, t_3 = 0.1, t_4 = 6$
$K_1 = 0.4, K_2 = 0.2, K_3 = 0.5, K_4 = 0.6$
$\bar{p}_{1o} = \bar{p}_{2o} = \bar{p}_{3o} = \bar{p}_{4o}, p_L \cong 1$
$\bar{c}_{1o} = 0$
$f_R(\bar{p})$ from Fig. 1
$k_F = 0.2(10)^6$ dollars
$f_L\left(\sum_i m_i k_i\right) = \left[0.1(10)^6 + 2(10)^6 \sum_i m_i k_i\right]$ dollars
$C_o = 15(10)^6$ dollars
$m_1 = 1$; m_2, m_3, and m_4 may be varied
$P = 0.95$

(See also Example 1.)

The values of m_i and $\bar{p}_i$ which provide the minimum C' were determined graphically by plotting C' for various values of m_i. Fig. 4 presents plots of C' for several values of m_i, including those giving the lowest cost. A cost tabulation for the minimum cost point of the two best sets of m_i for an integral value of n is presented in Table 2.

Comparison of the minimums for the no-redundancy case of Example 1, (1,1,1,1,) with (1,3,1,2) makes it readily apparent that a considerable cost savings is realized by the application of redundancies. Table 2 shows that little difference in total program cost exists between the (1,2,1,2) redundancy case, which requires three launches, and the (1,3,1,2) case, which requires only two to achieve the necessary probability of mission success; a significant difference does, however, exist in the program cost distribution.

Example 3

In this illustration a mission of 1,000 hours' duration is assumed with guidance and controls subsystems 1, 2, 3 (subsystem 1 being incapable of redundancy), a power supply subsystem 4, of very low complexities, and an instrumentation subsystem 5. The low complexities are assumed to illustrate application of the optimization model to developments reflecting advances in fabrication process technologies which may be realized in the next 5 or 10 years. The assumed values of all parameters are:

$s_1 = s_2 = s_3 = s_4 = s_5 = 1$
$t_1 = t_2 = t_3 = t_4 = 100, t_5 = 0.2$
$K_1 = 0.05, K_2 = 0.06, K_3 = 0.05, K_4 = 0.04, K_5 = 1.5$
$\bar{p}_{1o} = \bar{p}_{2o} = \bar{p}_{3o} = \bar{p}_{4o} = \bar{p}_{5o} = 0.55$
$k_F = 0.2(10)^6$ dollars
$f_L\left(\sum_i m_i k_i\right) = \left[0.3(10)^6 + 4(10)^6 \sum_i m_i k_i\right]$ dollars
$f_R(\bar{p})$ from Fig. 1
$C_o = 20(10)^6$ dollars
$m_1 = 1$; m_2, m_3, m_4, and m_5 may be varied
$P = 0.95$

Table 2. Cost Components for Minimum Total Cost Programs (Example 2)

Item	m_i: (1,2,1,2) n: 3	m_i: (1,3,1,2) n: 2
	Cost, Dollars × 10^{-6}	
Fixed cost (basic design development)	15	15
Fabrication and launch costs	15.7	11.6
Reliability improvement costs:	28.2	32.1
Guidance and controls		
Subsystem 1	(12.6)	(14.8)
Subsystem 4	(12.6)	(15.0)
Power supply (Subsystem 2)	(3.0)	(2.3)
Instrumentation (Subsystem 3)	(0)	(0)
Total	58.9	58.7

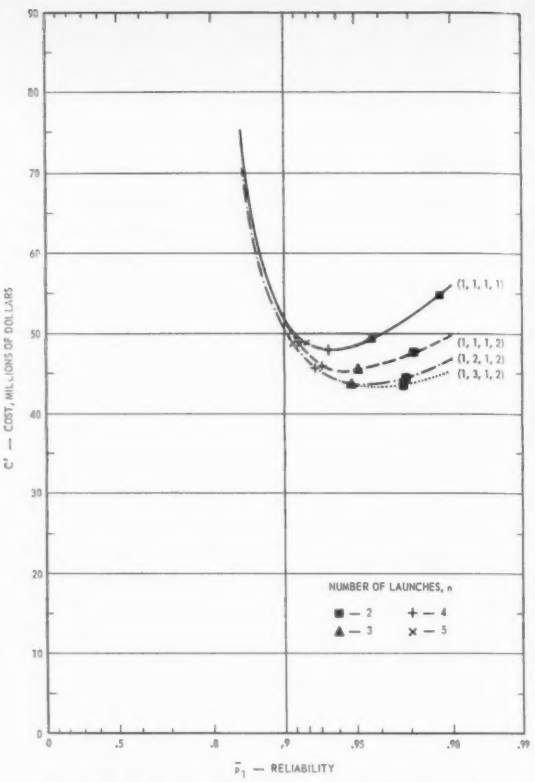

Fig. 4. Cost vs. reliability and redundancies (Example 2).

Plots of cost C' are shown in Fig. 5 for the no-redundancy case and the two lowest cost redundancy combinations, (1,3,3,3,1) and (1,3,3,3,2). The program cost breakdowns for the latter are shown in Table 3.

As was the case with Example 2, a cost savings is realized by the application of redundancies. The minimum program cost is obtained for the redundancy set (1,3,3,3,2), employing a single launching; the program cost indicated is $45,400,000. It is apparent that reliability improvement costs—$10,400,000, for this example—are much smaller than for the previous examples owing to the assumption of less complex subsystems. It should be recognized that the cost figures used for fabrication, launch, and basic development, though adequate for this illus-

tration, are hypothetical and may not be realistic for the type of mission assessed.

If the same subsystem performance requirements and associated complexities which exist today were required for this 1,000-hour mission, the resulting program cost would be in the $300–400 million range, assuming that the same fabrication and launch cost constants and factors apply.

Conclusions and Comment

Application of the reliability optimization model derived in the preceding section to three one-shot mission examples shows that considerable savings in overall cost are probable through such systematic trade-off calculations. It is believed, too, that the examples show that an effort in reliability improvement of considerably different magnitude than might be generally assumed is required for such missions. In the 60-hour mission example, the optimum reliability improvement effort was 50 percent of the total experiment cost and amounted to $32 million of a total cost of $63 million. This is believed to be more money than would usually be allocated to reliability improvement, even if one trial instead of the optimum number of four were optimistically planned.

Application of this approach requires use of the basic relationship between reliability improvement effort cost and the reliability resulting from this effort as shown in Fig. 1. It has already been pointed out that the Fig. 1 curve is calculated and extrapolated from actual, but somewhat limited, data. It should be noted, too, that, although the curve is applicable to other than "one-shot" projects, it is not applicable to some types of project. For instance, the specific Fig. 1 curve is not applicable to most airplane and some ground support system developments in which that portion of the reliability improvement effort concerned with disclosure of possible modes of failure—contributing a sizeable portion of Fig. 1 costs—can be largely absorbed in costs charged to training and actual operational testing.

Whereas the on-board redundancy model can be applied to "element" as well as "subsystem" standby redundancy possibilities, some modification should be made to allow for finite probability "switching" mechanism failures if applied to complex element-redundant networks. Also, as pointed out earlier, the improvement-cost vs. reliability-obtained curve of Fig. 1 is not precisely applicable to subsystems of too-small complexity. From strictly a cost standpoint, the model can be applied to cover consideration of manual "switching."

If the approach described in this paper is used in planning the development of "one-shot" mission projects, it should also be pointed out that such use should be recognized in the proposal request initiating the project. That is, the requester either should perform the optimization calculations and then specify the resulting number of vehicles to be launched, general on-board redundancy requirements, and the magnitudes of subsystem reliability improvement programs, or else should specify the required probability of experiment success and require that the bidder furnish and justify the optimization plans.

Table 3. Cost Components for Minimum Total Cost Programs (Example 3)

	m_i:	(1,3,3,3,1)	(1,3,3,3,2)
	n:	2	1
Item		Cost, Dollars × 10^{-6}	
Fixed cost (basic design development)		20	20
Fabrication and launch costs		17.5	15
Reliability improvement costs:		9.1	10.4
Guidance and controls			
Subsystem 1		(3.6)	(4.2)
Subsystem 2		(2.3)	(2.7)
Subsystem 3		(1.9)	(2.0)
Power supply (Subsystem 4)		(1.3)	(1.5)
Payload (Subsystem 5)		(0)	(0)
Total		46.6	45.4

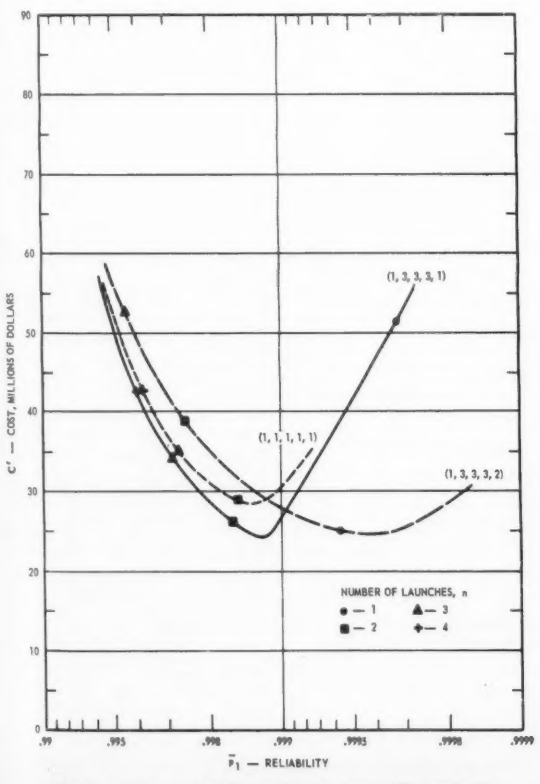

Fig. 5. Cost vs. reliability and redundancies (Example 3).

Reference

[1] Moskowitz, F., and McLean, J. B., *Some Reliability Aspects of Systems Design*, IRE Trans. on Reliability and Quality Control, Sept. 1956.

Radioisotope Auxiliary Power (Continued from page 9)

Table I. Typical Radioisotopic Heat Sources

Nuclide	Mode of Decay	Half Life	Fuel Form	Density (g/cc)	Power (Thermal) (watts/cc)	Power (Thermal) (curies/watt)	Estimated Costs ($/watt) Current	Estimated Costs ($/watt) Projected
Po^{210}	alpha	138 days	Po	9.3	1,320	31.2	—	—
Cm^{242}	alpha	162 days	Cm_2O_3	11.75	1,169	27.2	80*	45*
Pu^{238}	alpha	86.4 years	PuC	12.5	6.9	30.3	—	1,600
Ce^{144}	beta	285 days	CeO_2	6.4	12.5	128	87	14†
Pm^{147}	beta	2.6 years	Pm_2O_3	6.6	1.1	2,700	3,000	1,630†
Cs^{137}	beta	33 years	CsCl	3.9	0.27	320	500	54†
Sr^{90}	beta	28 years	$SrTiO_3$	4.8	0.54	153	455	23†

* Radiation cost not included (increase is @ $100/watt).
† AEC estimates based on construction of major separation facility.

research in this direction.

SNAP Devices

Research and development of isotope-fueled generators for use in space has been in progress since 1956. A well-diversified group of generator designs has resulted (Table 2): SNAP 3, a 2.8-watt, 6-month thermoelectric generator is now operational; SNAP 1A, a 125-watt, 1-year thermoelectric generator is in the advanced hardware stage; and a curium-242 fueled thermionic generator is also in the testing stage. Design configurations have been established for additional thermoelectric generators with power capabilities from 10 to 100 watts and operational lives up to 10 years. Table 2 lists generator specifications for several of the systems under development. Only SNAP 1A, SNAP 3, and Transit are described in some detail.

SNAP 1A Generator

SNAP 1A consists of a central fuel container supported by tubular truss members within two concentric shells. A cylindrical block of Inconel X, $3^3/_4$ in. in diameter and 11 in. long, contains the radioisotope. Seven thin-walled stainless-steel tubes loaded with ceric oxide pellets are inserted into holes drilled in the block. The loaded block may be transported separately in its own shipping cask and installed, with portable ground handling equipment, through a port in the generator at the launch site. Physical relationships are illustrated in Fig. 1.

Heat generated in the central source is radiated to the inner shell made of stainless steel. The inner shell serves as a hot junction for the thermoelectric elements installed between the shells. Unconverted thermal energy conducted through the elements and escaping through the insulation is radiated from the outer aluminum shell. Excess energy, resulting from the excess fuel loaded initially to compensate for isotope decay, escapes from an exposed area of the inner shell. Insulated shutters, actuated by a mercury vapor bellows, control the amount of exposed area as required to maintain a constant hot junction temperature.

Approximately 6,000 thermal watts would be produced by an initial load of 880,000 curies of cerium-144. Over a period of one year, the output will decay to 2,700 watts, the generator design output. The outer shell, 24 in. in diameter and 34 in. long, must be of sufficient area to radiate this energy to the space sink. At initial loading, 3,300 watts can be dumped from the exposed inner shell with the shutters completely open. A fibrous insulation, Min-K-1301, is used between the shells to minimize heat losses.

The SNAP 1A system uses 277 thermoelectric couples (P-N pairs) connected in series to produce 125 watts at 28 volts. Operating at a hot junction temperature of 1,000°F. and a cold junction temperature of 335°F, these elements attain a thermoelectric efficiency of 6.75 percent, which, because of the thermal losses through the generator insulation and structural members, decreases to an overall efficiency of 4.7 percent. Significant design characteristics are summarized in Table 2.

Cerium-144, a fission product, is the radioisotope heat source for which this generator was designed. It decays through beta emission, with a half life of 285 days, to praseodymium-144, which, in turn, decays through beta emission with a half life of 17.5 min. The third element in the decay scheme, neodymium-144, with a half life of 1.5×10^{15} years, is considered to be stable. The major source of energy is derived from the energetic beta decay of praseodymium. In addition to the decay gammas, a large portion of the photon radiation results from the slowing down of these energetic beta particles (bremsstrahlung).

To reduce the radiation level to a reasonable amount for ground handling purposes, sufficient volume exists between the heat source and the inner shell to contain approximately 4,000 lb of mercury. Because of the source and shell geometry, shield thickness and dose rates vary from point to point around the unit. With the mercury in place, radiation levels one meter from the generator surface would vary from 2 to 95 milliroentgens/hour and 11 to 750 mr/hour on the generator surface. The design radiation level 100 ft from the bare core is 22 roentgens/hour.

Two SNAP 1A units, using an electrical heater in lieu of a radioisotope heat source, have been constructed for test purposes.

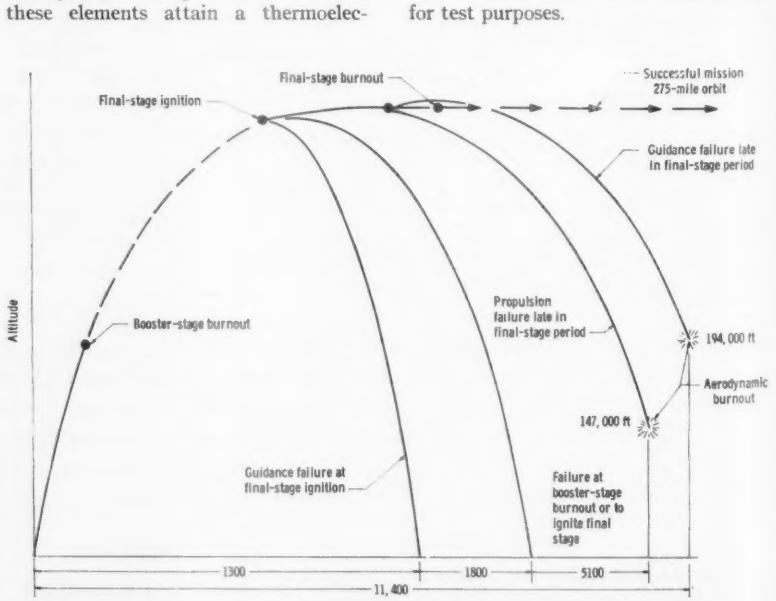

Fig. 4. SNAP 3 aborted mission.

Table 2. SNAP Generator Specifications

	SNAP 1A	SNAP 3	Satellite	SLLG*	HLLG†	SPG‡	TIPS**
Design power, watts	125	3	14.5	19	13	100	5
Design life (constant power)	1 year	90 days	5–10 years	6 mo.	2 mo.	6 mo.	3 mo.
Weight, lb	200	4	11.9	16.6	6.2	77	0.9
Initial thermal input, watts	6,500	70	260	655	370	7,500	120
Fuel nuclide	Ce-144	Po-210	Pu-238	Cm-242	Cm-242	Cm-242	Cm-242
Half life	285 days	138 days	89 years	163 days	163 days	163 days	163 days
Quantity	880,000 c	2,300 c	475 g	6.3 g	3.1 g	70 g	1 g
Voltage	28	3	3	3	3	28	0.7
Efficiency							
Thermoelectric	6.75	6.0	6.54	6.51	5.4	5.2	4.6
Device	4.7	5.75	5.5	4.8	5.2	5.0	4.2
Hot junction temperature, °F	1,050	1,050	900	1,000	1,400	1,000	2,240
Cold junction temperature, °F	335	300	235	370	458	490	1,110
Length, in.	34	5.5	7	8.4	6	21.5	2
Diameter, in.	24	4.75	12.5	7.5	2¾	19.5	2

* Soft lunar landing generator.
† Hard lunar landing generator.
‡ Space probe generator.
** Thermionic system (in conjunction with Thermo Electron Engineering Corp.).

SNAP 3 Generator

This device (Fig. 2) was the first to produce a practical amount of electrical power by direct conversion of the heat resulting from radioisotope decay. It was demonstrated at the White House on January 16, 1959. The characteristics of this unit are listed in Table 2.

Polonium-210, with a half life of 138 days, is used as the radioisotope heat source, and its thermal energy results almost entirely from the emission of a 5.3-mev alpha particle. A low-gamma emission coincident with a 4.5-mev alpha particle occurs in 0.0012 percent of the disintegrations. With no shielding other than the fuel-encapsulating material, the SNAP 3 dose rate is only 3.5 mr/hour at one meter. Mound Laboratory has provided the polonium for all generators fueled to date. Double stainless-steel capsules are inserted in a heavy-walled heat source cylinder. This cylinder is then closed with a threaded plug and sealed by fusion welding. In this unit, the thermoelements support the central heat source. (Minnesota Mining and Manufacturing Co. designed and fabricated the thermal-to-electrical conversion section.)

Three additional units have been fueled with various amounts of polonium, ranging upward to 2,320 curies. A maximum output of 4 watts at 4 volts has been attained with an efficiency of 5.75 percent. The last two units were subjected to over 2,000 hours of severe environmental testing prior to being fueled. Their operation has been satisfactory to date.

The output of SNAP 3 was given earlier as 2.8 watts, as opposed to the 4 watts stated previously. This is the result of two effects. First, in a space environment the isotope load must be reduced slightly to avoid overheating. Since radiation is the only method of heat transfer from the cold junction, its temperature increases slightly over that in air, causing a corresponding increase in hot junction temperature if the same thermal input is provided.

Second, the electrical output would fall off to approximately 1.8 watts over a 90-day period without some method of power flattening. A method of obtaining a constant output has been devised through tests in Martin laboratories. Conductivity of the Min-K insulation decreases rapidly at pressures less than one atmosphere. Thus, by introducing a conductive gas mixture of helium and hydrogen into the shell, the conductivity may be increased initially and then decreased by allowing the gas to leak to space. This conductivity change may be controlled, by proper selection of a fixed orifice, so as to be inversely proportional to thermal energy decrease. Initially, with a gas charge of one atmosphere, heat losses through the insulation are high, and generator output is decreased to approximately 2.8 watts. As this gas charge leaks out, generator efficiency improves so that a constant output is produced for a 90-day period.

Transit Generator

The Transit IV-A satellite (Fig. 3; see also Cover illustration), a development of the Applied Physics Laboratory of The Johns Hopkins University, is designed to produce constant frequency transmission to ships at sea for a minimum of 5 years. Through Doppler shift techniques, accurate navigational information is made available to such vessels. One of the major problems associated with this satellite was the development of a power source capable of meeting the 5-year life requirement. Early Transit satellites used solar cell

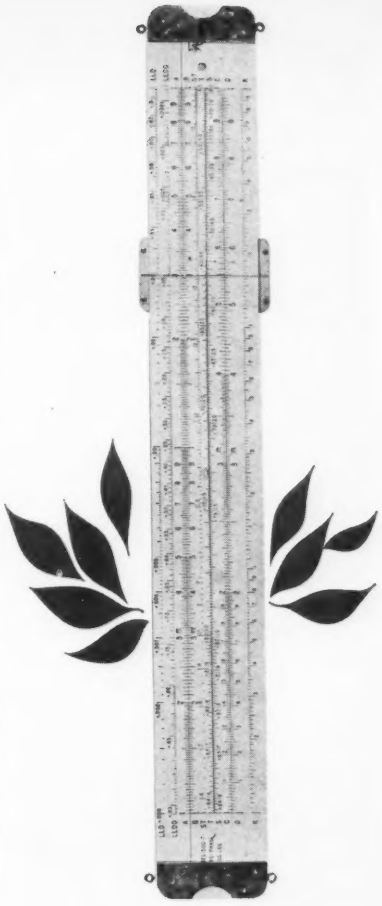

Creative minds thrive best where the climate is best

Lockheed-California Company proves this every day. For nowhere do Scientists and Engineers find a more creative, more stimulating, more academic climate.

In this environment Scientists and Engineers are encouraged to try the untried; to express new ideas; experiment, explore.

Small wonder Lockheed's future in *Spacecraft and Aircraft* is brighter than ever! **Scientists and Engineers** of initiative and talent will find it worthwhile to examine immediate openings in: Aerodynamics; thermodynamics; dynamics; electronic research; servosystems; electronic systems; physics (theoretical, infrared, plasma, high energy, solid state, optics); hydrodynamics; ocean systems; structural design (wing, empennage, fuselage).

Write today to Mr. E. W. Des Lauriers, Manager, Professional Placement Staff, Dept. 2611, 2415 N. Hollywood Way, Burbank, California. An equal opportunity employer.

LOCKHEED-CALIFORNIA CO.
A DIVISION OF LOCKHEED AIRCRAFT CORPORATION

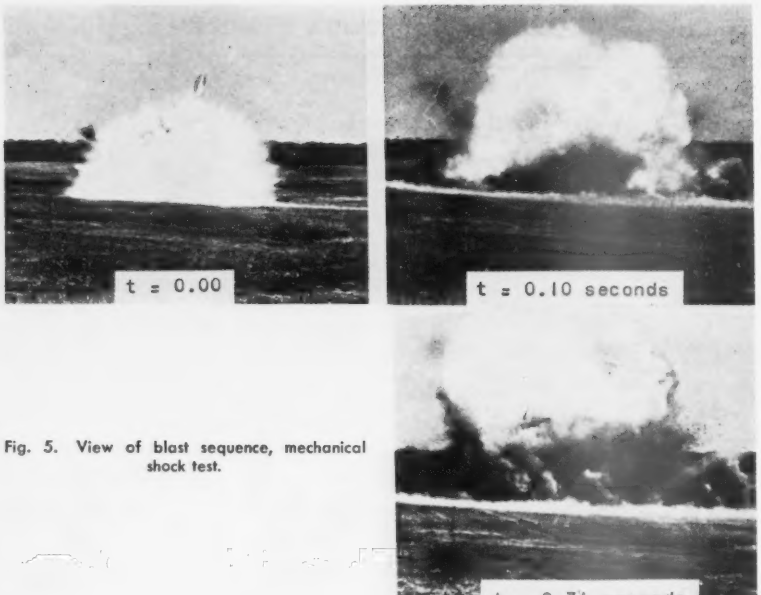

Fig. 5. View of blast sequence, mechanical shock test.

Fig. 6. Development of second Fireball 5 sec after ignition.

Fig. 7. SNAP 1A cores after successful impact on granite.

battery power supplies. The battery system, however, was required to go through many recharge cycles over the 5-year period and therefore presented a major reliability problem.

It was a natural development that the Transit program and the SNAP program should merge. It was decided that an initial system including a low-powered isotopic generator should be developed to demonstrate operational capability. The fuel selected for this mission was plutonium-238.

The generator system which finally evolved contains 1,600 curies of plutonium-238; it is $4^3/_4$ in. in diameter, $5^1/_2$ in. in height, and weighs only about 4 lb. The power output from the generator is 2.7 watts.

The operating voltages of the two transmitters powered by the radioisotope generator are considerably higher than the output voltage of the generator itself. Consequently, a d.c.-to-d.c. converter was designed and manufactured to provide the proper voltages. The tolerance permitted in voltage was ±5 percent with a maximum of 1 percent ripple. The converter provided met these specifications and is operating at better than 70 percent efficiency.

The generator-converter system was first subjected to flight qualification tests, which included vibration and thermal vacuum, simulating launch, and orbital conditions. It was then mounted on the satellite for flight acceptance tests. The system passed all tests.

Radiological Safety

One of the most significant factors in establishing the practicability of isotopic power for space applications is the assurance that can be provided for the radiological safety of operational systems employing such devices. During the ascent of a space vehicle, a great many abort conditions can take place. These may be defined in detail by analyzing a typical trajectory (Fig. 4), which may be divided into four fundamental phases:

(1) Failure at launch.

(2) Ascent failures.

(3) Final-stage or injection-stage failures.

(4) Orbital decay and re-entry before the design lifetime of the satellite in question.

The first phase involves those failures that can occur on the launch pad or shortly after launch and are usually of the type where fuel tank rupture occurs or guidance system failures require command destruct of the vehicle. In either case, two severe environmental conditions can occur—explosion of the unused fuel, and fire. The most severe fire or explosion occurs while the vehicle is actually on the launch pad and none of its fuel has been expended in flight. Generator fuel cores have been subjected to tests simulating these environments and have completely contained the fuel (Figs. 5 and 6).

The second type of failure is that which occurs during ascent of the vehicle to orbital altitudes. This range is considered to be above 10,000 ft up to the design orbital altitude of the vehicle in question. The most severe environmental condition that can occur during this phase of the trajectory is that of impact of the isotope core. The most stringent impact conditions occur if the injection stage fails to ignite. Maximum impact velocities are determined by the drag factor associated with the core in question but are generally of the order of 200 to 500 fps. The core impacts at its operating temperature, and impact can conceivably occur on any type of surface. With our present missile ranges, Vandenberg Air Force Base or Cape Canaveral, it is generally the practice to fire the missile system over large expanses of ocean area. Hence, the most probable impact location is the sea. Should this occur, the problem of salt water corrosion on the isotope core would be a major consideration. Impact on hard media such as granite can occur in the case of a misaligned trajectory where the command destruct system fails. The probability of this occurrence, however, is extremely low. The SNAP 1A, SNAP 3, and Transit cores have been tested in impact at Aberdeen Proving Ground's Supersonic Ballistic Sled Track. Target media ranged in hardness from water to granite. Impact velocities up to 500 fps at core operating temperatures were investigated. The cores successfully survived these experiments (Fig. 7). Sea water corrosion studies on fuel cores conclusively prove that the cores will not release the fuel until the activity level has been greatly reduced by the passage of time.

Final-stage failures occur when the injection or transit phase of the flight vehicle undergoes a propulsion or guidance malfunction. This results in

impact of the core far downrange. The area in which this impact can occur can be defined only by the missile system in question and the azimuth under which it is flown. Detailed trajectory analyses for the missions anticipated have been performed. These studies include aerodynamic heating occurring during re-entry, and determine the percentage of core burnup and the point of impact for propulsion failures and guidance failures.

The fourth condition involves orbital decay and re-entry of the SNAP device. This problem has been studied in detail by the SNAP Hazards Committee and the Aerospace Nuclear Safety Committee of the AEC. The basic design philosophy adopted by these committees is that, where impact can be controlled, it is desirable to contain the isotope. If, however, an orbital status is achieved and it is no longer possible to control the point of impact reliably, the fuel core should burn up to very fine particle size at very high altitudes—specifically, particles averaging less than 10 microns at altitudes greater than 100,000 ft. Detailed aerodynamic heating studies, coupled with plasma arc tests, have established that the three generator systems discussed here meet these criteria (Fig. 8).

When the fuel burns up at altitudes greater than 100,000 ft, the fuel debris behaves very much like weapon fallout—it is widely dispersed, and, when finally it does descend, it constitutes only a minor increase in the radiation levels already present on the earth's surface. In the case of SNAP 1A, these levels are approximately 5 millicuries/sq mile, in comparison with 2,000 millicuries/sq mile already present on the ground. The conditions for Transit and SNAP 3 are significantly less than this.

The test programs described briefly here have conclusively demonstrated the operational safety of the SNAP systems in question. Such tests will be repeated for all space systems to assure that they, too, can meet these requirements.

The Future

The problems confronting the users of radioisotope auxiliary power systems are primarily those of radioisotope availability and the practical upper limits of their power-producing capabiltiy. Their energy-production ability is currently in the order of only several hundred watts, although this may be boosted simply by using more than one generator in a single satellite—just as rocket engines are clustered to increase total thrust. As for availability, the problem is not so much one of quantities of radioisotopes as it is one of facilities for separating, purifying, and processing

WORLD'S MOST ACCURATE OPTICAL DIVIDING HEAD

VINCO GUARANTEES the Optical Master Inspection Dividing Head to be accurate within ± 1 second of arc; the ball bearing spindle runout to be 25 MILLIONTHS of an inch, total indicator reading; the master disc graduations to be spaced to an accuracy within ± ½ second of arc.

Shown above is a heavy duty dividing head and a dual recorder console with a ball slide electronic indicator stand. This ultra precision equipment will check and record tooth to tooth errors and accumulated errors to within 50 millionths of an inch on a 15″ D.P. gear. Single recorder consoles are available.

DIVIDING HEAD APPLICATIONS

- Inspection of missile guidance system components.
- Measurement of gear and spline spacing and bore relationships.
- Calibration of index plates, involute and master involute profiles.
- Calibration of lead bars or helical precision components.
- Inspection of two and three dimensional cams as well as ellipses, cycloids, etc.
- Measurement of angular transmission of motion by gears and gear trains.
- Measurement of angular displacement of turntables.

SEND FOR THIS FREE EIGHT PAGE BROCHURE. THE DIVIDING HEAD IS FULLY ILLUSTRATED AND EXPLAINED.

A 720 TOOTH, 32 D.P. 14½° P.A. PRECISION GEAR

Tolerances on this 22.500″ P.D. gear are .0002″ involute profile; .0003″ T.T.E.; .0006″ T.C.E. The same craftsmen who build the world's most accurate dividing head produce gears of even closer tolerances daily for use in missile guidance systems, jet aircraft, instrumentation or wherever needed. **Call Vinco on your sub-contract requirements.**

VINCO DIV., VINCO CORP.

9111 SCHAEFER HIGHWAY • DETROIT 28, MICHIGAN

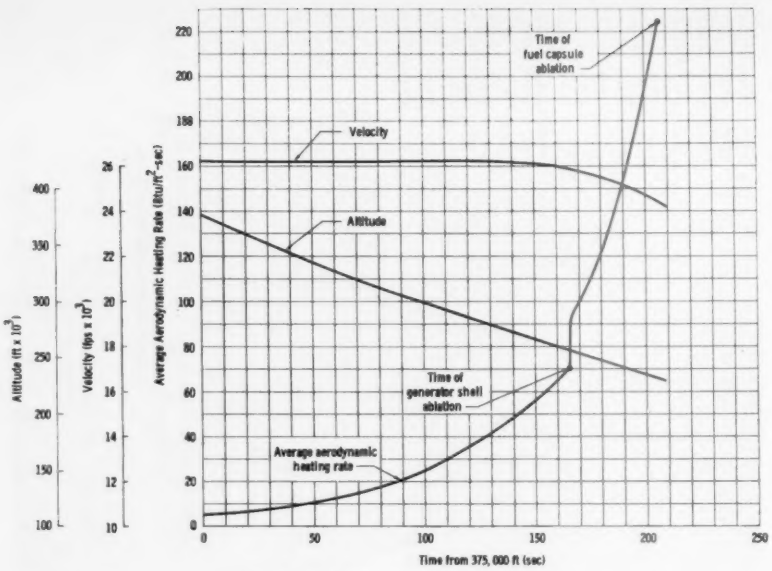

Fig. 8. SNAP 3 postorbital re-entry.

the active materials into forms useful for power applications.

Improvements in the technology of direct conversion will lead to higher temperature, more efficient thermoelectric materials allowing smaller fuel inventories, and systems of lighter weight. Thermionic technology, which is also developing at a rapid rate, offers these improvements plus the added factor of higher heat rejection temperatures. Within a dollar framework, these growth factors are reflected in Table 3. The fuel cost is considerably greater than the cost of the remainder of the power system.

Table 3. Cost of 100-Watt (e) Ce-144 Power Supply (1-Year Life)

System	Thermal Power (watts)	Curies	Fuel Cost ($)*
Thermoelectric, 5 percent efficiency (available today)	5,000	675,000	70,000
Thermionic, 13 percent efficiency (1965)	2,000	270,000	28,000

* Production cost.

Basic to the use of nuclear energy in space is the technical assurance that established safety criteria have been met. A considerable portion of the AEC-SNAP program has been directed toward establishing such criteria and subsequent testing of core, containment, and generator configuration for each system against these criteria.

Bibliography

[1] Barmat, Anderson, and Bollmeier, *SNAP III—Electricity From Radionuclides and Thermoelectric Conversion*, Nucleonics, Vol. 17, No. 5, 1959.

[2] Bustard, Thomas S., and Wilson, Robert J., *Applicability of Radioisotope Fueled Thermoelectric Generators as Power Supplies for Unmanned Soft Lunar Landing*, AIEE Aero-Space Transportation Conf., Philadelphia, June 1961.

[3] Morse, Jerome G., and Harvey, Douglas G., *Radionuclide Power for Space Missions*, Nucleonics, Vol. 19, pp. 69–72, April 1961.

[4] Seaborg, Glenn T., *The Transuranium Elements*, Nuclear Science and Engineering, Vol. 9, No. 4, pp. 475–487, April 1961.

[5] Snyder, Nathan W., *Power Supplies for Space Vehicles*, Astronautica Acta, Vol. 6, Fasc. 6, p. 271, 1960.

[6] Wilson, Robert J., *Operational and System Testing of SNAP 3 Thermoelectric Generator*, The Martin Co., Nuclear Div., RP-61-2-37, January 1961.

✦ ✦ ✦

CAI-IAS Joint Meeting Papers

Ottawa, October 23–24, 1961

61-214 The Use of Helicopter Support in Polar Operations—W. C. E. Loftus and J. P. Croal

61-215 Transpolar Jet Navigation—E. S. Pedersen

61-216 Naval Aviation in Antarctica—William H. Munson

61-217 Aircraft Landings on Ice—T. G. Dunkin

61-218 Flight Testing the C-130BL "Hercules" in the Antarctic—P. D. Gillich and H. B. Dees

61-219 Some Aspects of Cold Weather Testing and Operation of Aircraft—K. Weinstein

61-220 Commercial Experience in Cold Weather Operation—P. A. Hartline

IAS Member Price—$0.50 each **Nonmember Price—$1.00 each**

Order by number from: **Special Publications Dept., IAS, 2 E. 64th St., New York 21, N.Y.**

generated out of sheer desperation when Maj. Gen. W. Austin Davis, then Director of Hq AMC Procurement and Production Staff Office and now Commander of ASC, got tired of these periodic "crash" inquiries and "panic" operations and decided that "there must be a better way of doing things."

The Operations Research teams set up to develop this "better way" consisted of representatives from six of the major aircraft companies (Boeing, Convair, Douglas, Lockheed, North American, and Northrop) and of AMC and ARDC. The program was called the "WSPACS Study" (an acronym for *W*eapons *S*ystems *P*rograming *A*nd *C*ontrol *S*ystem), and represents the Operations Research study in scientific management techniques for decision making, although its final configuration differs somewhat from the simple "panic averter" that it started out to be.

It was planned originally that WSPACS would provide simply the mathematical model by which the Air Force could answer these "crash" inquiries without resorting to or disturbing the contractors whose programs might be affected, but the development of the tool has indicated even greater usefulness and illustrates the benefits of good Operations Research applications in management principles.

Before continuing, it should be explained to the uninitiated or novitiates in Operations Research that the term "mathematical model" represents simply a mathematical statement of equalities and/or inequalities in the relationships of the various parameters involved in the system described by the model and the constraints upon these parameters. It does not imply that the model is a single simple or complicated mathematical expression describing the system since it actually may consist of many mathematical statements, but the term refers to the group of mathematical expressions describing the system, its behavior, and in some cases, the manipulation of the system to achieve specific objectives such as optimization based upon certain ground rules.

With this introduction, let us approach the specific example of scientific management described herein in true Operations Research fashion by first defining the problem, then determining the inputs, parameters, and constraints, and then describing the model itself and how it is used in scientific management.

The Problem and the WSPACS Objectives

Within the total program complex under its jurisdiction, it is not easy for the Air Force to break its decisions regarding programs into small, independent packages, each of which relates only to a single program and is therefore easy to understand and manage.

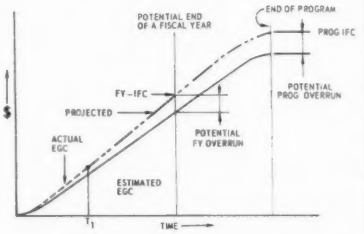

Fig. 4. Estimated vs actual expenditure growth curve.

Instead, there is a very strong interdependence between many of the programs in this complex, not only because any one of the programs may be in direct support of some of the other programs but also because of the relation of each program to the total force complex.

For example, decisions made on the B-70 program are not independent of the Atlas program because they are not only drawn from a common source of funds but their joint cost must not exceed fund ceilings. In addition, they at least partially replace each other in the weapons systems mix so that more of one means fewer of the other. If one system is delayed, maintaining continuity of deterring capability means that the other must be accelerated correspondingly. There are many other examples that indicate how decisions made in respect to one weapons system affect one or more other weapons systems and, hence, must be considered in management decision-making. Therefore, WSPACS must provide decision-making information not only on the individual weapon system but also upon the total program complex.

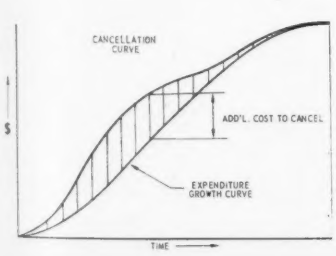

Fig. 3. Cancellation curve.

NEW
STRAIGHT WALL
TANTALUM
CAPACITOR
CAN'T LEAK

Meets MIL C 3965-B, Style CL-64, CL-65.

A new space-saving approach to the design of wet tantalum capacitors ends mounting problems encountered with flanged types and yet will not leak.

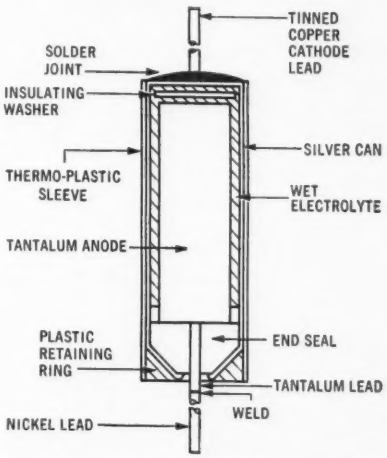

ITT's compact, sintered slug tantalum capacitor features a wedge-shaped seal held under compression by an epoxy retainer ring formulated for thermal characteristics inverse to those of silver. Ordinary, straight-wall capacitors leak along the lead when elastomer compression is reduced as the silver can expands. Not so with the new ITT design!

This new, compact capacitor conforms to specifications MIL C 3965-B, Style CL-64, CL-65 and provides both the compactness and rugged reliability required in missile, airborne and mobile equipment. For details, write today requesting Bulletin No. 610.

ITT
CAPACITOR DEPARTMENT
COMPONENTS DIVISION
INTERNATIONAL TELEPHONE AND TELEGRAPH CORPORATION, PALO ALTO, CALIFORNIA

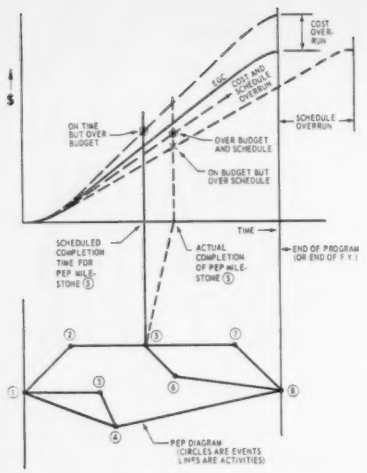
$
COST OVER-RUN
EGC
COST AND SCHEDULE OVERRUN
ON TIME BUT OVER BUDGET
OVER BUDGET AND SCHEDULE
SCHEDULE OVERRUN
ON BUDGET BUT OVER SCHEDULE
TIME
SCHEDULED COMPLETION TIME FOR PEP MILE-STONE ⑤
ACTUAL COMPLETION OF PEP MILE-STONE ⑤
END OF PROGRAM (OR END OF F.Y.)
PEP DIAGRAM (CIRCLES ARE EVENTS LINES ARE ACTIVITIES)

Fig. 5. Progress vs cost performance.

Stated broadly, the WSPACS model must provide the decision-maker with a system for obtaining better program and reprograming data, for assessing rapidly the impact of alternate decisions upon program variables, and for detecting real or potential deviations from planned programs in time to make adjustments. In other words, it must provide the Air Force management with a broad planning device and provide the USAF and industry with a means of maintaining control and surveillance over the expenditure of their development and production moneys.

The WSPACS is a man–machine operation. The concept is that a body of data supplied by the various USAF contractors will be stored in a computer. These data will represent the current Air Force program and, in addition, information that will permit the Air Force to estimate development and production costs, system-connected costs incurred as a result of introduction of weapons into the inventory, and various other types of pertinent information. When a reprograming requirement arises, management will input into the computer a reprograming action which they consider most desirable in the face of the reprograming requirement.

In a relatively short time, the computer will return to management the results of the proposed action. If the solution is not feasible because it calls for expenditures above the current or projected limitations, additional suggested solutions may be attempted until one is found which satisfies all financial and other constraints and, in addition, is compatible with management's decision with respect to a desirable USAF structure.

It must be remembered that WSPACS, like any other mechanized, "scientific" management system, will be a decision-aiding and not a decision-making tool. It will accept relatively large amounts of information and manipulate it according to the rules and constraints built into the model, but the results will be given to management for evaluation and revision.

This really constitutes a "man-machine feedback" scheme that yields an iterative technique for reaching decisions through the use of simulation. In other words, the manager again and again imposes new restrictions and constraints, lets the machine operate using its store of data and logical procedures, and views the outputs. The results of the computations are predictions of the conditions that would exist for the specific management plan under the current situation data.

Based upon these results, the manager can modify his plan, let the machine simulate the real world situation again, view the new results, and again modify the plan as necessary. Thus, he iterates toward or "homes in on" a solution

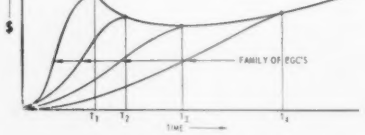

Fig. 6. Time-cost (T/C) curve for any quantity.

which, if not best, is at least acceptable to him.

It must be remembered that the WSPACS system is not meant to be a day-to-day administrative tool but rather a reprograming tool suitable for fiscal and force structure planning but with not enough precision to provide detailed budgets and contractual figures. Thus, WSPACS should be considered purely as a broad planning tool in which any estimates provided are only carried to within "order of magnitude" limits. This is an extremely important point and should be emphasized because additional and more detailed planning is required before final decisions with respect to specific numbers of dollars to be allocated or committed can be made.

Stated in greater detail, the WSPACS model will provide to the Air Force manager answers to the following areas of "What if . . . ?" questions:

(1) The cost implications of stretch-out, acceleration, or cancellation of a program.

(2) The time implications of reducing or increasing the rate and/or amount of total program expenditures.

(3) The time and/or cost implications of a change in the number of end products or in the objectives of a program.

Such data from each of the contractors on each of their programs will provide the information for a simulation model that can be manipulated in accordance with strategic or tactical constraints in time and/or cost and which will then provide information to the decision makers on the effects of the proposed changes in programs not only on the remaining programs but also upon the various time and budget constraints under which the Air Force must operate. This simulation or gaming model is referred to hereafter as the "total" or "reprograming" model since its function is to permit prediction of the effects of reprograming upon controlling variable parameters.

There is one other phase of the WSPACS model that is developed from the input data described above as well as other data which describes the relationship of cumulative dollar expenditures to physical program progress. This input will provide both to the contractor and to the Air Force as the customer, periodic and timely indications of controlled performance or potential "out-of-control" conditions that will require either control action by the contractor or reprograming action by the Air Force. Since this component of the WSPACS model is the one that raises a warning flag to direct attention to the need for action, it is referred to hereafter as the "early warning" model.

The Inputs

The minimum that the problem will accept as inputs is information regarding the following variable parameters and their interrelation:

From the Contractor

(1) Time schedules for performance.

(2) Estimated and actual costs as expenditure rates.

(3) Cancellation costs.

(4) Quantity of end products or

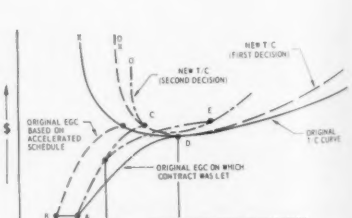

Fig. 7. Effect of reprograming on T/C curve.

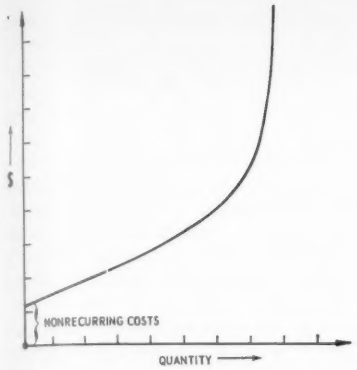

Fig. 8. Quantity-cost relationship (for constant time).

scope of a research and development task.

(5) Performance milestones to be reached in the program.

From the Customer

(1) The planned budget ceilings for the expenditure rates of all programs in the program complex.

There are other factors than the aforementioned that should appear in a complete overall model, particularly if the model is to develop true optimization. These include:

From the Contractor

(1) Anticipated reliability factors.
(2) Constraints based on contractor capabilities.

From the Customer

(1) The relative priority of the various programs.
(2) Potential modifications of the program or end products.
(3) The "value" of the program.
(4) The defense posture (including the weapons systems mix) based on economic, political and strategic considerations.
(5) Training effort required for the program.
(6) Logistics support and facility construction required.

Although subsequent and more sophisticated versions of the WSPACS model will take into account more of the latter factors, the initial version of the model will consider only the minimum inputs described.

The first of these input data is the rate of expenditure curve which usually is of the form indicated in Fig. 1. Any well-managed contractor will develop such a curve in planning a program whether it is a direct contractual requirement or not because this is a natural factor in planning the pursuit of any proposed program from a basic research program to a follow-on production program or any combination between these two extremes.

The data in the expenditure rate curve can be accumulated in a form that indicates the total estimated cost of the program as a function of time, as shown in Fig. 2. This curve is usually referred to as the cumulative expenditure or expenditure growth curve and is very important in the WSPACS concept as the basic curve relating most of the other WSPACS factors.

For example, this expenditure growth curve is also the basis for the "cancellation" or the "termination liability" curve, which is of the general form shown in Fig. 3. This curve can be estimated in advance as a function of the estimated expenditure curve and then maintained in relation to the actual expenditure growth curve.

By continuously plotting the actual expenditure growth curve against the estimated and projecting the actual growth curve to an Indicated Final Cost (IFC), the contractor and the Air Force have an indication not only of cost performance in comparison with the planned performance at any time but also a warning flag that indicates a potential out-of-control condition that will exist at some future time, the probable degree of this perturbation, and the need for immediate action to obviate the threatened condition. (See Fig. 4.)

This expenditure growth curve can also be utilized to correlate performance and cost where performance is measured by the activity and event network (like a precedence matrix) such as that provided by the PERT (Navy) or PEP (Air Force) concept of performance evaluation. Fig. 5 indicates such a relationship using an over-simplified PEP network and shows how this provides another tool for management by raising warning flags that a potential out-of-control condition exists or is threatened. This is the PEPCO concept.

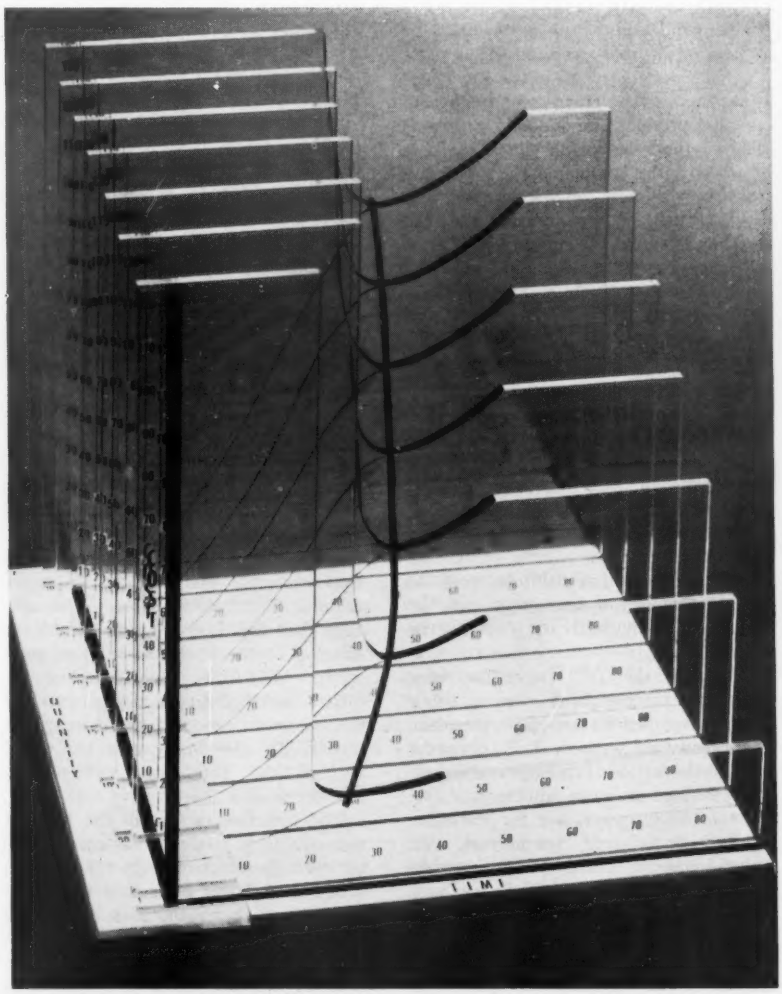

Fig. 9. Three-dimensional model of T/Q/C (time-quantity-cost) relationship as it exists at the beginning of a contract.

There is another relationship between time and cost in the performance of a contract that is not generated normally by contractors in estimating and planning proposed work but which is necessary in providing data for the WSPACS model. This is the time–cost (T/C) relationship for any particular program or quantity of product and has the general shape shown in Fig. 6. This is a curve that compares the cost of pursuing a certain task (whether it be a research program or the production of a specified number of end product items) to the time within which that same task is completed.

In a sense, the T/C curve is the locus of the end point of a family of expenditure growth curves (EGC) as indicated in Fig. 6, or, in other words, as generated by the EGC waving around the origin. It is important to recognize that the T/C curve is not a *static* curve but is a very *dynamic* curve which changes as a function of time after go-ahead of a contract. Once a particular EGC and, therefore, a point on the T/C curve has been selected and some work performed, the original T/C curve ceases to be valid and a new curve must be generated if reprograming occurs at any time during the life of the contract.

Assuming that there is no change in the end product and the only change is that of the time within which the program is to be completed, Fig. 7 shows the effect of first, an acceleration and subsequently a deceleration of the program on the T/C curve (which actually is a shrinking curve and physically culminates in a single point at the end of a program).

It is logical to believe that the T/C curve has a vertical asymptote which represents the minimum time within which a program can be completed regardless of cost. Experience, in turn, indicates that the T/C curve usually is relatively flat near the optimum or minimum cost but does rise again as the time is increased beyond that required for minimum cost. There would appear to be some relationship between the rise of this leg of the curve and the fixed costs involved in a particular program.

Although the T/C curve has been discussed as though it were a single curve developed for an entire program, there really are separate T/C curves for each of the various functions and operations that go to make up the performance of a program, as, for example, engineering, tooling, production, etc. In addition, the T/C relationship exists for the various components of a weapons system or of the air vehicle such as the airframe, propulsion unit, etc. In other words, there is an actual matrix of T/C curves for any total system, although, for simplicity, we shall continue to refer to a T/C curve for the total system, keeping in mind that the total system is comprised of many elements.

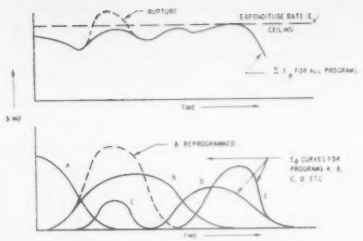

Fig. 10. AMC cumulative expenditure rate curves.

There is a similar relationship that exists between the quantity of product produced and the cost for any specified time of performance, and this curve has the general shape shown in Fig. 8, although there may be certain discrete discontinuities that are a function of contractor capabilities in tooling, equipment, and manpower. Reprograming changes in the Q/C relationship for any specified time will depend upon the number of products produced up to that time and upon a number of factors such as the status of the tooling, plant capabilities, manpower, etc.

Obviously, the time-quantity-cost (T/Q/C) relationship produces a three-dimensional surface which reprograming affects like a shrinking universe that ultimately winds up in a single point in space. Fig. 9 is a photograph of a three-dimensional model of this T/Q/C relationship as it exists at the beginning of a contract. Similar models could be prepared for this three-way relationship at any point in time in the performance of a contract.

The Output

From the standpoint of the individual programs, the PEPCO correlation and the IFC projection yield outputs that give warning of existing or potential out-of-control conditions requiring action by contractor management or reprograming by the Air Force. The only time that the total program complex is affected by the Early Warning segment of the WSPACS model is when the contractor's inability to regain control of the program necessitates reprograming by the Air Force and hence the use of the total or reprograming model.

The principal output of the total or reprograming model is a comparison between the costs of the total program complex and the budget ceilings prescribed by higher authorities. The total expenditure rate generated by all of the Air Force programs must lie below the expenditure rate ceiling as indicated in Fig. 10. If, at any time, this ceiling is ruptured by the acceleration, deceleration, or cancellation of a single program or group of programs (as indicated by the dotted conditions in Fig. 10), then action must be taken by the USAF in order to bring the monthly rate of expenditure back under control.

This action is the simulation of a new program complex and the determination by the WSPACS model of whether the proposed reprograming (such as acceleration, deceleration, cancellation, or change in quantity) causes a rupture in the budget ceiling.

By repeated simulated reprograming or gaming, it is possible to arrive at a new program complex that will meet all of the requirements of military policies and philosophies and will not rupture the budget ceiling. It is even possible by this trial-and-error method to arrive at a reasonable optimization in which the proposed program complex will not only not rupture the budget ceiling but will accomplish the Air Force's objectives at minimum cost. However, it is possible to develop the model in such a way that it will perform automatically the iterative processes of optimization within the constraints defined by management.

Similarly, this total reprograming model of WSPACS can be used to determine whether a new proposed program not yet in the Air Force program inventory, will cause a rupture in the budget ceiling and, if so, how it can be fitted into the budget by proper reprograming of the existing programs.

The Model

As explained before, a number of the desirable variables or parameters that should be included in the WSPACS model have been frozen or limited in the initial study in order to accelerate the study and avoid too much complexity. Even so, it is necessary, in order to get a useful model for the Air Force, to cover at least one major segment of the total weapons system responsibility. In this case, the segment chosen is the air vehicle consisting of the airframe, the propulsion, the electronics or guidance, and the ground support equipment. The model must be capable of handling each of the components of this segment of the weapon system.

Furthermore, the model must be capable of embracing any segment of the time period from planning for source selection through production and follow-on, with some consideration for the span of time when operational use of the weapon causes a significant cash drain for training and ground support.

In order to develop a model of such complexity and magnitude, it was necessary to first consider only one component of the air vehicle—the airframe, and its counterpart, the missile frame. Having once developed the model for the airframe, it is expected that this can be

extrapolated to the other components of the air vehicle.

In developing the input section of the reprograming model, it became evident that there are many elements involved in this model (such as basic engineering, sustaining engineering, basic tooling, sustaining tooling, experimental flight testing, production flight testing, manufacturing, etc), each of which may have its own manpower loading curves and learning curves for the performance of work.

Since these may have different characteristics and do not all start simultaneously, or have the same rate of rise and/or spread, it is not possible to normalize these curves to single curves for all elements. Accordingly, it became obvious that the model must include a summation of several such components.

However, in considering the manpower loading curve and learning curve for these various components in an airframe or missile frame program, it was found possible to group some of these of sufficient similarity and to make certain assumptions regarding the definition of these various components as a function of time or point in the performance of the contract. Obviously, the summing of component information in arriving at the total model has definite advantages in setting up the model because it allows the operator to sum only those components that are applicable to a specific type of program. For example, a research and development program would include basic engineering and might include experimental flight testing but would not include maintenance or sustaining engineering, tooling, or production.

A production program would include all of the components involved in any type program and would involve, then, the summation of all of the elements. A follow-on program would not include basic engineering or basic tooling, experimental flight test and other elements of research and development phases of the work, but would include only the balance of the production operations or components. Thus, the summed-component approach to the input model permits its adaptation to any type of program whether it be a follow-on, production, or strictly research and development.

In developing the model for the summed-component approach, two courses were followed—one empirical and one analytical. The empirical course attempted to reduce historical data to a mathematical model capable of analysis and application to the various types of programs in the Air Force complex.

The analytical model attempted to find an analytical expression for the various elements of a program and then prove the validity of the mathematical expressions by their application to existing programs or proposals for programs.

Although an empirical approach to the problem was found and an expression derived which could serve as the input model to WSPACS, it was not possible to ascribe analytical significance to each of the terms involved in a meaningful way. Accordingly, despite the apparent validity of the empirical expressions for a number of different types of programs, there was some doubt as to the universal application of this type of solution without some means of analytical verification, and this approach was dropped.

On the other hand, the analytical approach was readily adaptable to the summed-component philosophy and the mathematical model is currently complete and ready for testing (although it must first be programed for large-scale computers in order to perform the necessary testing). In this analytical model, suitable manpower loading curve and learning curve data have been developed to satisfy the variations in the use of such data by each of the six companies represented and present a reasonable approximation of a standard set of curves for the industry.

However, it is not to be implied that each of the manufacturers represented used the identical curve except in contour and configuration because each will have his own factors and coefficients that apply to the equation describing the curve or curves.

It has been generally accepted by the group that T/C relationship can best be approximated by a regular hyperbola with its vertical asymptote defined by the minimum time within which the program can be completed regardless of cost, and its horizontal asymptote related to the fixed costs for each program and each manufacturer.

The total or reprograming model has been developed so that it can accept and utilize these inputs, test for input compatibility with the constraints imposed upon the reprograming model, determine whether the expenditure rate ceiling is ruptured by the proposed reprograming and, if not, what the remaining budget will be, and even find a minimum total cost solution based upon predetermined information by management.

For this total model, industry would provide to the Air Force for each weapons system:

(1) An estimate of the expenditure rate to produce any particular number of units of that weapon system given a go-ahead date and a delivery date.

(2) An estimate of the liability commitment rate or cancellation costs to support an expenditure rate.

(3) A set of industry restrictions on the quantity, go-ahead date, and end delivery date dictated by conditions peculiar to that contractor.

Also, the reprograming model would require inputs from the USAF, three of which apply specifically to each of the weapons systems to be considered and two of which describe the monetary restrictions imposed upon USAF spending by Congress:

(1) An estimate, for each weapon system, of the future expenditures by the Air Force as a result of the expected expenditure rate necessary to obtain the inventory of that weapon system based on the original go-ahead and completion dates.

(2) A set of military restrictions on the values of the weapons systems parameters consistent with WSPACS.

(3) A set of functions indicating the relationships between weapons systems or between weapons systems and supporting systems.

(4) An estimate of the USAF expenditure ceilings related to time.

(5) An estimate of nonsystem USAF expenditure rates for such things as overhead, training, etc.

Each of the variables (quantity, go-ahead date, and completion date) has two sets of restrictions imposed upon it—one set provided by industry and the other by the Air Force. The industry restrictions have to do with such things as its production capacity and the accuracy of the expenditure rate estimates. The USAF restrictions deal with defense requirements and/or relationships among weapons systems. Inasmuch as these restrictions are provided for different purposes, it is conceivable that they may be in conflict on occasion. Therefore, the WSPACS reprograming model should first check for consistency in order to avoid wasting valuable time.

The next step in the use of the reprograming model is to develop the relationship of the total expenditure rates for all programs in the program complex to the budget ceiling at that time. If all program changes have been selected so that there is no overrun or rupture of the budget ceiling, then a feasible solution exists and the reprograming is acceptable.

If, however, there is a rupture of the budget ceiling and the proposed reprograming is incompatible with the moneys available, then the model can be used again for alternative reprograming until a satisfactory solution has been arrived at. However, it is desirable to have the model accommodate a program of repeated reprograming without having to go in and out of the computer with each potential solution.

This is an "idea-testing mode" of operation in which the failure of the proposed programing to satisfy the constraints in the model would cause

the transfer of the computer to the "idea-testing mode" of operation in which USAF management could experiment with various changes in reprograming and observe the effects of these changes on the expenditure rate of the total complex. Allowed changes would include changes in weapon system quantities, delivery times, and cancellation.

While in this mode, none of the initial input to WSPACS would be changed but, once USAF had decided upon a change, the computer would accept the change, estimate its effect upon the budget ceiling, and return to management information for subsequent proposed changes in the simulation gaming.

The foregoing might well complete the first phase of this initial WSPACS study of scientific management techniques for the Air Force, but these techniques permit the development of even greater usefulness to Air Force management. For example, at the end of the effort described, we will have arrived at any one of the following situations:

(1) All compatibility tests have been satisfied and a set of values has been found for all programs which cause no overrun and which were found without using the Idea-Testing Mode. In other words, for a compatible set of USAF–Industry restrictions, a feasible solution exists.

(2) All compatibility tests were satisfied and a set of values found for all programs which cause no overrun but the Idea-Testing Mode was used.

(3) The Idea-Testing Mode was used, all low priority programs have been cancelled, all remaining programs have been cut to minimum quantities, but an overrun condition still exists.

Following these conditions, the model might develop a solution in which optimization takes place according to management-chosen criteria. For example, a total program complex might be determined that will affect maximum reserve funds by minimizing the total expenditure rate, that is, one that optimizes the program complex to minimum cost.

Another optimizing procedure that might be effected would be for the model to determine that program complex which would utilize all of the available moneys without overrunning the budget ceiling.

Finally, even when the Idea-Testing Mode is used and a feasible solution is not found, the model can still be used to give USAF management and answer to the effects of pursuing the only two courses open to it—that of cancelling some of the high-priority weapons systems or approaching Congress for more funds.

Subsequent Course of WSPACS

The completed model as accepted by the Air Force and industry will be programed for large-scale electronic data processing equipment and will be tested by the various USAF contractors in an attempt to fit it to their past, present, and future operations and test the validity of the WSPACS model concept. This means the application of their own coefficients and factors that will make the model applicable to their particular programs and company operations.

When the model has thus been proved or modified to fit realistic conditions and accepted by both the Air Force and industry, an investigation will be made into the current methods of data acquisition and presentation for all AMC (AFLC) contractors. This is necessary because some of the data needed for WSPACS is currently in other Air Force reports while some of the data has never been reported. Obviously, one of the objectives of WSPACS will be to attempt to reduce the total amount of reporting to the USAF rather than increase it so that the WSPACS report will include not only the data necessary for its use by the Air Force as a management tool but also will include any other data currently covered by other related reports.

It is conceived that WSPACS will have usefulness at every level of Air Force weapons systems management from Hq USAF to major contractors. Each level will look at different aspects in more or less detail but it is assumed that the picture will appear more and more in aggregate as the decisions to be made become broader in their scope. Hq USAF, with ultimate Air Force responsibility, will make use of the overall model covering all weapons systems and stressing the budget implications. The AFLC and ARDC will use parts of this model to recommend decisions to Headquarters and will also look at more detail (through the WSPO) for planning within given systems. Industry, which supplies most of the event-activity-cost data, will look at reprograming as it affects each individual company's participation in the program.

When all of the elements of the weapons systems programs have been incorporated into the WSPACS concept and made capable of being applied as true management tools for the USAF, the final step will be the incorporation of the visual display so that management can perform its simulation or gaming in a manner that will permit the most effective utilization of this scientific management tool in scientific management decision making. This is as near the ultimate in man–machine relationship as we care to go since there must be reserved to man those decisions requiring human judgment that cannot be built into machines.

✦ ✦ ✦

Change of Address

Since the Post Office Department does not as a rule forward magazines to forwarding addresses, it is important that the Institute be notified of changes in address 30 days in advance of publishing date to ensure receipt of every issue of the *Journal* and *Aerospace Engineering*.

Notices should be printed legibly and sent directly to the Institute of the Aerospace Sciences, Inc., 2 East 64th Street, New York 21, N.Y.

✦ ✦ ✦

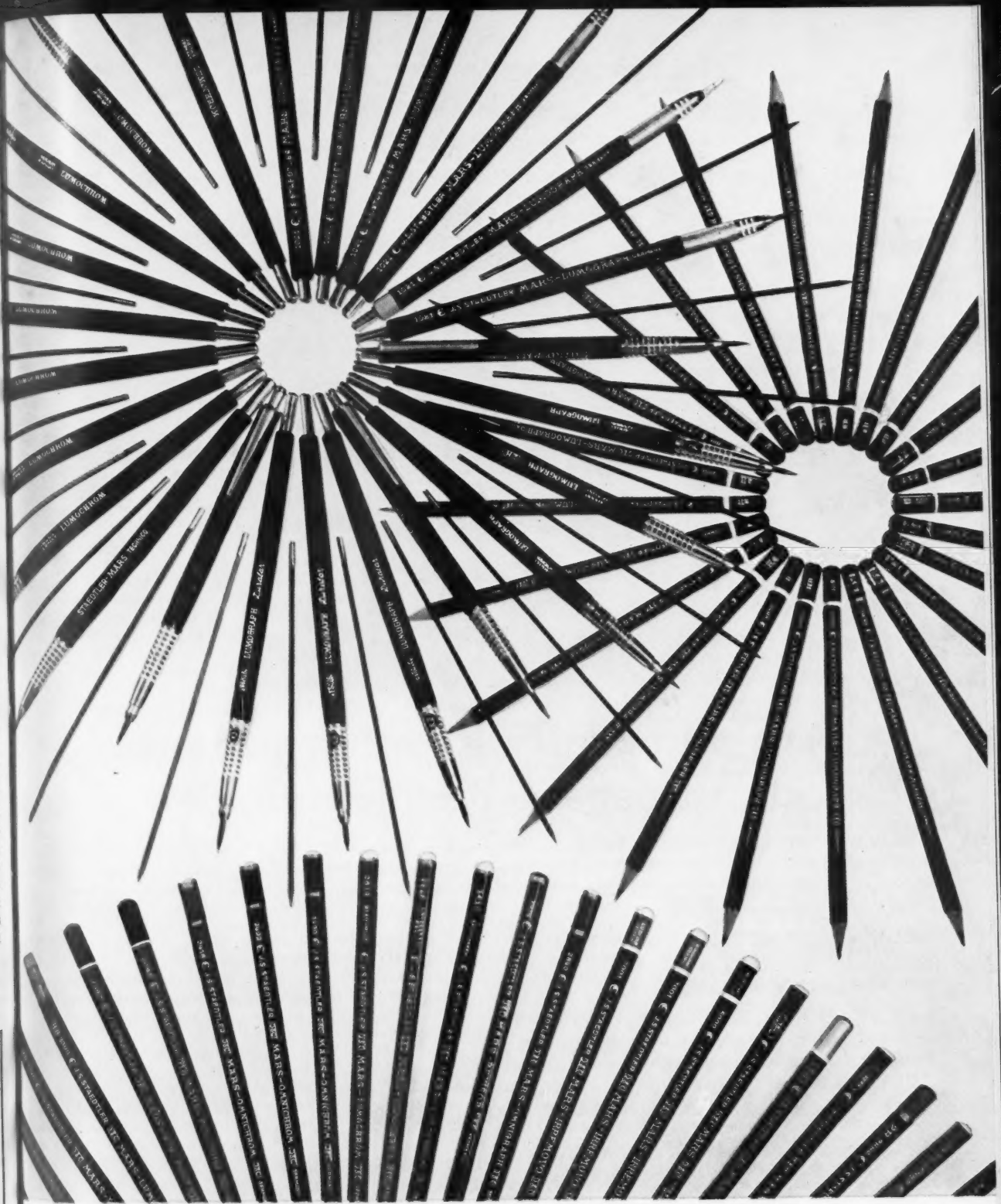

ALL MARS – ALL TOPS

.... all imported from West Germany, made to meet the highest standards of professionals.

the pencil that's as good as it looks

MARS

J.S. STAEDTLER, INC.
HACKENSACK, NEW JERSEY

Mars products are available at better engineering and drafting material suppliers everywhere.

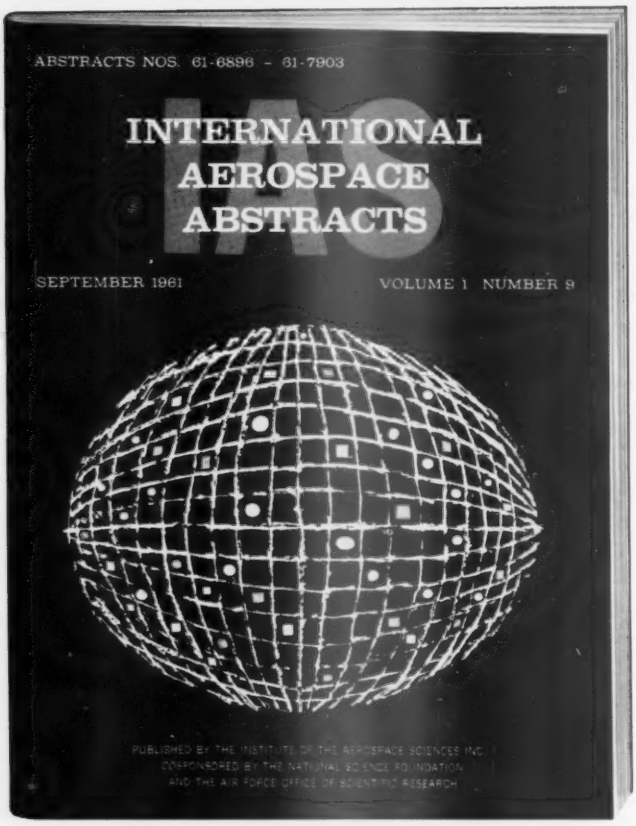
ABSTRACTS NOS. 61-6896 - 61-7903
INTERNATIONAL AEROSPACE ABSTRACTS
SEPTEMBER 1961
VOLUME 1 NUMBER 9
PUBLISHED BY THE INSTITUTE OF THE AEROSPACE SCIENCES INC.
COSPONSORED BY THE NATIONAL SCIENCE FOUNDATION
AND THE AIR FORCE OFFICE OF SCIENTIFIC RESEARCH

Are you really keeping abreast of aerospace developments?

Today's aerospace technology moves *fast*. Every forward-looking engineer and scientist *must* know the results of all aerospace research related to his own work *wherever accomplished*.

INTERNATIONAL AEROSPACE ABSTRACTS is ideally suited to help you with this task—made enormous by an avalanche of publications.

INTERNATIONAL AEROSPACE ABSTRACTS saves you time. Each monthly issue gives you about a thousand abstracts of the latest reports, articles, meeting papers, and books—selected because they *are* important to aerospace technology. You can immediately put your finger on the work being done in your field. COVERAGE IS WORLD-WIDE.

INTERNATIONAL AEROSPACE ABSTRACTS is cosponsored by the National Science Foundation and the Air Force Office of Scientific Research. For detailed information on this indispensable R & D tool, write to the address below.

Enter Your Subscription Now!

INTERNATIONAL AEROSPACE ABSTRACTS
2 East 64th Street, New York 21, N. Y.

Please enter ___ subscription(s) for the year 1962 at the following rates:

- ☐ Individual IAS Member Rate – $20/yr
- ☐ Corporate IAS Member Rate – $40/yr
- ☐ Nonmember Rate – $60/yr
  - ☐ Payment is enclosed.
  - ☐ Please send bill.

Name_____ Title_____

Company_____

Address_____

City_____ Zone_____ State_____

INSTITUTE OF THE AEROSPACE SCIENCES, INC.

X-15 Flight Simulation Program (Continued from page 17)

major research objectives of the X-15 program include hypersonic stability and control at low dynamic pressure, aerodynamic heating, exit from and re-entry into the atmosphere, and simulation. In these areas flight experience is needed to verify theoretical prediction and testing techniques. However, simply flying high and fast will not provide the necessary data. In order to accomplish the research objectives, precise piloted maneuvers are required during maximum performance flights. The use of the simulator in preparing for these critical flights ensures an optimum flight plan for each research objective, and provides the training necessary to utilize the full capability of the pilot in obtaining the required data. Included as a major research objective is simulation itself. The requirements for adequate simulation are increasing rapidly as more advanced space vehicles enter the design stage. Correlation between the X-15 simulator and flight test will provide information regarding validation of simulators and simulation techniques, and will serve as a guide for future simulation programs.

Early in the X-15 development, it became apparent that a six-degree-of-freedom simulation, covering as much of the complete flight regime as possible, was necessary in order to explore the problems of manually controlled boost, re-entry, and space flight. In past airplane designs, stability and control problems could be adequately analyzed and solved by utilization of a five-degree-of-freedom (constant velocity) simulation at a large number of given flight conditions. The addition of the sixth degree of freedom—namely, the variation in velocity and altitude—entailed much increased complexity in the mechanization required and was not warranted since the effects of these variations were not significant in the overall stability analysis. However, the X-15 can transverse its flight profile at a rate much greater than any encountered before. The rates of change of velocity and altitude, and correspondingly of dynamic pressure, during the boost and re-entry phase of the X-15 mission become large enough to influence greatly stability and control characteristics. The performance range of the X-15 makes the number of flight conditions which would be required to be investigated on a five-degree-of-freedom simulation prohibitively large. Also, it was necessary to allow the pilot to evaluate all the various phases of the mission during continuous simulated missions to establish proper compatibility with the human of the control systems, instruments, etc., during design. Thus, the requirement for at least a limited six-degree-of-freedom simulation was obvious purely from a stability, control, and human engineering standpoint, without regard to the many added advantages it would provide in pilot training, mission evaluation, and flight planning.

Because of the need for adequate aerodynamic data and early limitations of analog equipment, it was not expedient to initiate a six-degree-of-freedom simulation immediately. Consequently, during the first year of the program, efforts were directed toward specialized problems which could be solved on simpler simulations. Fig. 3 presents a time schedule of the various simulation activities from the initiation of the X-15 program to the present time. The capability of including the pilot in the control loop was provided in the simulation program from the beginning. The early studies utilized a simple cockpit with a reaction and aerodynamic control stick. It is of interest to note the increasing sophistication of these studies. It is also interesting to note that the problems of early interest were those about which we knew the least—namely, the exit and re-entry problem and the problems associated with reaction control. A simple reaction control mechanization was initiated in early 1956 and provided preliminary criteria for the reaction control system design. This was followed by a three-degree-of-freedom longitudinal mode mechanization of the exit and re-entry flight characteristics, utilizing very early aerodynamic data, for preliminary evaluation of control characteristics during these phases of the mission. This program showed that, in the longitudinal mode at least, manual control without augmentation was possible, but that augmentation was desirable. Next a "programed q" analog mechanization was utilized to evaluate the compatibility of reaction and aerodynamic controls during the transition phases of exit and re-entry. Reaction control duty cycle requirements were also finally determined. This simulation programed the dynamic pressure variations of a design altitude mission and utilized constant aerodynamic data estimated at Mach 6.

The first six-degree-of-freedom mechanization which was utilized in the X-15 program was limited to Mach numbers greater than 2 and altitudes greater than 50,000 ft in order to simplify the mechanization. In this manner we were able to eliminate the complex variations in

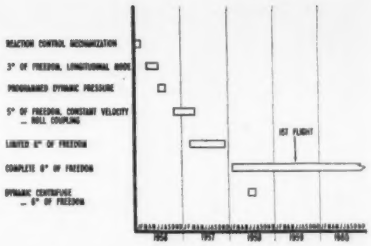

Fig. 3. Flight simulation summary.

aerodynamic characteristics in the transonic regions and to minimize the range of variations of air density which had to be simulated. The limited six-degree-of-freedom mechanization was utilized with the cockpit portion only of the flight control simulator. The actual control system hardware was still in the design stage and was not available for simulator operation. Consequently, it was necessary to simulate the control system in addition to the aerodynamic characteristics. This simulation was utilized for approximately 8 months during 1957. During this period, the major design and development of the primary control system and the stability augmentation system on the X-15 was accomplished. Also, additional stability requirements were determined, and several design changes were incorporated in the basic configuration.

The five-degree-of-freedom analog program shown on the schedule was run simultaneously with the early six-degree studies in order to evaluate stability and control characteristics, including roll coupling, at subsonic and transonic conditions.

One other simulation program which was accomplished during this period is worthy of note before we discuss the complete six-degree-of-freedom simulation. Since there was some concern as to the pilot's ability to control the X-15 under the dynamic loading conditions characteristic of exit and re-entry, a simulation program was conducted in the human centrifuge at the U.S. Naval Air Development Center,

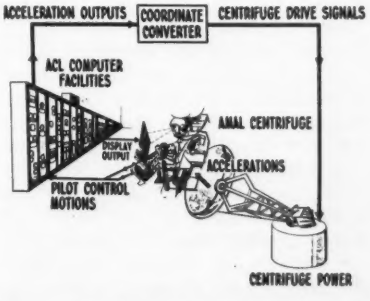

Fig. 4. Dynamic simulation.

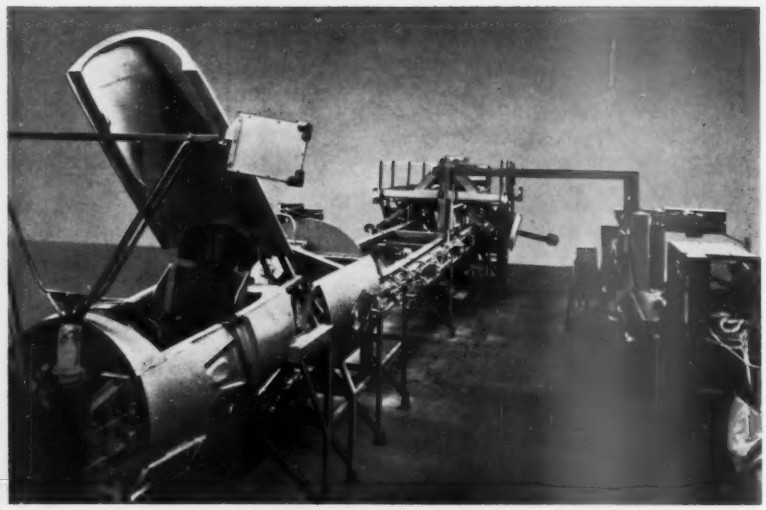

Fig. 5. Flight control simulator.

Johnsville, Pa., during the summer of 1958. In this program, the centrifuge was driven by computed signals from a limited six-degree-of-freedom analog simulation of the X-15 which was very similar to the one just described. Fig. 4 shows, schematically, the method in which the analog computer was used to drive the centrifuge with a pilot operating as a closed-loop controlling function. The centrifuge was driven to follow the computed values of accelerations resulting from pilot inputs and airplane stability and response characteristics, so that the pilot was subjected to the actual g loads of a specific mission or maneuver.

The centrifuge program had, as its prime objective, the evaluation of the pilot's ability to control the airplane during high angle of attack re-entries with the Stability Augmentation System (SAS) failed. Static simulation had shown this to be a critical control problem. Also of interest in the program were the physiological effects of extended high g loads, the adequacy of the pilot restraint system, and the characteristics of the side arm controller under g. During the program a total of 287 dynamic flights, consisting of boost and/or re-entry, were accomplished by the seven participating pilots. Normal accelerations of up to 7g and longitudinal decelerations of 4g (brakes open) were encountered simultaneously for as long as 20 sec during some of the re-entries. The results of this program showed that the pilot could control the X-15 during its most severe re-entry conditions, and further showed that, for the X-15 missions, static simulator results were not significantly different from those obtained under dynamic conditions. Consequently, no additional dynamic simulation effort has been necessary in the X-15 program. This, however, does not imply that the centrifuge program was unnecessary. It provided a verification of the design under severe environment, and made possible a higher level of confidence which has allowed the flight-test program to proceed at a more rapid rate.

Although the limited six-degree-of-freedom simulation provided invaluable information in early design of the airplane, it was soon apparent that it was inadequate. Because of limitations imposed on Mach number and altitude, problems associated with launch and roundout, space positioning, subsonic and transonic stability, and landing could not be investigated. By this time the potential value of the simulator in flight-test mission planning and pilot training was apparent, and, in these applications, complete simulation capability over the X-15 flight regime would be required. Therefore, the unlimited six-degree-of-freedom simulation was developed and has been in operation continuously since March 1958. This simulation is capable of piloted or nonpiloted analysis throughout the X-15 flight regime, including launch maneuvers, boost and exit phase, reaction-controlled ballistic flight, re-entry, and glide to landing flareout. The performance capability of the simulation covers the Mach range from 0.2 to 10.0, altitude to 500,000 ft, and angles of attack to 35 deg. Simulated flights may be accomplished with speed brakes open or closed, with flap and landing gear extension effects, ventral jettisoning characteristics, and other nonlinear effects. Missions may be flown using either the XLR-11 or the XLR-99 engine, including the effects of engine throttling and thrust misalignment. Missions may be accomplished from the design B-52 carrier aircraft or from other advanced carriers such as the B-70. The dynamic effects of nonlinear changes in mass and moments of inertia during engine burning are simulated. Premature burnout of either engine may be simulated at any time, and propellant jettisoning may be accomplished at the required rates.

This simulation capability permits evaluation of all important contributions to the complete mission, with the exception of temperature. A simplified computation of skin temperature at critical points on the vehicle was mechanized on the analog computer and incorporated in the real-time problem solution early in the program. Temperature at one of several points on the vehicle was displayed to the pilot as an aid in remaining within limits during re-entry. However, it was found that this information merely told the pilot that he had exceeded limits and did not provide sufficient lead time to allow corrections once it was established that an overtemperature condition was imminent. Because of the limited application for which the temperature mechanization was suitable, and the equipment required, this part of the simulation was discontinued.

The capability of permitting piloted flights of the X-15 with this simulation is obtained by integration of the mechanization into the X-15 flight control simulator (Fig. 5). It consists of duplication of the airplane cockpit, instruments, and control system. The complete operational flight control system provides exact system characteristics under operating conditions. Actual production components, including cables, push rods, bell cranks, the hydraulic system, artificial feel, etc., are utilized in exactly the same manner as in the actual airplane. The electronics of the X-15 stability augmentation system are also included. The control system is duplicated in this detail in order to include all nonlinearities in closed-loop systems evaluation, and to provide the pilot with the feel characteristics of the airplane. All control displacements are available to the analog computer by means of electrical pickoffs on each aerodynamic control surface. The cockpit area (Fig. 6) is a realistic simulation of the airplane configuration. The simulator has the same provisions for aerodynamic control as in the airplane, utilizing either the center stick or the right-hand console stick and rudder pedals. Reaction control is provided with the left-hand three-axis controller. The pilot has normal control over the stability augmentation system by means of the same controller panel as installed in the air vehicle. The flight instruments, which are simulated in complete opera-

tional form, are driven by voltages from the analog computer. They include the inertial attitude indicator which provides pitch, roll, and heading; the inertial velocity, altitude, and rate-of-climb instruments; indicators of angles of attack and sideslip, roll rate, normal load factor, and indicated air speed; and for simulator test purposes only, an indication of dynamic pressure.

The equations utilized to simulate the X-15 in the unlimited six degrees of freedom are presented in Fig. 7. These are basically the classical equations of motion of the aircraft with respect to an Eulerian frame of reference. The equations and all aerodynamic parameters are mechanized in a body-axis system of coordinates. Orientation of the gravity vector and the geographical distance and position are obtained by means of conventional Eulerian angles. Because of the limited ground distance traveled by the X-15 in its design mission, a flat earth may be assumed as a reference. However, the centrifugal acceleration effect is included as a function of the X-15 horizontal velocity component and adds directly to the normal gravity vector which is mechanized as a function of altitude. The terms and the equations which are considered variable include thrust, mass, velocity, gravity, inertia, and all aerodynamic coefficients which may not be assumed constant within the accuracy desired.

The analog computer complex used in the X-15 simulation is shown in Fig. 8. The linear equipment consists of five Model 16-31 Electronic Associates analog computers, incorporating 330 operational amplifiers. Additional nonlinear equipment required in the mechanization includes approximately 80 diode function generators, 25 computing servos, and three electronic multipliers; part of this equipment is shown in Fig. 9. The nonlinear variations of stability derivatives with Mach number and angle of attack are accomplished on four special interpolating servos which provide 17 interpolating points selected, as necessary, over the Mach range for each of the derivatives. The nonlinear variation of the derivatives with the angle of attack at the required Mach number points are obtained from a rack of 60 fixed-base diode function generators.

The greatest utilization of the simulator is obtained when the pilot is included as part of the control loop. Before discussing specific applications of the simulator in the X-15 program, it might be well to review a complete simulated flight of the X-15. Typical analog traces of a piloted design altitude mission as flown on the simulator are shown in Fig. 10. The flight begins at drop conditions, at Mach 0.8, at approximately 45,000 ft. The throttle is opened immediately after drop, and the pilot makes a pullup to $\alpha = 8$ deg, which is maintained until the proper climb angle is established. (For a 250,000-ft-altitude mission, this angle is 30 deg.) Pitch angle is then held constant until burnout, at which time an $\alpha = 0$ ballistic trajectory is established. It is well to note that this represents only one of several acceptable techniques for performing the exit phase. During the period of engine burning, control is required to correct for thrust misalignment. Burnout occurs approximately 90 sec from drop, at a velocity of 6,200 fps, at 160,000 ft. The effects of thrust misalignment are seen in the oscillations in angle of attack and sideslip. At burnout, the pilot begins use of the reaction control and continues this means of control throughout the ballistic phase of the trajectory. The recovery used in this particular flight was an angle of attack of 15 deg, established at approximately 200,000 ft during re-entry. The required aerodynamic trim for this attitude can be set at any time, and the reaction control system then used to establish the required angle of attack. As the dynamic pressure builds up, the load factor is seen to increase, and for this mission, the pilot performed the recovery with the maximum of 5g. Following the successful recovery, which occurs in this case at approximately 85,000 ft at approximately Mach 5, the altitude is held constant as the airplane decelerates until the desired descent speed is reached.

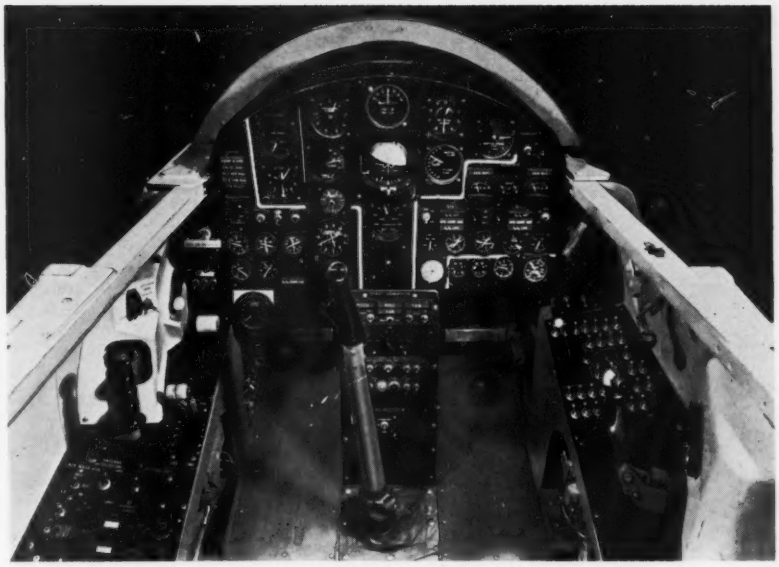

Fig. 6. Simulator cockpit.

Consider now what this complete flight simulation allows in the way of system development and testing. Since the pilot can essentially fly the complete mission, a complete evaluation of controls, displays, and augmentation devices is possible long before flight. In the case of the X-15, the complete flight control system (including the stability augmentation system) which was originally designed and specified on the limited 6-deg simulation was later included in a closed-loop simulation in its exact prototype form on the complete mechanization. The simulation tests on the complete system revealed several inadequacies due to the nonlinear characteristic of the control system; these were corrected before flight. An example of these was a SAS-induced lateral oscillation which occurred at high gain flight condition. Fig. 11 shows this effect during a simulated re-entry before and after corrective action was taken. This was first encountered on the simulator when the prototype SAS was included in the loop. Additional

$$\dot{V}_x = g \sin\Theta + \frac{T - Y_0 S C_c}{m} - V_y \psi + V_y r$$

$$\dot{V}_y = g \cos\Theta \sin\Phi + \frac{Y_0 S}{m}\left(C_{Y_\beta}\beta - 1.6\, C_{Z_{\delta_N}} \delta_N - 1.5\, C_{n_{\delta_r}} \delta_r\right) - V_x r + V_y p$$

$$\dot{V}_y = g \cos\Theta \cos\Phi - \frac{Y_0 S}{m}\left(C_{X_{\delta_{SB}}} - \frac{\bar{c}}{\ell_T} C_{m_{\delta_N}} \delta_N\right) - V_y p + V_x \psi$$

$$\dot{p} = \frac{Y_0 S b}{I_{xx}}\left(C_{\ell_\beta}\beta + C_{\ell_{\delta_N}} \delta_N + C_{\ell_{\delta_r}} \delta_r + \frac{b}{2V} C_{\ell_p} p\right) + \frac{I_{yy} - I_{zz}}{I_{xx}} qr$$

$$\dot{q} = \frac{Y_0 S \bar{c}}{I_{yy}}\left(C_{m_{\delta_{SB}}} + C_{m_{\delta_N}} \delta_N + \frac{\bar{c}}{2V} C_{m_{\dot{\alpha}}} \dot{\alpha}\right) + \frac{I_{zz} - I_{xx}}{I_{yy}} pr$$

$$\dot{r} = \frac{Y_0 S b}{I_{zz}}\left(C_{n_\beta}\beta + C_{n_{\delta_N}} \delta_N + C_{n_{\delta_r}} \delta_r + \frac{b}{2V} C_{n_p} p\right) + \frac{I_{xx} - I_{yy}}{I_{zz}} pq$$

$$\dot{\Theta} = q \cos\Phi - r \sin\Phi \qquad V_0^2 = V_x^2 + V_y^2 + V_z^2$$

$$\Phi = p + \dot{\Psi} \sin\Theta \qquad \alpha = \sin^{-1}\frac{V_z}{V_0 \cos\beta}$$

$$\dot{\Psi} = \frac{q \sin\Phi + r \cos\Phi}{\cos\Theta} \qquad \beta = \sin^{-1}\frac{V_y}{V_0}$$

$$\dot{x} = \left[V_x \cos\Theta + (V_y \sin\Phi + V_z \cos\Phi)\sin\Theta\right]\cos\Psi + \left[V_y \sin\Phi - V_z \cos\Phi\right]\sin\Psi$$

$$\dot{y} = \left[V_x \cos\Theta + (V_y \sin\Phi + V_z \cos\Phi)\sin\Theta\right]\sin\Psi - \left[V_y \sin\Phi - V_z \cos\Phi\right]\cos\Psi$$

$$\dot{h} = V_x \sin\Theta - V_y \cos\Theta \sin\Phi - V_z \cos\Theta \cos\Phi$$

$$g = 32.17 - k_1 h - k_2 h^2$$

Fig. 7. Six-degree-of-freedom equations of motion.

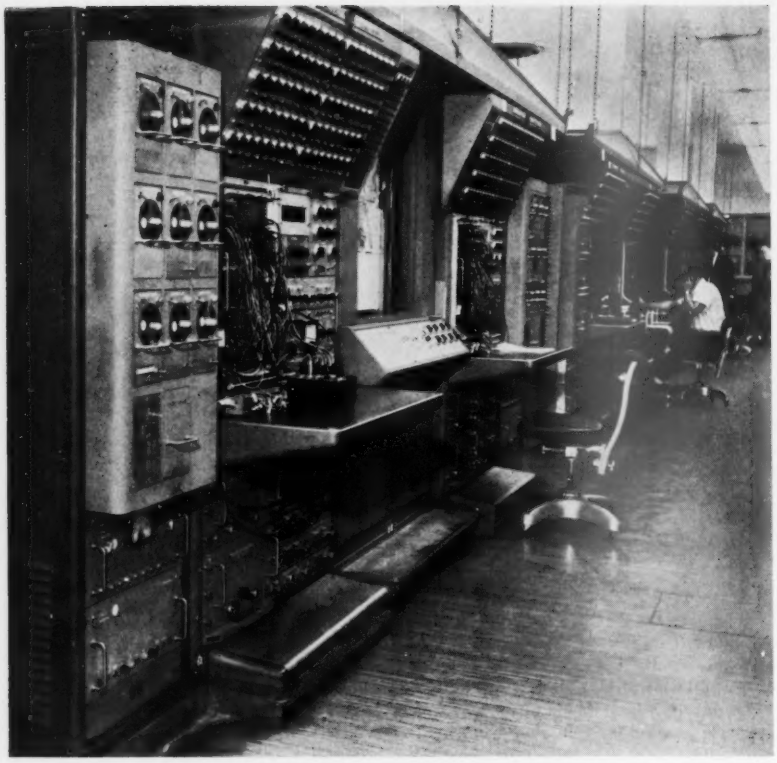

Fig. 8. Analog simulation.

study showed that this effect was caused by mechanical lags due to linkage deformation not accounted for in the design analysis.

The simulator was used extensively for pilot evaluation of the cockpit control and instrument hardware under simulated flight conditions. This resulted in changes or modifications in the control system feel characteristics and instrument location, and a redesign of the right-hand console stick. The centrifuge tests described earlier were also very instrumental in optimization of the side stick configuration. Fig. 12 shows the right-hand stick in its present configuration, compared with two early designs which progressed to the stage of simulator evaluation. It is significant that these early configurations appeared satisfactory from both the pilot's and human engineer's viewpoint when evaluated in an early cockpit mockup. It was not until the pilot was able to utilize the stick to perform the required control function during simulated flight that the deficiencies and limitations of the controller were evident.

The versatility of the combined simulator and analog mechanization has been more recently demonstrated by the design evaluation and hardware testing of two separate autopilot systems on the simulator. Both of these were complex, adaptive-type autopilots which included attitude-hold modes, reaction and aerodynamic control integration, and other refinements to the basic X-15 control system. These autopilots were included as a part of the closed-loop control system, and their performance was completely evaluated under conditions of the X-15 mission profile. Considerable design changes and improvements were made as a result of these tests, and at the present time, one of these advanced systems is being readied for X-15 flight evaluation. During flight testing of this system, a simulator support program will provide the pilots with preflight training and familiarization with its operational characteristics.

In addition to systems development and stability analysis applications, the simulator has proved invaluable in studies involving the pilot, his control requirements and training, and flight-test planning and support. An example of these is the early development of reaction control techniques. Since the basic X-15 originally had no provisions for stability augmentation through the reaction control system, the control characteristics were those of a perfectly neutral, undamped system unlike any vehicle with which pilots were familiar. Prior to establishment of final reaction control fuel requirements, several pilots were trained on the simulator to perform this type of control, and a realistic duty cycle was then obtained. It is significant that gross reductions in fuel requirements were obtained after a pilot had experience on the simulator. Also, it was found that only a minimum amount of experience was required (10 to 20 "flights") for the pilot to reach his near-optimum degree of efficiency.

More recently, the simulator has been utilized by the Air Force, NASA, and North American almost exclusively for pilot training and flight planning. In order to appreciate fully the value of a simulator in this capacity, it is necessary to consider in some detail the

Fig. 9. Nonlinear computing equipment.

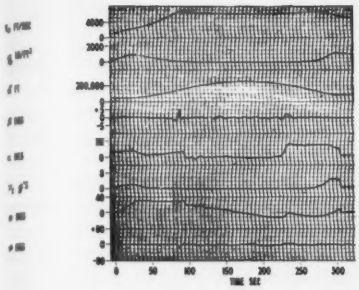

Fig. 10. Design altitude mission.

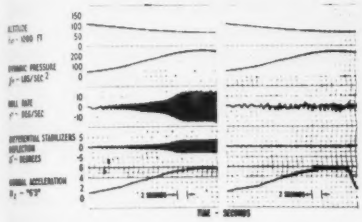

Fig. 11. Stability augmentation system residual oscillations (*left:* original SAS; *right:* modified SAS).

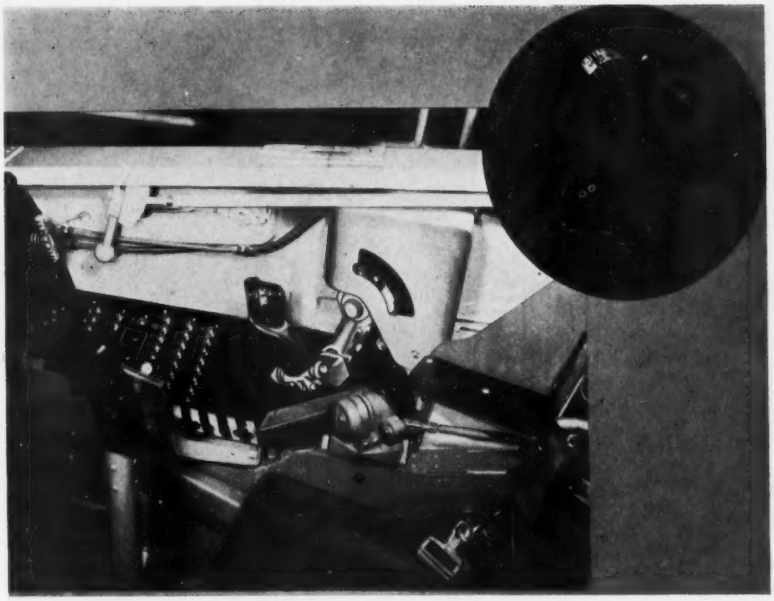

Fig. 12. Side-located aerodynamic controller.

X-15 flight-test program. First, of course, the cost of an X-15 flight is quite high, requiring that all possible benefit be derived from each mission in terms of research data. The cost factor is also reflected in the necessity for taking reasonably large steps in performance during the flight buildups, which requires that each flight be thoroughly evaluated prior to its acceptance. The safety aspect of research flight planning provides the greatest single requirement for adequate simulation. The simulator allows the research pilot to evaluate thoroughly all aspects of a proposed flight, including all conceivable malfunctions or emergency situations.

The ground positioning, or navigational problem, is a critical consideration in flight planning because of the limited glide range of the X-15. This problem is analyzed on the simulator, with the aid of a detailed map of the flight area (Fig. 13) on an X-Y plotter upon which the simulated flight path is plotted. This permits the pilot actually to fly simulated emergencies, such as premature engine shutdown, at all points along the proposed flight path, and to determine the optimum approaches to the selected emergency landing sites. It is interesting to note that the plotting board used in the simulation is identical to the ones used at the ground station during an actual flight—except, of course, that, at the actual control station, the flight path is plotted from radar tracking signals rather than from analog signals. This permits the flight-test engineer to review, or rehearse, the proposed flight with the pilot on the simulator.

As a result of 3 years of continuous operation of the X-15 simulator in many various applications, certain general conclusions may be drawn regarding operation, accuracy, and efficiency of complex analog mechanizations. The six-degree-of-freedom analog simulation has been operated in excess of 10,000 hours in support of the X-15. Over 5,000 hours have been logged in the flight control simulator. The simulator is generally on a two-shifts-per-day schedule, and on this basis, an operational utilization of approximately 85 percent is realized. Down time may be attributed equally to equipment problems and to checkout. It has been found that, for a computer complex as large as this, daily problem checks are a requirement. So-called "dynamic" checks, or stability checks, are made by comparing the simulator with IBM-computed transients obtained during preprogramed roll maneuvers at several constant-velocity flight conditions. These five-degree-of-freedom checks have been found to be most adequate in ensuring correct stability characteristics throughout the flight regime. Good accuracy is obtainable with the analog computer in stability computations since they generally involve short time transients for which the analog is well suited.

Performance checks are also made at regular intervals, and involve comparison of IBM-computed trajectories with analog results. It is in this area that the checks become most critical. Minor discrepancies in the computer operation can cause excessive errors in performance checks, primarily in altitude and range. This is because of the long time computations involved (from 5 to 20 min, depending on the condition) and the resulting susceptibility of the solution to computer drifts and noise, and to nonlinear servo characteristics. It has been possible, however, to recognize the source of these errors and, by proper computer checks, obtain the accuracy necessary for the X-15 performance problem. The accuracy usually obtained in computing such parameters as range, altitude, and velocity over a 20-min simulated flight is within 2 percent.

Final proof of the validity of the simulation is, of course, demonstrated in how well it compares with actual flight results. The pilots who have flown the X-15 consider the simulator to be a very close simulation of the actual airplane flight characteristics. In fact, the simulator has become an integral part of the pilot's flight preparation program as a result of the pilot's own acceptance of the accuracy and value of the simulator. Fig. 14 shows a performance comparison of XLR-11 maximum-speed flight with the analog-predicted flight run prior to the actual flight. The discrepancies noted are, to a great extent, the result of atmospheric variations—i.e., nonstandard days and wind shears. Fig. 15 shows the same comparison for the maximum-altitude flight with the XLR-11 engine. During all speed and altitude buildup flights, simulator-predicted performance has been matched to within 0.1 Mach and 3,000 ft altitude. The stability characteristics of the X-15 have also been adequately predicted on the simulator,

Fig. 13. Variplotter for simulated high-range plotting.

although it is in this area that minor discrepancies in wind-tunnel data reflect the largest differences in simulator matches. The simulation is used, in this regard, to determine the variation in stability derivatives necessary to obtain exact flight data matches, and in this manner the validity of wind-tunnel data is established.

Fig. 16 shows a simulator comparison of the data obtained during the landing of the first X-15 glide flight. This demonstrates the validity of the simulation in duplicating the low-speed dynamics and performance of the airplane, but at the same time, it may be used to indicate an area in which the simulation was proved to be deficient The pitching oscillation experienced during the landing flareout, although duplicated almost perfectly on the simulator after the flight, was not predicted from simulator experience prior to flight. The problem resulted from a higher level of control sensitivity associated with the side-arm controller than was expected. This characteristic was not predicted on the simulator because of lack of critical cues, such as the visual horizon and the actual motion of the airplane, during the landing simulation.

It is of interest to compare the X-15 simulation requirements with those of currently projected manned space vehicles, and to consider some of the expected problem areas in view of X-15 experience. In the X-15 program, the major simulation requirements have been described as being related to control system development and testing, stability evaluation, pilot task studies, mission planning, and pilot training.

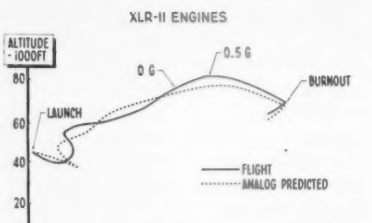

Fig. 14. X-15 maximum-speed flight.

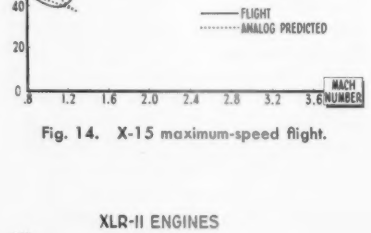

Fig. 15. X-15 maximum-altitude flight.

These requirements result primarily from the fact that the vehicle utilizes the man for command and control, and that it is designed to fly at conditions far advanced over any encountered at the time of the vehicle design. The extension of this reasoning to manned space systems is obvious. The system development and testing requirements for these advanced vehicles will far exceed those of the X-15 because of the greater number of systems requiring integration and pilot evaluation and because of their increased sophistication and complexity. The importance of early simulator evaluation of subsystems critical to the space mission is demonstrated by the advanced system programs which have been accomplished, or are being planned, on the X-15 simulation. The stability and control characteristics of aerospace vehicles, particularly during re-entry, will require simulator analysis and pilot evaluation over a much greater range of flight conditions than for the X-15. The effects of the expanded flight envelope will also be reflected in increased simulation requirements in areas of human engineering, mission planning, and pilot training.

Even these very general considerations leave no doubt that simulation will play an even more important part in space vehicle development and testing than was required on the X-15. Consider next the problems which may be expected in providing this required simulation capability. The critical problem areas which have been encountered in the X-15 simulation have already been described as being related primarily to performance. These resulted from long time computation requirements in which computer drift and accuracy limitations become critical. It is apparent that these problems will become more serious in space mission simulation because of the larger mission time. The ranges of important variables which must be mechanized for a

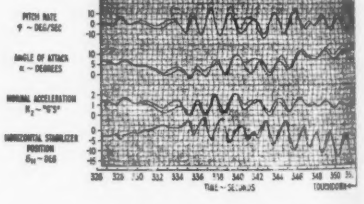

Fig. 16. First glide flight landing flareout.

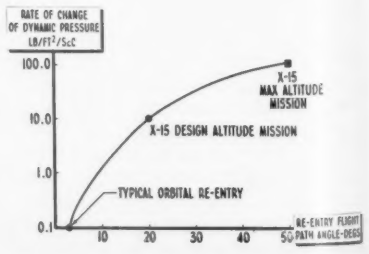

Fig. 17. Re-entry dynamic pressure variation.

typical aerospace configuration will be, in many cases, greater than those required in the X-15 simulation and will create additional scale-factoring problems. Typical of these are velocity, Mach number, and altitude. In some instances, however, the X-15 requirements may be the more severe. For example, the range of dynamic pressure for which the X-15 is designed (0 to 2,500 psf) is much greater than will be required in winged re-entry vehicles. The rates of change of dynamic pressure in the X-15 mission are even more significant. Fig. 17 shows dynamic pressure rate of change during re-entry as a function of re-entry angle. It is seen that the steep re-entry angles required for the X-15 result in much more severe dynamic pressure changes than are experienced by orbital re-entry vehicles.

Space simulation requirements will allow particular phases of the complete mission to be mechanized individually in order to limit the range of variables and minimize the computation time required. For instance, simulation of the boost, orbit, and re-entry phases of a complete orbital mission in a single mechanization becomes impractical by current analog techniques. However, if each phase is mechanized individually, with appropriate scale factoring, satisfactory results may be obtained for most applications. For example, the major portion of the orbital re-entry problem may be simulated at altitudes above 100,000 ft. Since the X-15 simulation adequately duplicates air density from sea level to 250,000 ft, the requirements for simulation of air density for an orbital re-entry problem are no more severe than for the X-15.

Some preliminary studies have been conducted utilizing conventional analog techniques to mechanize various aerospace missions. The vehicles simulated were an orbital re-entry system and a lunar return vehicle. The X-15 flight simulator was used to allow pilot participation in analysis of such problems as high-angle-of-attack stability during re-entry and flight path control during aerodynamic deceleration from lunar return velocities. Analog data showing a piloted lunar return maneuver are shown in Fig. 18. As the vehicle approaches the earth at approximately 36,000 fps along an optimum flight path which has been established many hours earlier, the pilot rolls 180 deg and, by utilizing aerodynamic lift, maintains a constant altitude as the velocity slows to suborbital. In this application, the analog simulation was found to be quite adequate in establishing pilot capability and control techniques since the critical portion of the problem—namely, the establishment of the proper approach trajectory—was assumed to have already been accomplished. Also the maneuver considered required relatively high aerodynamic forces at velocities appreciably greater than orbital, so that the differences between gravity and aerodynamic effects were not critical. Fig. 19 shows the effects of a 0.1 percent error in either of the components of acceleration during a simulated re-entry from a near-circular orbit in which aerodynamic drag is used to decelerate the vehicle at perigee. Here the effects on performance during re-entry are seen to be quite severe because of the near-equal values of gravity and centrifugal acceleration.

It was apparent from these studies that the analog mechanization provided adequate simulation of dynamic characteristics but that very accurate performance results could not be obtained; thus providing verification of the trends extrapolated from X-15 results. In order to obtain the accuracy necessary for orbital or near-orbital space simulation applications while maintaining the flexibility inherent in analog computation techniques, the need for combined analog-digital computation is apparent. It is believed that the X-15 simulation program pushed analog techniques to their limits, and, in fact, instances were noted where the accuracy obtained was marginal. Based on these results, it is apparent that digital techniques must be resorted to in future simulations.

To summarize, it would be well to reiterate that the X-15 flight simulator, as it exists today, is the result of design requirements as projected early in the program. The requirement to include the pilot in the loop as an integral part of the systems development and testing

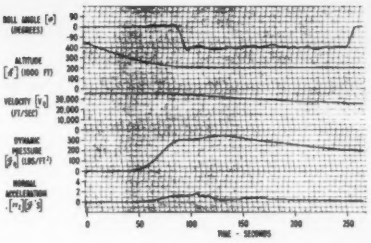

Fig. 18. Lunar vehicle re-entry.

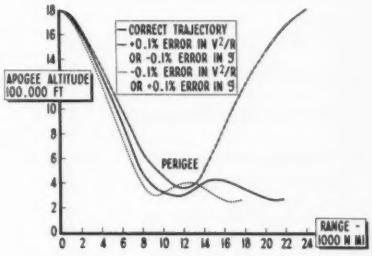

Fig. 19. Effects on analog errors in near-circular orbit computations.

provided the major justification for the detailed duplication of displays and flight controls, and for the extensive six-degree-of-freedom analog simulation of the airplane motion. Since the application for which the simulator has been utilized in the latter phases of the program—namely, mission planning and pilot training—was not clear-cut in the beginning, we were fortunate that early requirements dictated the simulation approach which was pursued. It has been indicated that the X-15 simulation requirements were similar in many respects to those which may be expected in simulation of more advanced vehicles, and that the problems which were encountered are a definite indication of the difficulties which may be expected. Consequently, it appears that the X-15 simulation requirements, techniques, and problems should prove helpful in future programs, both in early definition of the overall simulation program to be followed and in determining the best approach to accomplish the program.

✦ ✦ ✦

IAS SCRIP COUPONS

IAS SCRIP COUPONS may now be used as payment for IAS Papers, dues, subscriptions, and all other IAS services. This method will save you from writing checks, sending money orders or cash. Sheets of 5- and 25-cent coupons are available in book form of $5, $10, $25, or any amount desired, from the Special Publications Dept. Scrip may be ordered by foreign and domestic members and nonmembers.

IAS CORPORATE MEMBERS

AC Spark Plug Division, General Motors Corporation

Academy of Aeronautics

Aerojet-General Corporation

Aeronca Manufacturing Corporation

Aeronutronic, Division of Ford Motor Company

Aerospace Corporation

Agawam Aircraft Products, Inc.

Airborne Instruments Laboratory, Division of Cutler-Hammer, Inc.

Allied Research Associates, Inc.

Allison Division, General Motors Corporation

American Airlines, Inc.

American Bosch Arma Corporation

American Oil Company

Amoco Chemicals Corporation

Arde Associates

ARO, Inc.

Avco Corporation, Research and Advanced Development Division

Avco-Everett Research Laboratory

Avien, Inc.

Beech Aircraft Corporation

Bell Aerospace Corporation

The Bendix Corporation

The Boeing Company

Booz, Allen Applied Research, Inc.

Bulova Research & Development Laboratories, Division of Bulova Watch Company, Inc.

Canadair, Ltd.

Chance Vought Corporation

The Chase Manhattan Bank

Chicago Aerial Industries, Inc.

Continental Motors Corporation

Cornell Aeronautical Laboratory, Inc.

Cox & Company, Inc.

Curtiss-Wright Corporation

Daniel, Mann, Johnson & Mendenhall

The Decker Corporation

Defense Systems Division, General Motors Corporation

Del Mar Engineering Laboratories

Delco-Radio Division, General Motors Corporation

Delco-Remy Division, General Motors Corporation

Douglas Aircraft Company, Inc.

Dzus Fastener Company, Inc.

Eastern Air Lines, Inc.

Eaton Manufacturing Company

Edo Corporation

Elastic Stop Nut Corporation of America

Fairchild Camera and Instrument Corporation

Fairchild Stratos Corporation

The Garrett Corporation

General Applied Science Laboratories, Inc.

General Dynamics Corporation

General Electric Company

General Precision, Inc.

The B. F. Goodrich Company

Goodyear Aircraft Corporation

Grumman Aircraft Engineering Corporation

Hoffmann Aircraft Company

Hughes Aircraft Company

IBM Space Guidance Center

Insurance Company of North America Companies

The International Nickel Company, Inc.

ITT Federal Laboratories, Division of International Telephone and Telegraph Corporation

Janitrol Aero Division, Midland-Ross Corporation

Johns-Manville Sales Corporation

Kollsman Instrument Corporation

Lavelle Aircraft Corporation

Lawrence Aviation Industries, Inc.

Lear, Incorporated

C. W. Lemmerman, Inc.

The Liquidometer Corporation

Arthur D. Little, Inc.

Lockheed Aircraft Corporation

The Marquardt Corporation

The Martin Company

McDonnell Aircraft Corporation

Meletron Corporation

Minneapolis-Honeywell Regulator Company

Mobil Oil Company

National Credit Office, Inc.

North American Aviation, Inc.

Northrop Corporation

Pan American World Airways, Inc.

The Ralph M. Parsons Company

Piasecki Aircraft Corporation

Poly Industries, Inc.

Radio Corporation of America, Defense Electronic Products

Republic Aviation Corporation

Rohr Aircraft Corporation

Ryan Aeronautical Company

Shell Oil Company

Simmonds Precision Products, Inc.

Solar Aircraft Company

Southwest Products Company

Space Technology Laboratories, Inc.

R. Dixon Speas Associates

Sperry Gyroscope Company, Division of Sperry Rand Corporation

Standard-Thomson Corporation

Stanley Aviation Corporation

Therm, Incorporated

Thiokol Chemical Corporation

Thompson Ramo Wooldridge Inc.

Trans World Airlines, Inc.

Union Carbide Metals Company, Division of Union Carbide Corporation

United Air Lines, Inc.

United Aircraft Corporation

United States Aviation Underwriters, Inc.

Vehicle Research Corporation

Western Gear Corporation

Westinghouse Electric Corporation

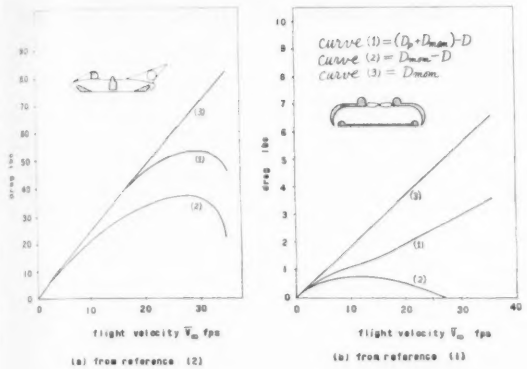

Fig. 2. Two examples of drag breakdown for peripheral jet GEM.

Third, a peripheral jet GEM will be considered. This type of GEM makes up a flow pattern similar to that of a plenum chamber GEM. The main difference is that, for a peripheral jet GEM, the ejected airflow is apt to suffer some additional energy loss as a result of impingement against the ground surface. Essential part of the internal drag, however, may result from rotation loss as in a plenum chamber GEM, according to the present authors' opinion.

Concludingly, the present authors think that the *internal flow brings about a drag through essentially similar mechanism, "rotation loss," for ram wing, plenum chamber and peripheral jet.*

(3) Two Examples of Drag Breakdown of Peripheral Jet GEM

There are two data published by Kuhn and Carter[1] and Nixon and Sweeney[2] which concern drag breakdown of peripheral jet GEM. Two sets of curves in Fig. 2 are constructed by the present authors, using these data. The curves (1) show us that total drag with internal flow is much less than $D_p + D_{mom}$. Furthermore, the curves (2) show that total drag D is less than D_{mom} only; thus, *the parasite drag in power-on condition $D_{p,p}$ can become negative* in a range of (especially low) velocity. The value of curves (1) suggests that there exists large "interference thrust." The authors cannot know on what conditions drag was measured by the writers[1,2]; for example, were the air intake and nozzle exit faired or not during measurement of power-off drag, and was the attitude of the GEM carefully controlled or not during measurement of power-on drag? It is clear, however, that the interference thrust, sufficiently large to make parasite drag negative in power-on condition, should be mainly attributed to partial conversion of the ejected jet momentum into the propulsive force. It is the authors' opinion that any reduction of frictional drag on the base surface and disappearance of dead area, such as air intake and jet nozzle exit, in power-on condition are rather minor parts of the interference thrust.

(4) Tentative Model of Flow Pattern About a GEM

Many previous writers showed that some types of jet, being located near the jet exit, induce vortices and change remarkably the pressure distribution over the ground surface and/or body surface. Fig. 3 shows some of these situations. Especially (a), (b), and (e) in Fig. 3 attracted the present authors' attention, and suggested the following image of the flow pattern around a GEM. A preliminary experiment confirmed this pattern for a few rugged ram wings, but the image will be only a tentative one for general types of GEM such as plenum and air curtain.

The image of the flow pattern is shown in Fig. 4. To simplify the description, we use the following terms:

external flow, airflow not passing inside of a GEM
internal flow, airflow passing inside of a GEM, through compressor fan
ingested air, from infinite upstream to air intake of a GEM
ejected air, from nozzle exit of a GEM to infinite downstream

First let us consider the flow pattern of the ejected air. In front of a GEM, the external flow curls up the ejected air, which energizes a trapped vortex located ahead of the GEM and passes partly over the GEM to infinite downstream.

A part of air ejected at the rear of a GEM seems to run simply along the ground surface to the infinite downstream. No trapped vortex exits behind the GEM because the external flow and ejected air prevent each from curling the other.

A part of air ejected at the sides of a GEM will induce a vortex parallel to the free stream at each side. These vortices seem to be joined together by the trapped vortex ahead of the GEM, thus a horse-shoe vortex will appear. *A GEM will run dragging such a U-type vortex on the front edge.* The present authors think a mechanism generating is created by the side vortices, as follows: A part of the air ejected at both sides of a GEM will separate from the outside surface of the GEM, not running close to it; the external flow here will be induced to construct a vortex. Furthermore, the discharged internal flow will be curled up, being sucked by a negative pressure area over the GEM upper surface. Thus the two reasons, separation of ejected air and suction by the negative pressure over the GEM upper surface, can be thought of as a possible mechanism of the side vortices. At present it is not clear which reason is predominant.

At larger flight velocity than a critical value, the trapped vortex will vanish and only the side trailing vortices will remain. The cruising condition perhaps gives this situation. If the ejected air would not suffer any loss and run with complete propulsive momentum, then the GEM would get the thrust expressed by

$$T_j' = mV_j' = m\sqrt{2P_{tj}/\rho}$$

which is a major part of the ideal interference thrust.

This value is, of course, sufficiently large to cancel the ingested airflow drag—namely, momentum drag. Unfortunately, for most current GEM's, this ideal situation does not occur. The energy (or momentum) dissipation of ejected air results from the two mechanisms; the one is direct mixing mainly due to impingement of the air against the ground surface, and the other is trailing vortices loss—viz., rotation loss. For a plenum chamber GEM, rotation loss is predominant and the direct mixing loss is negligible. For a peripheral jet GEM, the direct mixing loss may not be negligible, nevertheless the rotation loss may still be a major part of the total loss.

The propulsive thrust caused by the ejected air is a component, parallel to the free stream, of the ejected air momentum sufficiently rearward of the GEM. The GEM, however, must feel the thrust as the favorable change in pressure distribution over its surface. For the plain GEM, thrust-feeling surface is the upper surface only. For the forward-inclination GEM, the major thrust-feeling surface is, of course, the

IAS/ARS JOINT MEETING

LOS ANGELES, JUNE 13–16, 1961*

61-88 -1782 Trends in Air Cargo—H. Carter & J. Jackovich
61-89 -1783 Factors Underlying the Future Domestic Market for Air Cargo Service—G. Busch & K. Mayer
61-91 -1785 Air Trailer Transportation—W. Ligon
61-92 -1786 Economics of Air Eligibility—L. Regan & G. Harris
61-95 -1789 Maximizing Reliability for One-Shot Space Missions—S. Morrison
61-96 -1790 One-Shot Mission Success for Minimum Cost—W. Cox & W. Harter
61-104-1798 Short Haul Air Transportation—W. Kennedy
61-105-1799 Aerodynamic Characteristics of Subsonic V/STOL Transport Airplanes—M. Kelly & C. Holzhauser
61-106-1800 Application of Laminar Flow Control to Transport Aircraft—W. Gasich
61-115-1809 Prediction of Optimum Approach & Landing Techniques-Manned Reentry Gliders—L. Gaines & T. Surber
61-116-1810 Second Order Theory of Entry Mechanics into a Planetary Atmosphere—W. Loh
61-118-1812 Instrument Flight Simulator Study of VTOL Controllability-Control Power Relationship—J. Patierno & J. Isca
61-119-1813 Design Characteristics of a Lifting Fan V/STOL Logistic Transport—E. Kazan & W. Bergen
61-120-1814 Influence of Two-Dimensional Stream Shear on Airfoil Maximum Lift—R. Vidal
61-123-1817 Age Concept of Management for Ground Environment Area—S. Tremaine
61-124-1818 Universal Program-Comparator Checkout Equipment & Logistical Considerations—E. Metsker & M. Beeson
61-125-1819 Role of Operational Analyses in Planning Effective Missile Ground System—S. Firstman
61-126-1820 Compiling of Automatic Test Equipment Programs—E. Quinn and C. Chipps
61-129-1823 Study of Solid-Fuel Ramjet Applications—P. Munter
61-134-1828 Description of Weapons Assignment Research Model (WARM)—R. Totschek
61-135-1829 General Purpose Simulator for Airborne Computers—E. Carter
61-143-1837 Design Alternatives for In-Flight Maintenance—R. Demaree
61-144-1838 Human Engineering Principles of Design for In-Space Maintenance—L. Pigg
61-146-1840 Predicting Human Reliability-Implications for Operations & Maintenance in Space—R. Kaufman, T. Oehrlein, & M. Kaufmann
61-147-1841 Some Experiments of Human Maintenance Behavior—M. Grodsky
61-149-1843 Unified Engineering Theory of High Stress Level Fatigue—S. Valluri
61-150-1844 Structural Aspects of Low Drag Suction Airfoils—J. Wieder & W. Pfenninger
61-151-1845 Leading Edge Design with Brittle Materials—F. Anthony & A. Mistretta
61-158-1852 Mercury Animal Program—J. Henry and J. Mosely
61-162-1856 The Mini-Recorder System—J. Renfro
61-183-1877 Directive Non-Oriented Reflectors as Passive Satellites in Long Distance Communications—Y. Stahler & A. Johnson
61-190-1884 The Magnetic Particle Clutch–A Versatile Control Element for Rocket Systems—B. Grau & B. Chubb
61-194-1888 X-15 Flight Simulation Program—N. Cooper
61-195-1889 Piloted Simulation Studies of Re-entry Guidance & Control at Parabolic Velocities—R. Wingrove & R. Coate
61-196-1890 The Simulator as a Human Factors Research Tool for Manned Space Flight—G. Simon
61-210-1904 Flow Past Slender Blunt Bodies–Review & Extension—R. Capiaux & L. Karchmer

*See pp. 30 and 62 for other IAS publications available. **IAS/ARS Member price, 50c each. Nonmember price, $1.00 each.**

Order by number from: Special Publications Dept., IAS, 2 E. 64th St., New York 21, N.Y.

✦ ✦ ✦

IAS SPECIAL PUBLICATIONS

	Member	Nonmember
Vehicle Systems Optimization Symposium Proceedings, 1961 (168 pp.)	$5.00	$10.00*
IAS/Army Aviation Meeting Proceedings - 1961 (68 pp.)	2.50	5.00*
National Midwestern Meeting on Air Logistics Proceedings - 1960 (116 pp.)	5.00	10.00*
Weapons Systems Management - National Midwestern Meeting Proceedings - 1957 (60 pp.)	1.50	2.50*
National Symposium on Hypervelocity Techniques Proceedings - 1960 (176 pp.)	5.00	10.00*
Recovery of Space Vehicles Symposium Proceedings - 1960 (104 pp.)	4.00	8.00*
National Specialists Meeting on Dynamics & Aeroelasticity Proceedings - 1958 (136 pp.)	3.50	6.00*
1961 National Telemetering Conference Report	3.50	5.50*
1960 National Telemetering Conference Report	4.50	6.50*
1959 National Telemetering Conference Report	3.00	4.00*
Frontiers of Science & Engineering Symposium Proceedings - 1959 (132 pp.)	5.00	10.00*
Fourth Turbine-Powered Air Transportation Meeting Proceedings - 1959	2.00	4.00*
Second Turbine-Powered Air Transportation Meeting Proceedings - 1955	3.50	6.00*
7th Anglo-American Aeronautical Conference Proceedings - 1959	20.00	25.00*
5th International Aeronautical Conference Proceedings - 1955	15.00	20.00*
2nd International Aeronautical Conference Proceedings - 1949	5.00	5.00*
National Naval Aviation Meeting Proceedings - 1957 (124 pp.)	3.00	5.00*
Index to Books on Selected Technical Subjects in the IAS Library (up to 1950), unbound	2.00	2.00*
Aerospace Engineering Index - 1958	10.00	15.00*
Aeronautical Engineering Index - 1956 and 1957 (each)	10.00	15.00*
Aeronautical Engineering Index - 1947 through 1955 (each)	3.00	5.00*

* Add $1.00 for orders outside the U.S.A.

These may be obtained by writing to: Special Publications Dept., IAS, 2 E. 64th St., N.Y. 21, N.Y.

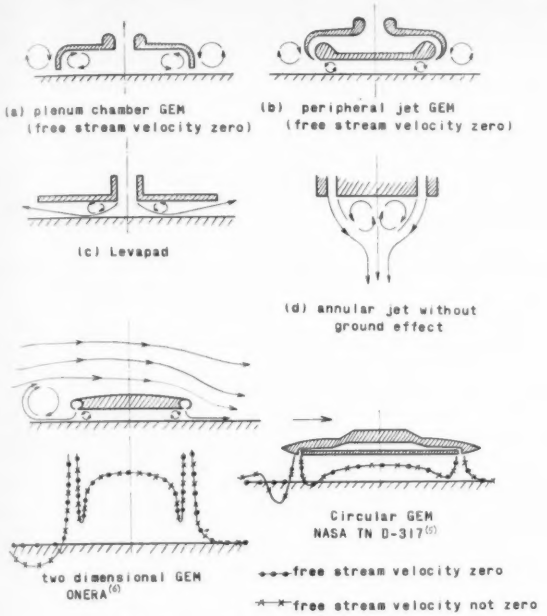

Fig. 3. Jets induce various types of vortices, which reduce the pressure on the ground surface or body surface.

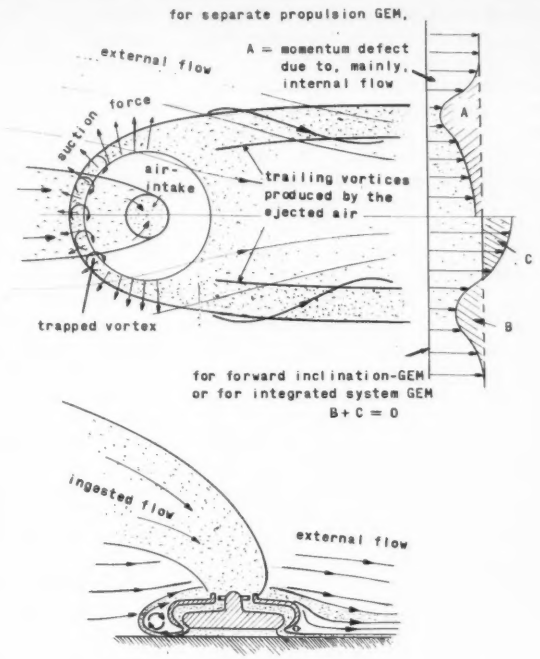

Fig. 4. Tentative model of flow pattern around a GEM.

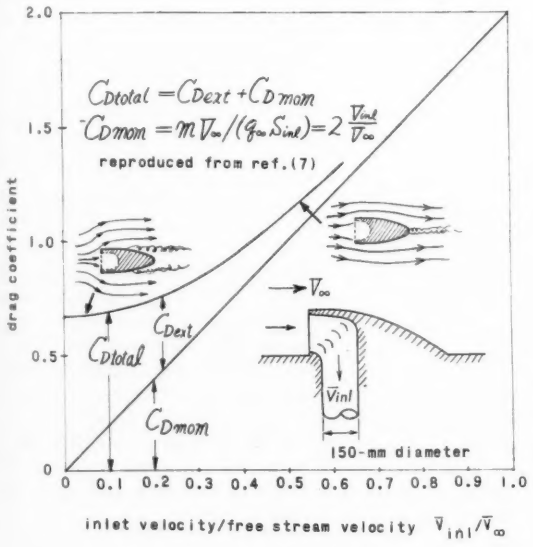

Fig. 5. Drag breakdown of air scoop.

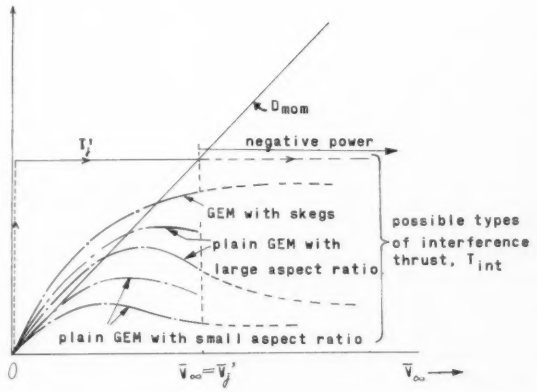

Fig. 6. Schematic diagram of interference thrust for some typical GEM's.

GEM base surface which forms a "nozzle" converting the pressure energy of the ejected air to the rearward momentum together with the ground surface. It has been believed that the propulsive force is a forward component of the lift vector acting on the GEM base surface. But the present authors think there exists some additional interference thrust acting on the GEM upper surface. For the integrated air curtain GEM, the major thrust-feeling surface is nozzle exit, again the lower portion of the GEM. Nevertheless, the authors believe that some additional thrust may be felt on the GEM upper surface and total available thrust in forward motion seems to be much larger than the value assumed by Chaplin,[3, 4] which is equal to the value for a hovering GEM.

It is noteworthy that the flow pattern produced by a forward-inclination GEM may be similar to the flow pattern produced by an integrated air curtain GEM, when one observes the flow from a point sufficiently behind the GEM's. If these two GEM's fly at a steady speed, then the resultant rearward component of the all-airflow momentum should be zero. Breakeven point thus depends on cushion power required to conquer a given roughness of the ground surface at the same flight velocity. But this subject is out of the range of the present paper.

Second we consider the effect of the ingested air; the ingested airflow seems to play a rather minor role when contrasted with the ejected airflow. Nixon and Sweeney[2] suggest that interference thrust (*momentum recovery*, in their terms) would be attributed mainly to sink effect on the external flow. However, this effect is not sufficient to explain the negative parasite drag. Let us suppose a uniform flow over an infinite flat surface. Let us then add an arbitrary hump on this surface and an air-ducting system, which has an arbitrarily tilted air intake in the hump and sucks in the air at some mass flow rate. If we restrict this to a potential flow, then the resultant force felt by this complete arrangement should be mass flow rate times free-stream velocity. It is important to note that this force results from the pressure change over the entire surface which contains not only the duct system but also the hump. Thus, it is the present authors' opinion that GEM momentum drag should be felt distributedly over the entire upper surface of the GEM, not just restrictedly in the air intake. However, the following viscous effects should not be neglected:

(1) The boundary layer developed on the GEM upper surface will decrease the momentum drag and ram effect; the layer should be removed from the ingested air.

(2) The ingested air tends to reduce the upper surface drag to the level of $D_{mom} + D_{friction}$, through the considerable reduction of external flow separation. This favorable effect was pointed out by Nixon and Sweeney,[2] and was justified roughly by the data shown in Fig. 5 which is cited from Hoerner.[7] It should be noted that this effect cannot decrease the parasite drag to a negative value.

Consequently, the generating mechanism of interference thrust is thought to be as follows:

(1) T_{int1}—The disappearance of dead area at the air intake and nozzle exit, and considerable reduction of frictional drag on the GEM base in power-on condition.

(2) T_{int2}—The ingested air and the air ejected at the rear bring about a favorable effect on the external flow; they tend to prevent the external flow from separating and to reduce the parasite drag to the level of the frictional drag only.

(3) T_{int3}—The ejected air has energy in the form of its total pressure P_{tj}, some part of which is converted to propulsive work in the process of expansion; the air ejected at the rear works most effectively and that ejected at the front has some propulsive effect through its curl-back and suction force which are caused by the front-trapped vortex. The air ejected at the sides, however, may lose its major energy. Note that *points (1) and (2) can explain the reduction of the parasite drag to a very small level of frictional drag only at the ideal limit*, but the *negative parasite drag should be attributed to point (3)*. Most ideal would be the case where all terms of T_{int1}, T_{int2}, and T_{int3} have their maximum values respectively.

Furthermore, the authors point out that there exists a fundamental difference between the induced drag of a conventional finite-span-wing and the internal drag of a GEM. The lift power of a conventional airplane is inevitable due to some essential downwash. On the other hand, *"true lift power" of a GEM is not always necessary*; what is necessary is to maintain some of excess pressure, not to give power to the air cushion. The air cushion requires power only when the air scatters from the GEM base irrespective of the scatter direction. Thus, for an ideal GEM in which the cushion air scatters only rearward, it could be said that the GEM requires power for propulsion only.*

(5) Tentative Expression of Aerodynamic Drag

Considerations presented in the preceding paragraph seem to justify the following expression for the drag of a GEM:

$$D = \underbrace{(D_p' + D_{mom} - T_{int})}_{\text{felt on the GEM upper surface}} + \underbrace{(D_{lf} + W\tan\alpha - \gamma T_j) + D_{water\ spray}}_{\text{felt on the GEM base}} \qquad (5.1)$$

where

D_p' = fictitious parasite drag; measured drag on the GEM the air intake and nozzle exit of which are shut by fairing covers, minus skin friction drag over fairing covers and base surface

D_{mom} = mass flow rate × flight velocity

T_{int} = interference thrust $T_{int2} + T_{int3}$

D_{lf} = frictional drag on base surface

$W\tan\alpha$ = drag due to attitude of GEM (α is positive when front part is up, in radian; this drag results from c.g. shift, change in jet thrust distribution, or existence of water wave drag)

γT_j = propulsive component of jet momentum, measured at nozzle exit; not zero for integrated air curtain GEM

$D_{water\ spray}$ = drag due to water spray; in general, negligibly small at cruising speed

Eq. (5.1) reduces to the following simple form for typical GEM's:

$$D \doteqdot (D_p' + D_{mom} - T_{int}) = T_s \qquad (5.1'a)$$

for plain GEM

$$D \doteqdot (D_p' + D_{mom} - T_{int}) - W\tan(-\alpha) = 0 \qquad (5.1'b)$$

for forward-inclination GEM

$$D' \doteqdot (D_p' + D_{mom} - T_{int}) - \gamma T_j = 0 \qquad (5.1'c)$$

for integrated system GEM

where two terms $D_{water\ spray}$ and D_{lf} are neglected. In the present state of the art, one cannot estimate T_{int} with sufficient accuracy, despite its significance.

To understand the nature of interference thrust T_{int}, let us consider change in this quantity with increasing flight velocity. It is instructive to consider the upper limit of the interference thrust T_{int}'. The reasonable value of T_{int}' is simply given by the following form, as mentioned in the preceding paragraph:

$$T_{int}' = T_j' + D_{sep}' \qquad (5.2)$$
$$T_j' = m\bar{V}_j' = m\sqrt{2P_{tj}/\rho}$$

where D_{sep}' is the pressure drag, contained in D_p'. $\bar{V}_j'$ is a fictitious velocity reached by the ejected jet if the jet would expand isentropically from the pressure P_{tj} to the free-stream pressure (zero), and T_j' is the corresponding fictitious thrust. If P_{tj} is equal to $P_{t\infty}$—viz., no power or loss is added—then T_j' is equal to D_{mom} as expected. Thus Eq. (5.1) for the most ideal GEM becomes

$$D \doteqdot (D_{uf} + D_{lf}) - m(\bar{V}_j' - \bar{V}_\infty) \qquad (5.1'')$$

where D_{uf} represents the skin friction on the upper surface.

Chaplin[3] presented the very instructive theory, "simplified ideal theory," which takes into account the momentum drag only as the inevitable loss, whereas the *present authors propose the most ideal type of GEM which suffers the frictional drag only in contrast with Chaplin's theory*. The most ideal GEM makes GEM's future more promising than in the previous investigations, and also shows us the decisive direction

* For example, a diffuser-recirculation type GEM requires no cushion power, according to the simplified ideal theory.[3]

in order to improve performance of the present GEM's.

The actual interference thrust T_{int}, of course, cannot reach the value of T_{int}'. For illustrative purposes some curves for T_{int} are shown in Fig. 6. When the GEM is at rest, T_{int} must be zero. For small flight velocity, a suction force may appear ahead of the GEM owing to the trapped vortex. This force seems to be proportional to $\bar{V}_\infty \bar{V}_j$ and in practice it often has a sufficient amount to cancel the momentum drag completely (Fig. 2). For larger flight velocity, considerable difference occurs between various types of GEM. First, the amount of T_{int} rather close to T_{int}' may be appear for GEM's with skegs, in which the air quantity ejected at rear part of the GEM has large percentage and the air ejected at front part of the GEM is easily turned back with increasing flight velocity. *For a plain GEM, however, the air quantity ejected at the both sides of the GEM increases with the flight velocity because of the negative ambient pressure at the sides. Thus most part of the ejected air energy may dissipate in the form of rotation loss. The flow pattern model given by the present paper thus explains satisfactorily the reduction of interference thrust at high flight speed* which stimulated Nixon and Sweeney's attention. Indeed the fact how the actual interference thrust closes to its upper limit T_{int}' may essentially depend on the fact how much part of the air is ejected from the rear of the GEM.

It is noteworthy that interference thrust has a similar nature, for proportionality to $\bar{V}_\infty$ at low speed and for the amount itself, to the momentum drag. This fact may continue to high speed range for GEM with skegs or high aspect ratio planform. Therefore the following expressions will be valid as the first order approximation:

$$T_{int} = \lambda D_{mom} \qquad (5.3)$$

for GEM with skegs or high aspect ratio planform

which leads us to

$$D_{mom} - T_{int} = \mu D_{mom},\ \mu \ll 1 \qquad (5.4)$$

for GEM with skegs or high aspect ratio planform

where λ and μ are quantities nearly independent of flight velocity.

Of course contribution of the air ejected at the front of GEM, through suction force due to the trapped vortex and curl back of the ejected air, to the propulsive thrust should be determined by experimental data quantitatively. Nevertheless the present authors believe the excellent aerodynamic drag characteristics of GEM with skegs or large aspect ratio planform according to the following, somewhat different, reasons:

With increasing flight velocity from zero, strength of the trapped vortex ahead of the GEM becomes larger, reaches the maximum and then becomes smaller; size of the vortex becomes smaller and the vortex goes to the front of GEM closer monotonously. At flight velocity larger than a critical value, the ambient pressure ahead of the GEM becomes positive value which is nearly equal to the free-stream dynamic pressure; the cruising flight velocity perhaps gives this situation *Thus a flow rate of air ejected at the front becomes smaller with increasing flight velocity, whereas a flow rate of air ejected at the rear becomes larger, because some little separation of external flow here may be inevitable for any actual GEM.*

In conclusion, major part of the internal flow would be ejected from the rear of actual GEM with skegs or large aspect ratio planform, and thus the internal flow drag will be almost canceled.

(6) Some Possible Methods for Decreasing Aerodynamic Drag

The tentative flow pattern model presented in the previous sections leads us directly to the following method for decreasing the internal drag:

(1) Use of skegs.
(2) Large aspect ratio planform.
(3) Forward inclination of GEM.
(4) Integrated system.

Of particular interest is the third method. Forward inclination GEM requires large internal flow for heaving the rear part of the GEM; this type of GEM suffers large momentum drag. However, much larger percentage of air may be ejected from the larger clearance at the rear in contrast to plain GEM. The present authors think that combinations between (3) and (1) or (4)—i.e., forward inclination GEM with skegs or forward inclination GEM with aft-tilted jet nozzle—may show excellent cruising performance.

Conclusion

A qualitative theory is presented in order to reveal the essential nature of drag of the ground effect machine. This tentative theory will be applicable to ram wing, plenum chamber and air curtain GEM, especially to the first two. The interference thrust is brought about by considerable reduction of flow separation due to the ingested and ejected air and partial conversion of the cushion pressure energy to propulsive work. The previous explanation which deduced the interference thrust from mainly sink effect is insufficient. The plain GEM flies dragging a horse-shoe vortex ahead of the GEM. Ejected air loses its pressure energy essentially through flow rotation loss, which is brought about by the part ejected from the both sides. In order to increase the interference thrust or decrease rotation loss, several methods such as use of skegs, large aspect ratio planform, integrated system or forward-inclination of the GEM may be effective.

Lastly it should be noted that most of the description in the present paper is merely the present authors' opinion and has not yet been confirmed experimentally.

References

[1] Kuhn, R. E., and Carter, A. W., *Research Related to Ground-Effect Machines*, NASA, L-59-6087, Oct. 1959.

[2] Nixon, W. B., and Sweeney, T. E., *Preliminary Flight Experiments With the Princeton University 20-Ft. Ground Effect Machine*, AERO/SPACE ENGINEERING, Vol. 19, No. 4, pp. 32–36, 58, April 1960.

[3] Chaplin, H. R., *Ground Effect Machine Research and Development in the United States*, David Taylor Model Basin, Aero Report 994, Dec. 1960.

[4] Chaplin, H. R., *Ground Cushion Research at the David Taylor Model Basin—A Brief Summary of Progress to Date*, paper presented at Princeton Univ. Symposium on Ground Effect Phenomena, Oct. 21, 1959.

[5] Greif, R. K., Kelly, M. W., and Tolhurst, W. H., Jr., *Wind-Tunnel Tests of a Circular Wing With an Annular Nozzle in Proximity to the Ground*, NASA TN D-317, May 1960.

[6] ONERA, no details are available to the present authors.

[7] Hoerner, S. F., *Fluid-Dynamic Drag*, pp. 9–13, 1958 (published by the author, Midland Park, N.J.).

THE IAS LIBRARY

Publications treated in *International Aerospace Abstracts* are maintained by the Library for use by the IAS Membership. They are *not* for sale but are made available through the facilities of the Library.

LENDING SERVICES: Institute members, both Individual and Corporate, may borrow periodicals, reports, and books for a period of 2 weeks, excluding time in transit. Excepted are certain reference books and those IAS publications that may be purchased.

PHOTOCOPY SERVICES: The Library is equipped to provide, as a service, positive photocopies of certain materials in its collections. Rates on request.

For detailed information about these and other services, write to:

John J. Glennon, Manager,
Technical Information Service
Institute of the
Aerospace Sciences, Inc.
2 East 64th Street
New York 21, New York

Honors and Awards of the IAS

The IAS Honors and Awards program has for many years given recognition for distinguished achievement in the aerospace sciences. The IAS has a special brochure which covers the awards and their past recipients in detail. The following excerpts indicate the nature of this IAS program.

HONORARY FELLOWSHIP, the highest IAS honor may be accorded annually to two persons of eminence in aerospace technology, one of whom must reside in the U.S.A.

IAS FELLOWS have attained a position of distinction in aeronautics and have made notable and valuable contributions in one of the aerospace sciences or in aerospace engineering. Not more than ten residents of the U.S., and ten residing outside the U.S.A., may be elected in any one year.

THE OCTAVE CHANUTE AWARD established by the IAS in 1939 honors the memory of the pioneer U.S. aeronautical investigator for whom it is named. It is given for "a notable contribution made by a pilot to the aerospace sciences."

THE JOHN JEFFRIES AWARD, recognizing the importance to aeronautics of scientific endeavor in the field of medicine, honors the memory of the American physician who made the earliest recorded scientific observations from the air. The award is given for "outstanding contributions to the advancement of aeronautics through medical research."

THE LOUIS W. HILL SPACE TRANSPORTATION AWARD carries the largest honorarium available through a scientific society — $5,000 to an individual, or up to $10,000 in the event of a "team" contribution.

THE ROBERT M. LOSEY AWARD established in 1940 honors the memory of Captain Robert M. Losey, a meteorologist, the first officer in the service of the United States to die in World War II. It is presented "in recognition of outstanding contributions to the science of meteorology as applied to aeronautics."

THE SYLVANUS ALBERT REED AWARD, endowed by Dr. S. A. Reed, a founder member of the IAS, to be presented "for a notable contribution to the aerospace sciences resulting from experimental or theoretical investigations, the beneficial influence of which on the development of practical aeronautics is apparent."

THE LAWRENCE SPERRY AWARD, established in 1936 by the sister and brothers of Lawrence Sperry, pioneer aviator and inventor who died in 1923, is given "for a notable contribution made by a young man to the advancement of aeronautics."

THE IAS FLIGHT TEST ENGINEERING FELLOWSHIP provides for two years of graduate study in flight test engineering leading to a master's degree or doctorate in engineering. Program of study can be varied to meet the background and needs of the individual student.

THE MINTA MARTIN NATIONAL STUDENT AWARDS, endowed by Glenn L. Martin, are given for outstanding student papers presented at the annual regional conferences. The regional first-prize papers in each division are considered for national awards.

Personnel Opportunities

This section is for the use of individual members of the Institute seeking new connections and eligible organizations offering employment to specialists in the aero/space industry. Any member or eligible organization may have requirements listed without charge by writing to the Secretary of the Institute.

Wanted

Missile Propulsion Preliminary Design—Applying advanced propulsion concepts this engineer will prepare systems analyses and trade-off studies on new concepts in missile propulsion design. He will prepare technical proposals on rocket engine hardware problems including solid propellant nozzle design and motor insulation. A minimum of 6 years' related experience required plus M.S.M.E. **Controls Analysis**—Responsible for the analysis and evaluation of aircraft-missile-electromechanical, servo-control systems. Capability of defining stability performance and dynamics of physical systems in terms of differential equations necessary. Analysis techniques will include use of LaPlace transforms, Nyquist stability criteria, and Bode plots. Related degrees plus several years' experience. **Operations Research Specialist**—Apply theory of operations research to selection and optimization of military weapons systems. Background in game theory and information theory desirable. Man will work on advanced projects involving the entire spectrum of environments, from space to undersea. **Magnetohydrodynamics Specialist**—To plan and perform research in the field of magnetohydrodynamics, power generation, and plasma as related to nuclear power and space power systems. M.S. physics or engineering plus minimum 5 years' experience. **Plasma Engine Specialist**—To plan and perform basic research in the fields of plasma and ion engines, magnetohydrodynamics, and power generation as related to nuclear power and space power systems. Ph.D. physics or engineering plus minimum 5 years' experience. **Gasdynamics Engineer**—To undertake studies in gasdynamics, heat transfer, supersonic aerodynamics, and fluid flow for support of rocket nozzle programs, systems for thrust vector controls, hot gas steering systems, auxiliary power units, and similar advanced engineering programs. Advanced degree plus 3 years' experience. Write fully to R. J. Theibert, Employment Manager, Tapco Group, Thompson Ramo Wooldridge, Inc., 23555 Euclid Ave., Cleveland 17, Ohio.

Professors—The Air Force Institute of Technology, Wright-Patterson AFB, Ohio, has a vacancy in the Department of Mathematics. Most of the work is at advanced undergraduate and graduate levels. One quarter out of four free of teaching duties for research or other academic pursuits, plus vacation. Working conditions comparable to those in leading universities. Employment will be effected in accordance with Civil Service regulations. Rank and salary will depend upon qualifications of applicant and may be anywhere between assistant professor, GS-11, $7,560, and full professor, GS-14, $12,210. Applications should be made on Standard Form 57, available at any Post Office, or by letter to Head of the Department of Mathematics.

Aerodynamicists—The Cornell Aeronautical Laboratory has attractive openings for qualified scientists to perform research in the following areas: (1) magnetoaerodynamic effects on the flow over blunt bodies; (2) flow field analyses at hypersonic velocities and low densities; (3) aerodynamic characteristics of simple geometry hypersonic configurations; (4) aerodynamic aspects of air-data sensing at hypersonic flight conditions; (5) base heating of clustered rocket nozzle configurations; (6) structure of air heat transfer due to turbulent boundary layers at hypersonic Mach numbers. The Laboratory provides a desirable combination of the best features of industry as to financial and facilities resources coupled with a university associated atmosphere conducive to R & D activity at the highest level. Salary commensurate with qualifications and experience. Send complete résumé to A. A. Rentschler, Cornell Aeronautical Laboratory, Inc., 4455 Genesee St., Buffalo 21, N.Y.

138. Professor of Aerospace Engineering—Positions now available in department of aerospace engineering of state university. Openings are in areas of aerospace structures, aerodynamics, and magnetoaerodynamics. Rank and salary will depend upon qualifications of applicant. Liberal research and consulting policies. Furnish résumé with reply.

The number preceding the notice represents the Box Number of the Institute of the Aerospace Sciences to which inquiries should be addressed.

Notices of all change of address should be sent to the Circulation Department, Institute of the Aerospace Sciences, Inc., 2 East 64th Street, New York 21, N.Y., at least 30 days prior to change of address.

Available

141. Research Engineer—Age 39; former head of university engineering research organization, now VTOL project aerodynamicist for aircraft manufacturer, desires increased research managerial responsibility. Fifteen years' industrial and academic experience, as university aeronautical engineering option head, research project engineer, and project director for sponsored STOL and VTOL analytical wind-tunnel and flight research programs. Complete résumé on request.

140. Airline Executive—A.E. and M.E. degrees. Member IAS. Sixteen years' extensive experience in management, operational and technical fields, including proved capability in planning and coordinating aircraft integration programs, performance and economic evaluation of proposed aircraft, and development of airplane operating procedures. Experienced in airplane contract negotiations, development of corporate planning premises, and personnel and budget administration. Particularly interested in program or project planning. Wish opportunity to explore other possibilities with you. Résumé furnished on request.

139. Director of Engineering and Maintenance—Twenty-one years of progressively increasing technical and administrative responsibility for the design, analysis, procurement, operation, and maintenance of commercial transport and military aircraft in domestic and international service. B.S.M.E., aeronautical major. Colonel, USAF Reserve. Age 43. Résumé upon request.

137. British Aircraft Designer (AFIAS)—Interested in consultation and formation of design team in United Kingdom. Would be prepared to consider any design consignment. Work would be completed rapidly and at nominal cost. Résumé on application.

136. Aeronautical Engineer—Thirty years' experience—civil approval of power plants, power-plant supervisor with aircraft manufacturer, chief of AEDC engine test facility; also manager, engineering sales and advanced proposals. Desires engineering applications and Government contacts for advanced propulsion and space systems. B.S. in M.E. and LL.B. Ohio resident.

134. Project of Engineering Manager—Broad background in aeronautical and ballistic missile design and management. Experience in establishing structural design, criteria, performance of operational analysis, and weapon system analysis and development. Considerable experience as project manager handling all phases of design, budgeting, program planning, and support activities for an operational military system. Age 44. AFIAS. Reg. Prof. Eng. Desires position in program planning, project management, engineering management, or at staff level.

133. Aeronautical Engineer—Thirteen years' experience in high-speed wind-tunnel testing, data reduction, and data analysis. Ten years in a supervisory capacity. Experience includes research activities, technical report preparation, and aerodynamic data analysis. Work also accomplished in the field of plasma generation in connection with arc-heated wind-tunnel development and employment as a testing facility. West Coast location desired; other locations considered. Résumé furnished on request.

A word about our Advertisers

The many companies whose advertising appears in this issue are interested in you and your work. They are anxious to let you know what they are doing to help you solve research and design problems in missile, rocket, air, and spacecraft projects.

AEROSPACE ENGINEERING's advertising pages keep you posted on new and improved materials, components, services, and supplies useful to your professional work.

To request more information on any product or service advertised, may we suggest you write to the *advertiser* directly, at no obligation to you. It would be greatly appreciated if you would mention that you saw the ad in AEROSPACE ENGINEERING.

AEROSPACE ENGINEERING
Established 1934
2 E. 64th St., New York 21, N. Y.

Index to Advertisers

AiResearch Mfgs. Divs., The Garrett Corp. ..... inside front cover
J. Walter Thompson Co.

American Machine & Foundry Co., Government Products Group 1
Cunningham & Walsh, Inc.

The Bendix Corp., Scintilla Div. ..... outside back cover
MacManus, John & Adams, Inc.

The Boeing Co., Wichita Div. 36
Jones and Hanger, Inc.

Components Div., International Telephone & Telegraph Corp. 63
Gaynor & Ducas, Inc.

Defense Electronic Products, Radio Corporation of America 34, 35
Al Paul Lefton Co., Inc.

Electro-Optical Systems, Inc. 31
Epic Advertising, Inc.

The Garrett Corp., AiResearch Mfg. Divs. ..... inside front cover
J. Walter Thompson Co.

General Precision, Inc., Kearfott Div. ..... inside back cover
Gaynor & Ducas, Inc.

Government Products Group, American Machine & Foundry Co. 1
Cunningham & Walsh, Inc.

International Aerospace Abstracts 70

International Telephone & Telegraph Corp., Components Div. 63
Gaynor & Ducas, Inc.

Kearfott Div., General Precision, Inc. ..... inside back cover
Gaynor & Ducas, Inc.

Lockheed-California Co., A Div. of Lockheed Aircraft Corp. 59
Hal Stebbins, Inc.

Lockheed-Georgia Co., A Div. of Lockheed Aircraft Corp. 33
Donahue & Coe, Inc.

MPB, Inc., Split Ballbearing Div. 5
Watson-Manning Advertising

Northrop Corp. 2
Doyle, Dane, Bernbach, Inc.

Radio Corporation of America, Defense Electronic Product 34, 35
Al Paul Lefton Co., Inc.

Scintilla Div., The Bendix Corp. ..... outside back cover
MacManus, John & Adams, Inc.

Southwest Research Institute 29

Split Ballbearing Div., MPB, Inc. 5
Watson-Manning Advertising

J. S. Staedtler, Inc. 69
Geer, DuBois & Co., Inc.

Vinco Corp. 61
Rolfe G. Spinning, Inc.

Wichita Div., The Boeing Co. 36
Jones & Hanger, Inc.

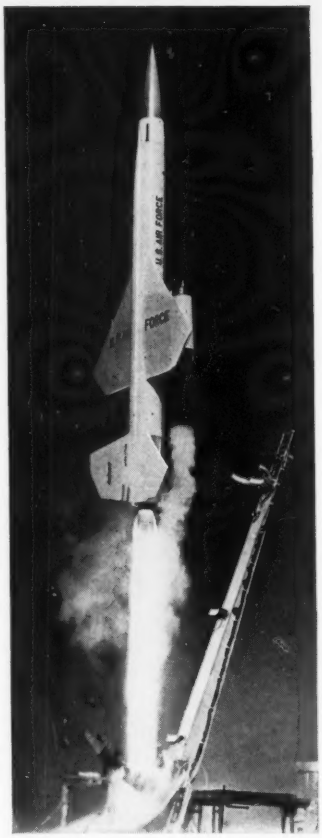

KEARFOTT developed

and now produces

the Bomarc-B all-attitude

mid-course

guidance system.

Engineers: *Kearfott offers challenging opportunities in advanced component and system development.*

KEARFOTT DIVISION
Little Falls, New Jersey

GENERAL PRECISION, INC.
Other Divisions: GPL, Librascope, Link

IN ELECTRICAL CONNECTORS, TOO

Craftsmanship produces enduring quality

For over three centuries, the Stradivarius has provided unmatched violin quality, reflecting the integrity of its maker. Similarly, companies today achieve their goals—or fall short—through varying degrees of quality and integrity.

Bendix® Electrical Connectors, made by the Scintilla Division, are recognized by their users as products of the highest quality—with no premium in cost. If connector quality interests you, write us at Sidney, N. Y.

Scintilla Division

THE Bendix CORPORATION

Canadian Affiliate: Aviation Electric, Ltd., 200 Laurentien Blvd., Montreal 9, Quebec. Export Sales & Service: Bendix International, 205 E. 42nd St., New York 17, N.Y.